Università degli Studi di Roma “La Sapienza”

Facoltà di Scienze Matematiche Fisiche e Naturali

Tesi di Dottorato in Scienza dei Materiali

PhD Thesis in Materials Science

XXIII ciclo

Anchoring and reactivity of calixarenes and rotaxanes on semiconductor and metal surfaces, studied by XPS, AFM and electrochemistry

Candidate

Dr. Alice Boccia

Supervisor

Prof. Robertino Zanoni

ABSTRACT

This PhD thesis work deals with the extension to surfaces of the supramolecular concept of molecular recognition. Molecular recognition at interfaces is a key aspect in several important present and perspective applications, such as high-sensitivity sensors, drug-delivery systems and molecular electronics. Specific and reversible binding of guest molecules from a solution to a surface pre-treated with host molecules is a recent and active field of research.

Self-assembled monolayers may result from supramolecular interactions between cavitands possessing suitable anchoring groups and properly functionalized surfaces, adding distinct functionalities to the resulting hybrid species.

A compared study by surface techniques on the application of calix[n]arenes in the production of new functional materials is given. These new materials include two series of hybrids, based on the functionalization of Si(100) and polycrystalline Cu surfaces with calixarenes and derivatives, and gold nanoparticles (AuNPs), synthesized with the help of calixarenes. A very attractive topological property of AuNPs is the possibility to anchor onto the metallic core suitable receptors in a radial tri-dimensional arrangement for the recognition of charged and neutral species.

The anchoring systems chosen, calix[n]arenes (n=4,6), are one of the most relevant class of compounds in supramolecular chemistry, which own their popularity because of their flexibility as linkers, being, *i.e.,* efficient building blocks for constructing molecular devices based on rotaxanes.

New wet-chemistry recipes have been here developed and optimized to covalently anchor the appropriate molecules to Cu and Si substrates. The covalent functionalization on both Si(100) and polycrystalline Cu surfaces was obtained by making use of distinct, suitable terminations: a thiol (-SH) or C=C anchoring group, respectively for Cu or H-Si(100). In this latter case, an extra-mild photochemical activation via visible light was operated, which largely preserves the integrity of the molecular substrate. Anchoring on Cu was reached by dipping a clean substrate of this metal in a calixarene solution. Molecular adhesion has been

demonstrated by the presence and quantitation of XPS signals from specific elements in the molecules. The combination of different functionalities in a single SAM was tested on Cu by producing a mixed film.

AFM measurements performed on Si(100)/calix[4]arenes have revealed morphology consistent with the presence of surface aggregates with of the calixarenes. The availability of the calix[4]arene cavity to reversibly host further species after anchoring has been demonstrated by the complexation reaction with Cs^+ ions and a sequence of uptake and release cycles with pyridinium salts.

Self-assembled monolayers of oriented calix[6]arene-based rotaxanes and pseudorotaxanes were prepared on polycrystalline Cu. When these SAMs are suitably biased at a specific potential (experimentally inferred from solution studies on the molecular substrates), fully assembled rotaxanes detach from Cu, while in the case of pseudorotaxanes a selective detachment of the wheel results from biasing.

On Si(100) it can be observed that a nearly full monolayer can be obtained only in a two step-procedure, starting from the spontaneous formation of a mixed monolayer composed of pseudorotaxanes and axles, further reacted with a solution containing only the calixarenes.

We cross-checked the reactivity of the thiol and alkene terminal anchoring groups on the Cu and Si surfaces. No molecular uptake was observed when the two surfaces were exchanged, while each calixarene chemisorbed on the expected surface.

The characterization of a series of monolayer-protected gold nanoparticles (AuNPs) resulting from the reactions of monodentate, bidentate, tridentate and tetradentate thiolated calix[n]arene derivatives with the suitable percursor Au(III) compound, is reported. The compounds have been prepared by the research group led by prof. Pochini in Parma, following the Brust-Schiffrin synthesis. XPS, combined with TEM measurements, has shown that the particular multidentate structure of calix[n]arenes introduces a control element in the preparation of the gold nanoclusters. The interesting point is that such element allows, in the particular experimental conditions here reported, to obtain very small (< 1 nm) Au MPCs.

Index

Chapter 1
Introduction

This PhD thesis work deals with the extension to surfaces of the supramolecular concept of molecular recognition, which primarily implies self-organization of even complex chemical architectures via specific interaction and reversible assembling of molecular systems. Such an extension is very recent, and in the following an overview is preliminary given of both the basic concepts and the existing literature in the field.

1.1 – State of the art

In the frame of supramolecular studies, the combination of suitable molecules and surfaces of inorganic solids which have been pre-organized to produce a host-guest interaction, is relatively new and may lead to nanomaterials with new, tuneable and improved properties for perspective applications. These hybrid nanomaterials may develop additional and more attractive properties than their separate counterparts, because of the reciprocal interactions between them.

Supramolecular chemistry, established in 1980s, exploits the weaker and reversible non-covalent interactions between molecules. These forces include hydrogen bonding, metal coordination, hydrophobic and van der Waals forces, pi-pi interactions and electrostatic effects. Important concepts that have been demonstrated by supramolecular chemistry include molecular self-assembly, folding, molecular recognition, host-guest chemistry, mechanically-interlocked and dynamic covalent chemistry.

Nanotechnology emerged in the 1990s and involves the research and development of technology at the nanometer level. Nanoscience includes the study of objects and systems with dimension in 1-100 nm range. At these sizes, nanosystems can exhibit interesting and useful physical behaviours based on quantum phenomena (electron confinement,[1] near-field optical effects,[2] quantum entanglement,[3] electron tunnelling[4] and ballistic transport[5]) or subdomain phenomena (superparamagnetism,[6] overlapping double layers in fluids[7]). Chemistry has played a key role in the achievements of nanoscience. The development of new synthetic methods has allowed to produce uniform nanostructures with new shapes (spheres, rods, wires, half-shells, and cubes) and compositions (organics, metals, oxides, and semiconductors). One distinguishing characteristic of nanoscaled structures is that, unlike macroscopic materials, they typically have a high percentage of their constituent atoms at the surface. This scaling behaviour leads, in the most extreme case, to structures where nearly every atom in the structure is interfacial. In some sense, nanostructures are "all-surface" structures.

An important challenge of modern nanoscience and nanotechnology is obtaining molecular machines through the molecule-to-molecule bottom-up approach. The idea of constructing artificial molecular-level machines was first contemplated in 1959 by Richard Feynman in his historic address *There's a Plenty of Room at the Bottom*.[8]

Organic molecules are particularly interesting as nanoscale device elements because of our present ability either to manipulate their functional groups by synthesis, in order to satisfy rapidly changing technological requirements, and to achieve atomic-scale uniformity using a self-assembling process. When deposited on a substrate, organic molecules provide

[1] a) P. M. Petroff, A. Lorke, A. Imamoglu, Phys. Today 2001, 54, 46; S. A. b) Empedocles, R. Neuhauser, K. Shimizu, M. G. Bawendi, Adv. Mater. 1999, 11, 1243.

[2] a) M. M. Alkaisi, R. J. Blaikie, S. J. McNab, Adv. Mater. 2001, 13, 877. b) J. Jiang, K. Bosnick, M. Maillard, L. Brus J. Phys. Chem. B 2003, 107, 9964.

[3] a) A. N. Cleland, J. S. Aldridge, D. C. Driscoll, A. C. Gossard, Appl. Phys. Lett. 2002, 81, 1699. b) M. N. Leuenberger, D. Loss, Nature 2001, 410, 789.

[4] a) J. A. Stroscio, D. M. Eigler, Science 1991, 254, 1319. b) W. Wang, T. Lee, M. A. Reed, Phys. Rev. B: Condens. Matter 2003, 68, 035416.

[5] a) T. V. Torchynska, J. Appl. Phys. 2002, 92, 4019. b) A. I. Yanson, G. R. Bollinger, H. E. Van Den Brom, N. Agrait, J. M. Van Ruitenbeek, Nature 1998, 395, 783.

[6] Q. A. Pankhurst, J. Connolly, S. K. Jones, J. Dobson, J. Phys. D: Appl. Phys. 2003, 36, R167.

[7] R. Pericet-Camara, G. Papastavrou, M. Borkovec, Langmuir 2004, 20, 3264.

[8] R. Feynman, There's Plenty of Room at the Bottom, 1959

functionalities and high selectivity for applications such as selective catalysis, sensoring, lithography and optoelectronics, to name only a few.

A route to generate organized hybrid systems, such as inorganic-organic supramolecular structures, is to use inorganic solids with preorganized nanostructures and arrange functional molecules of different complexity on the scaffold. The functionalization of nanostructured solids with specific groups for the recognition of guests or for the switching of surface properties is a field where application of supramolecular concepts can be highly rewarding. Recent representative examples of hybrid frameworks that involve use of gold nanoparticles covered with functional alkanethiols have been reported for sensing. Astruc and coworkers described the electrochemical sensing of anions (Figure 1.1.1) by amidoferrocenyl moieties attached to AuNPs through simple alkanethiols[9] or dendritic structures.[10]

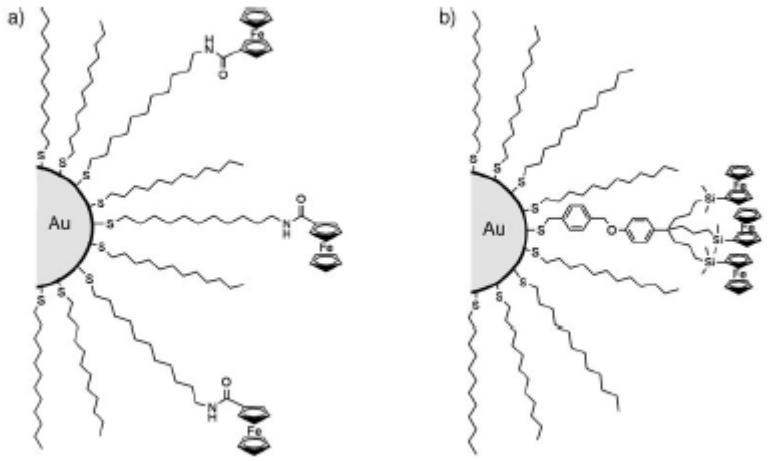

Figure 1.1.1: AuNPs functionalized with redox-active ferrocenyl units.

The research groups of Beer and Pochini developed systems with increased sensitivity for anion, organic cation and ion pair detection by assembling metalloporphyrins[11] and calix[4]arenes[12] (Figure 1.1.2) on the surface of AuNPs. Complex chemical structures can be

[9] a) A. Labande, D. Astruc, Chem. Commun. 2000, 1007. b) A. Labande, J. Ruiz, D. Astruc, J. Am. Chem. Soc. 2002, 124, 1782.

[10] a) M.-C. Daniel, J. Ruiz, S. Nlate, J. Palumbo, D. Astruc, J.-C. Blais, Chem. Commun. 2001, 2000; b) M.-C. Daniel, J. Ruiz, S. Nlate, J.-C. Blais, D. Astruc, J. Am. Chem. Soc. 2003,125, 2617.

[11] P. D. Beer, D. P. Cormode, J. J. Davis, Chem. Commun. 2004, 414 .

[12] a) A. Arduini, D. Demuru, A. Pochini, A. Secchi, Chem. Commun. 2005, 645.b) T. R. Tshikhudo, D. Demuru, Z. Wang, M. Brust, A. Secchi, A. Arduini, A. Pochini, Angew. Chem. 2005, 117, 2973.

synthesized from simple building blocks. Especially attractive examples are those where reversible assembly/disassembly processes can be controlled.

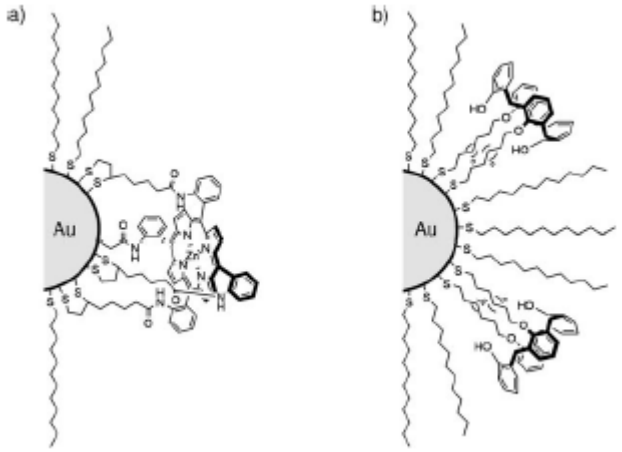

Figure 1.1.2: AuNPs functionalized with metalloporphyrins (a) and calix[4]arenes (b).

A step towards controlled and directional assembly was achieved by Reinhoudt and co-workers. They adsorbed tetraguanidinium calix[4]arenes functionalized with four adamantine units onto a ciclodextrines monolayer on gold by a two-step recipe: first, a complexation of the adamantane with the hydrophobic cavity of the cyclodextrines was induced (Figure 1.1.3);[13] second, tetrasulfonate calix[4]arenes were assembled onto the modified surface through electrostatic interactions.

Reversible control of the assembly and disassembly of a supramolecular structure should also have promising applications in the construction of molecular devices and nanomachines.

By covering surfaces and nanoparticles with an organic stabilizing shell, 2D self-assembled monolayers (2D-SAMs) or monolayer-protected clusters (MPCs or 3D-SAMs) can be obtained, respectively. The enticing aspect of these systems is that the nature of both the inorganic and the organic layer can influence the properties of the resulting hybrid material.[14] During the last decade, it became progressively clear that supramolecular chemistry, through the application of a "bottom-up approach", opens virtually unlimited possibilities to the design of nanomaterials and nanoscale objects.

[13] F. Corbellini, A. Mulder, A. Sartori, M. J.W. Ludden, A. Casnati, R. Ungaro, J. Huskens, M. Crego-Calama, D. N. Reinhoudt, J. Am. Chem. Soc. 2004, 126, 17050.

[14] A. B. Descalzo, R. Martinez-Manez, F. Sancenón, K. Hoffmann, K. Rurack, Angew. Chem. Int. Ed. 2006, 45, 5924.

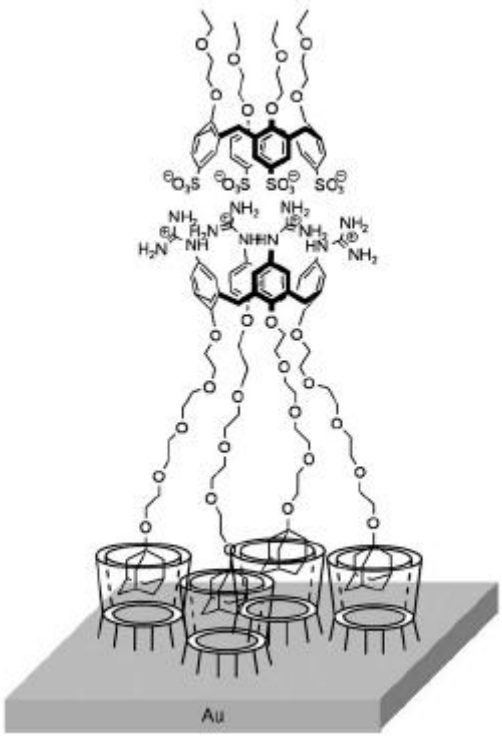

Figure 1.1.3: Tetraguanidinium calix[4]arene functionalized with four adamantyl units adsorbed on cyclodextrins monolayers and the subsequent assembly with tetrasulfonate calix[4]arene.

The modification of semiconductor surfaces by the covalent attachment of organic molecules has been an active topic of investigation in the field of surface science. The most important elementary semiconductor material is silicon. Organic monolayers immobilized on silicon substrates are crucial for microelectronics and sensors. Organic monolayers formed through a covalent Si-C bond provide electronic coupling between organic functionalities and semiconductor, without interference interfacial oxide thin film.[15]

Molecular recognition reactions at interfaces have been largely investigated in the past two decades, mainly by means of 2D-SAMs.[16] Nature teaches that molecular recognition can

[15] a) J. M. Buriak, Chem. Rev. 2002, 102, 1271. b) D. D. M. Wayner, R. A. Wolkow, J. Chem. Soc. Perkin Trans. 2 2002. c) M. R. Linford, C. E. D. Chidsey, J. Am. Chem. Soc. 1993, 115, 12631. d) C. H. de Villeneuve, J. Pinson, M. C. Bernard, P. Allongue, J. Phys. Chem. B 1997, 101, 2415. e) B. J. Eves, Q.-Y. Sun, G. P. Lopinski, H. Zuilhof, J. Am. Chem. Soc. 2004, 126, 14318. f) B. Fabre, D. D. M. Wayner, Langmuir 2003, 19, 7145.

[16] a) A. Aurora, F. Cattaruzza, C. Coluzza, C. Della Volpe, G. Di Santo, A. Flamini, C. Mangano, S. Morpurgo, P. Pallavicini. R. Zanoni, Chem. Eur. J. 2007, 13, 1240. b) F. Tancini, D. Genovese, M. Montalti, L. Cristofolini, L. Nasi, L. Prodi, E. Dalcanale, J. Am. Chem. Soc. 2010, 132, 4781. (c) G. G. Condorelli, A. Motta, M. Favazza, E. Gurrieri, P. Betti, E. Dalcanale, Chem. Commun. 2010, 46, 288. (d) E. Biavardi, M. Favazza, A. Motta, I. L. Fragala, C. Massera, L. Prodi, M. Montalti, M. Melegari, G. Condorelli, E. Dalcanale, J. Am. Chem. Soc. 2009, 131, 7447.

be achieved much more efficiently at appropriate interfaces.[14] In this framework, the use of versatile model surfaces of a high technological impact such as Si(100) to investigate molecular recognition can provide great insights into different classes of phenomena. The issue of immobilization on silicon oriented surfaces of molecules displaying single or multiple functions has grown rapidly in the last few years.[15a,16] Grafting reactions of organic molecules and ligands have been reported, with an aim at progressing into advanced fields of research such as nanoelectronics, nanosensing and, more recently, biological interfaces at the nanoscale. The advantages offered by a substrate as silicon are numerous, not only in terms of its low cost and high availability, but also because of its biocompatibility. Moreover, silicon can work as a semiconductor electrode, with applications in sensors and biosensors or, in the case of electroactive surfaces, charge-storage devices.

Supramolecular interactions have now started to diffuse into the realm of Si-anchored ligands, thus extending the control on reversibility typical for such type of chemical bond.[16] Research studies on Si oriented surfaces[17] looked at the establishment of a robust surface-to-organics bond, in order to reach the best possible conditions of reproducibility, in addition to an easier approach to a thorough characterization via surface spectroscopies and microscopies. The combination of a stable anchoring bond at the interface with the supramolecular interaction offered by the attached ligands leads to specific recognizing systems, which can be considered prototypical of more complex inorganic-organic hybrids.[14]

Literature on cavitands on Si(100)[16b-d] already exists on resorcinarenes, which have been used to control the self-assembly process in multistep growth of supramolecular structures on silicon.

Calix[n]arenes[19] are another class of synthetic macrocycles extensively employed for the preparation of efficient and selective receptors for neutral and charged species. More recently, they have been proposed as wheels in the oriented synthesis of rotaxanes and pseudorotaxanes.[18] Calix[n]arenes have found wide application as molecular platforms, on which a large variety of binding sites can be inserted and oriented in space, or as tridimensional receptors able to include into their aromatic cavities either neutral or charged species. They play an important role in molecular recognition as hosts for smal organic

[17] a) F. Cattaruzza, A. Llanes-Pallas, A. G. Marrani, E. A. Dalchiele, F. Decker, R. Zanoni, M. Prato, D. Bonifazi, J. Mater. Chem. 2008, 18, 1570. b) A. G. Marrani, E. A. Dalchiele, R. Zanoni, F. Decker, F. Cattaruzza, D. Bonifazi, M. Prato, Electrochimica Acta 2008, 53, 903. c) M. Cossi, M. F. Iozzi, A. G. Marrani, T. Lavecchia, P. Galloni, R. Zanoni, F. Decker, J. Phys. Chem. B 2006, 110, 22961. d) F. Decker, F. Cattaruzza, C. Coluzza, A. Flamini, A. Marrani, G. Andrea, R. Zanoni, E. A. Dalchiele, J. Phys. Chem. B 2006, 110, 7374.

[18] H. E. Zaugg, W. B. Martin in Organic Reactions; Ed.: A. Cope, Wiley, New York, 1965; Vol. 14, pp 52-269.

molecules, for ions, clusters or neutral guests. The main applications of calixarenes reported up to date are their use as sensors.[19]

Calix[6]arene derivatives functionalized with N-phenylureido groups have been recently employed as active components for the preparation of prototypes of molecular machines.[20] Owing to their particular shape and size, these macrocycles can act as asymmetric wheels for N,N'-dialkyl-4,4'-dipyridinium salts (viologen), to give rise to self-assembled species belonging to the class of rotaxanes and pseudorotaxanes. These latter are supramolecular complexes characterized by high thermodynamic stability, which can be reversibly disassembled in solution by external electrochemical stimuli.[21]

From the viewpoint of research advancements on molecular machines, the most interesting complex is pseudorotaxane, since it can be reversible dissociated into a free ring host and a free axle guest, giving rise to dethreading/threading motion. The external stimulus employed to operate this machine can be chemical, photochemical or electrochemical. Rotaxane-based molecular machines have been of early interest for their potential use in molecular electronics as logic molecular switching elements and as molecular shuttles. These molecular machines are usually based on the movement of macrocycle on the dumbbell.

The controlled production of organic SAMs on metal surfaces started in 1983, and is now a mature field. Early studies reported the behaviour of alkanethiols and dialkyl sulfide or disulfide on Au.[22] Various examples of functional species have thereafter been proposed, such as redox species,[23] biomolecules or selective receptors.[24] Use of model surfaces of a high

[19] Calixarenes in the Nanoworld, Eds.: J. Vicens, J. Harrowfield, Springer, Dordrecht, 2007 and references therein.

[20] a) M. Semeraro, A. Arduini, M. Baroncini, R. Battelli, A. Credi, M. Venturi, A. Pochini, A. Secchi, S. Silvi, Chem. Eur. J. 2010, 16, 3467. b) A. Arduini, R. Bussolati, A. Credi, G. Faimani, S. Garaudee, A. Pochini, A. Secchi, M. Semeraro, S. Silvi, M. Venturi, Chem. Eur. J. 2009, 15, 3230. c) B. Gadenne, I. Yildiz, M. Amelia, F. Ciesa, A. Secchi, A. Arduini, A. Credi, F. M. Raymo, J. Mater. Chem. 2008, 18, 2022. d) A. Arduini, A. Credi, G. Faimani, C. Massera, A. Pochini, A. Secchi, M. Semeraro, S. Silvi, F. Ugozzoli, Chem. Eur. J. 2008, 14, 98. e) A. Arduini, R. Bussolati, A. Credi, A. Pochini, A. Secchi, S. Silvi, M. Venturi, Tetrahedron 2008, 64, 8279.

[21] V. Balzani, A. Credi, M. Venturi, Molecular Devices and Machines: Concepts and Perspectives for the Nanoworld, Wiley-VCH, Wienheim, 2008 and references therein.

[22] J. C. Love, L. A. Estroff, J. K. Kriebel, R. G. Nuzzo, G. M. Whitesides, Chem. Rev. 2005, 105, 1103 and references therein.

[23] a) S. Watcharinyanon, E. Moons, L. S. O. Johansson, J. Phys. Chem. C 2009, 113, 1972. b) A. A. Yasseri, D. Syomin, V. L. Malinovskii, R. S. Loewe, J. S. Lindsey, F. Zaera, D. F. Bocian, J. Am. Chem. Soc. 2004, 126, 11944. c) J. Jiao, I. Schmidt, M. Taniguchi, J. S. Lindsey, D. F. Bocian, Langmuir 2008, 24, 12047. d) G. Fioravanti, N. Haraszkiewicz, E. R. Kay, S. M. Mendoza, C. Bruno, M. Marcaccio, P. G. Wiering, F. Paolucci, J. Am. Chem. Soc. 2008, 130.

technological impact such as Cu to investigate molecular recognition reactions can provide great insights into different classes of phenomena.

Molecular and nanoscale electronics are driven by the technological need for low cost devices or ever decreasing dimensions and the scientific desire to understand nanoscale charge transport. In molecular electronics, a critical issue is the establishment of a robust and reliable metal contact without damage of the organic layer or contamination of the interface (and Cu is a metal of choice for vias). In the literature, a few different methods are described to this aim, as producing Cu deposits on self-assembled monolayers (SAMs) covalently attached to a semiconductor as Si,[25] or depositing Cu nanoparticles on semiconductor surfaces.[26] We are interested in a selective functionalization procedure of a substrate as a key-step towards controlled deposition of suitable metals (also as nanoparticles) on semiconductors. In the case of Cu and Si, distinct and selective anchoring groups towards the two moieties are needed in case a bridging bond should be established between, *e.g.*, Cu nanoparticles and a pre-patterned Si surface. Moreover, investigations on the reactivity of polycrystalline Cu surfaces can be considered as preliminary to Cu single-crystal studies.[27]

Supramolecular chemistry can play an important role also in the development of a class of emerging hybrid organic-inorganic materials: 3D self-assembled monolayers (3D-SAMs). The members of this class, also known as monolayer protected clusters (MPCs), are compounds constituted by a discrete aggregate of metal atoms (inorganic core) of nanometric size, stabilized on the surface by an organic monolayer (shell). The properties of 3D-SAMs strongly depend on the nature of both the inner inorganic nanoparticle and the outer organic monolayer. The various functionalities of the latter (sensing, multivalency, solubility, etc.) makes nanoparticles excellent building blocks for the fabrication of new functional materials through the bottom-up approach of nanotechnology.

[24] a) B.-H.Huisman, E. U. T. van Velzen, F. C. M. van Veggel, J. F. J. Engbersen, D. N. Reinhoudt, Tetrahedon. Lett. 1995, 36, 3273. b) H. Schoenherr, G. J. Vancso, B.-H. Huisman, F. C. J. M. Van Veggel, D. N. Reinhoudt, Langmuir 1999, 15, 5541. c) F. C. J. M. Van Veggel, D. N. Reinhoudt, Chem. Eur. J. 1999, 5, 3595. d) C. Safarowsky, K. Wandelt, P. Broekmann, Langmuir 2004, 20, 8261.

[25] D. Cahen, G. Hodes, Adv. Mater. 2002, 14, 789.

[26] a) H.-F. Wang, Y.-G. Yan, S.-J. Huo, W.-B. Cai, H.-F. Wang, Y.-G. Yan, S.-J. Huo, W.-B. Cai, Electroch. Acta 2007, 52, 5950. b) O. Seitz, M. Dai, F. S. Aguirre-Tostado, R. M. Wallace, Y. J. Chabal, J. Am. Chem. Soc. 2009, 131, 18159.

[27] a) D. P. Woodruff, Appl. Surf. Sci. 2007, 254, 76. b) D. P. Woodruff, Surf. Sci. 2008, 602, 2963.

Recently, much attention has centered on colloidal metal nanoparticles because of their potential applications in areas of electronics, photonics, and catalysis.[28]

In antiquity, colloidal gold were used in an ecological sense for both aesthetic and curative purposes. The physical properties of nanoparticles in the diameter range 1-10 nm (intermediate between the size of small molecules and that of bulk metal) are neither those of bulk metal nor those of molecular compounds, but they strongly depend on the particle size, interparticle distance, nature of the protecting organic shell, and shape of the nanoparticles.[29]

Gold nanoparticles are the most stable metal nanoparticles. In particular, thiol-stabilized gold nanoparticles have become an important model system in nanomaterial research due to their stability, easy preparation and chemical versatility. Despite increasing efforts in the past few years, it is still a great challenge to fabricate well-controllable nanostructures by using colloidal particles as the structural elements. A key to achieving this goal will be the ability to assemble nanoparticles onto a desired surface. Much work has been performed to design and produce position-controlled assemblies of nanoparticles on solid surfaces, which are essential for nanodevice studies.[30] Silicon is clearly the most important material in modern technology, and several recipes reports have been published on the self-assembly of nanometer-sized materials attached to a silicon surface through strong Si-C bonds (347 $kJmol^{-1}$).[31] As a notable example, in a paper published by Nishihara et al. ω-alkene-1-thiol-functionalized gold nanoparticles covalently linked to a hydrogen-terminated Si(111) surface through a thermal hydrosilylation reaction are described (Figure 1.1.4).[32] The authors demonstrated the formation of an ordered monolayer on the surface that prevented the aggregation of nanoparticles and preserved the surface after long-term exposure to ambient conditions.

[28] a) M. C. Daniel, D. Astruc, Chem. Rev. 2004, 104, 293. b) G. Schmid, B. Corain, Eur. J. Inorg. Chem. 2003, 3081. b) A. C. Templeton, W. P. Wuelfing, R. W. Murray, Acc. Chem. Res. 2000, 33, 27.

[29] M. Brust, C. J. Kiely, Some Recent Advances in Nanostructure Preparation from Gold and Silver: A Short Topical Review. Colloids Surf. A: Physicochem. Eng. Asp. 2002, 202, 175.

[30] a) E. W. L. Chan, D.-C. Lee, M.-K. Ng, G. Wu, K. Y. C. Lee, L. Yu, J. Am. Chem. Soc. 2002, 124, 12 238. b) E.W. L. Chan, L. Yu, Langmuir 2002, 18, 311. c) H. X. He, H. Zhang, Q. G. Li, T. Zhu, S. F. Y. Li, Z. F. Liu, Langmuir 2000, 16, 3846. d) J. A. Harnisch, A. D. Pris, M. D. Porter, J. Am. Chem. Soc. 2001, 123, 5829 . e) T. Okamoto, I. Yamaguchi, J. Phys. Chem. B 2003, 107, 10 321. f) H. Tanaka, M. Mitsuishi, T. Miyashita, Langmuir 2003, 19, 3103. g) b) M. Yamada, H. Nishihara, Langmuir 2003, 19, 8050.

[31] R. T. Sanderson, Chemical Bonds and Bond Energy, Academic Press, New York, 1976.

[32] Y. Yamanoi, N. Shirahata, T. Yonezawa, N. Terasaki, N. Yamamoto, Y. Matsui, K. Nishio, H. Masuda, Y. Ikuhara, H. Nishihara, Chem. Eur. J. 2006, 12, 314 .

Ideally, it would be desirable to immobilize gold nanoparticles onto the surface by non-covalent, reversible bonds.

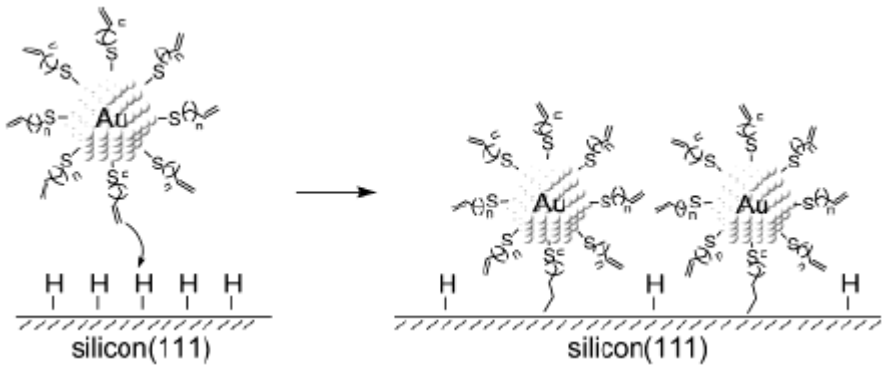

Figure 1.1.4: ω-alkene-1-thiol-functionalized AuNPs immobilized onto a hydrogen-terminated Si(111) surface.

The formation of mono- and multilayer films of small-ligand-stabilized metal nanoparticles is a significant research topic in the variety of possible applications (separations, chemical sensors) and their significance in fundamental science (such as the ligand dependence of electron-hopping conductivity within the films).

1.2 – Aim and outline of this thesis

The main object of this thesis is a compared study by surface techniques on the application of calix[n]arenes in the production of new functional materials. These new materials include two series of hybrids, based on the functionalization of Si(100) and polycrystalline Cu surfaces with calixarenes and derivatives, as discussed in Chapter 4 ad 5, and monolayer-protected gold clusters (MPCs), synthesized with the help of calixarenes, reported in Chapter 6.

The anchoring systems chosen, calix[n]arenes (n=4,6), are one of the most relevant class of compounds in supramolecular chemistry, which own their popularity because of their flexibility as linkers, being, *i.a.*, efficient building blocks for constructing molecular devices based on rotaxanes (Chapter 2).

The hybrids produced during the thesis work were mainly characterized by surface spectroscopy (XPS), and the experimental conditions and apparatus are described in Chapter 3. In some selected cases this technique has been supported by Atomic Force Microscopy (AFM), in order to obtain information on surface coverage and arrangements, and by electrochemical measurements, which can both provide relevant data on the redox processes and evidence the conditions for stimulating surface reactivity, as in threading-dethreading processes.

New wet-chemistry recipes, reported in Chapter 4 and 5, have been developed to covalently anchor the appropriate molecules to Cu and Si substrates, and optimized to obtain a high degree of coverage and to preserve surface from oxidation and contamination. The covalent functionalization on both Si(100) and polycrystalline Cu surfaces was obtained by making use of distinct, suitable terminations: a thiol (-SH) or C=C anchoring group, respectively for Cu or H-Si(100). In this latter case, an extra-mild photochemical activation via visible light was operated. Anchoring on Cu was reached by dipping a clean sample in a calixarene solution. Molecular adhesion has been demonstrated by the presence and quantitation of XPS signals from specific elements in the molecules. The availability of the calix[4]arene cavity to reversibly host further species after anchoring on both substrates has been demonstrated by a sequence of uptake and release cycles with pyridinium salts.

Self-assembled monolayers of oriented calix[6]arene-based rotaxanes and pseudorotaxanes were prepared on polycrystalline Cu. When each SAM is suitably biased at a specific potential, the rotaxane attached on Cu loses the entire molecular substrate, while a selective detachment of the wheel results from the pseudorotaxane (Chapter 4). On Si(100) it can be observed that a mixed monolayer, composed of pseudorotaxanes and axles, further uptakes free calixarenes from a solution (Chapter 5).

We cross-checked the reactivity of the different anchoring group on the Cu and Si surfaces. No molecular uptake was observed when the two surfaces were exchanged, while each calixarene chemisorbed on the expected surface.

In Chapter 6, the characterization of a series of monolayer-protected gold clusters (MPCs) stabilized by monodentate and multidentate thiolated calix[n]arene derivatives, is reported. The compounds have been prepared by research group led by prof. Pochini in Parma following the Brust-Schiffrin synthesis. The combination of XPS and TEM measurements shows that the particular multidentate structure of calix[n]arenes introduces a control element in the preparation of the gold nanoclusters that allows, in the particular experimental conditions here reported, to obtain very small (< 1 nm) Au MPCs.

Chapter 2

Investigated Systems

2.1 – Inorganic substrates

Atoms or molecules at the surface of a material experience a different environment from those in the bulk and thus have different free energies, electronic states, reactivities, mobilities, and structures. Whitesides et al. believe that surfaces represent a fourth state of matter.[22]

2.1.1 - Silicon surface

Silicon is the semiconductor most employed in electronics and nanotechnology, with an intrinsic conductivity of 4.3 × 10-6 Ω^{-1} cm^{-1}, and a band gap of 1.12 eV at 300 K. The electronic properties, such as its conductivity, can be manipulated by altering the dopant type (*p* or *n*) or concentration.

Silicon is a covalent solid that crystallizes into a face-centered cubic lattice structure, as illustrated in Figure 2.1.1.

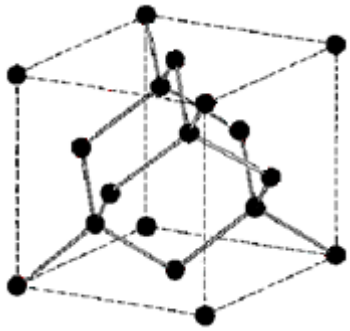

Figure 2.1.1: The face centered cube geometry of the crystal silicon.

Silicon forms a covalent solid, whose bonding is produced by the overlapping of highly directional electronic orbitals in a tetrahedral bonding configuration. While the diamond cubic lattice is preserved in the bulk, the solid is truncated on the surface of the material. The silicon surface reactivity is partly controlled by the unsaturated bonding orbitals, or dangling bonds, containing a single electron. On the surface, atoms can readjust themselves to minimize the total free energy of the system and eliminate or restrict the number of dangling bonds in a process known as "surface reconstruction".[33] Because of their importance in industry, the most common surface crystallographic orientations are Si(111) and Si(100) although other Si(hkl) orientations are known.[34] In Figure 2.1.2, the (111) and (100) ideal orientations and their respective dangling bonds are illustrated. The two surfaces have markedly different surface structures.[33]

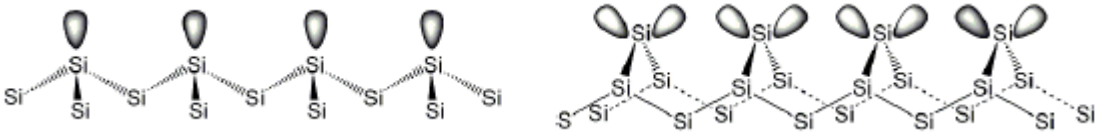

Figure 2.1.2: The Si(111) (left side) and Si(100) (right side) orientations.

The Si(100) surface reconstructs into 2x1 structure, where 2x1 designates the new periodicity of the surface atoms. The Si(100)-2x1 surface, illustrated in Figure 2.1.3, is made up of pairs of silicon atoms in adjacent rows that have bonded with each other, thereby this dimerization eliminates half of the dangling bonds. The Si(100)-2x1 dimers consist of a *s*

[33] a) J. J. Boland, Surf. Sci. 1991, 244, 1. b) A. Zangwill, Physics at Surfaces, Cambridge University Press, New York, 1988; c) C. B. Duke, Chem. Rev. 1996, 1237. d) H. N. Waltenberg, J. T. Yates Jr., Chem. Rev. 1995, 589.

[34] a) H. N. Waltenburg, J. T. Yates, Chem. Rev. 1995, 95, 1589. b) 8 R. J. Hamers, Y. Wang, Chem. Rev. 1996, 96, 1261.

bond (with a symmetry around the axis connecting the two atoms) and a *p* bond (with a nodal plane along the axis).[35] In any case, the silicon dimers are highly reactive towards reactions involving unsaturated bonds and have shown to produce ordered organic monolayers. The surface energy is further reduced by a surface distortion, in which the dimers are tilted, forming the so-called ‘‘up’’ and ‘‘down’’ dimers.

Figure 2.1.3: Si(100)-2x1 reconstruction, from DFT calculations.

By heating them to sufficiently high temperature under the Ultra-High Vacuum, the surface atoms of Si(111) rearrange themselves to a more energetically stable configuration called 7x7. Even after reconstruction, both the Si(100)-2x1 and Si(111)-7x7 surfaces are highly reactive. If exposed to the air, single crystal silicon is soon coated by a thin, native oxide.

In water solution silicon surfaces react quickly and result terminated -H, -OH and –O. In addition silicon wafer can be contaminated by metallic and organic species. Silicon surfaces can be made relatively stable in air for ten minutes, without any detectable growth of oxide (*i.e.* relatively resistant to oxidation) by hydrogen termination. It changes the surface structure, since Si–Si bonds of dimers are replaced by the stronger Si–H bonds, relaxing the surface reconstruction.[36] Due to the strong bonding and passivating nature of hydrogen atoms at the interface, hydride terminated silicon does not reconstruct itself, revealing instead a nearly bulk-like periodicity of the surface silicon atoms. Since the formation of a layer of oxide should be avoided when a covalent Si-C bond is established, the H-terminated p-Si(100), produced by wet chemistry procedures described in the Chapter 4, has been used as substrates for organic functionalization.

[35] J. J. Boland, Adv. Phys. 1994, 42, 129.

[36] P. Allongue, V. Kieling, H. Gerisher, Electrochim. Acta, 1995, 40, 1353.

The photochemical activation of H-Si – The photochemical approach is considered to be the mildest for functionalization of H-terminated Si surfaces via hydrosilylation reactions of terminal alkenes and alkynes. Due to the mild reaction conditions requested (room temperature and short reaction time) it is the most likely to be used in presence of biological and labile moieties. In the case of porous silicon such an approach has been taken by Buriak et al. through the use of a white light-promoted reaction.[37] It was demonstrated that excitons generated through illumination of the surface of photoluminescent porous silicon with white light (400 nm) are capable of driving a surface hydrosilylation reaction on hydride-terminated porous silicon, producing Si–C bonds. On the basis of the bond strength of the Si–H bond, a minimum energy of 3.5 eV (< 350 nm) is required to perform Si–H bond cleavage. Since Stewart and Buriak used wavelengths ≥ 400 nm, they concluded that the mechanism of hydrosilylation on porous silicon does not start with a homolytic cleavage of the Si–H bonds. For this reason a radical chain mechanism,[38] as operative in the case of thermal and UV hydrosilylation, was rejected, and a new mechanism was proposed, which involves attack by a 1-alkene or 1-alkyne on a surface-localized positive charge (the hole) in a nucleophilic fashion, resulting in Si–C bond formation (Figure 2.1.4).

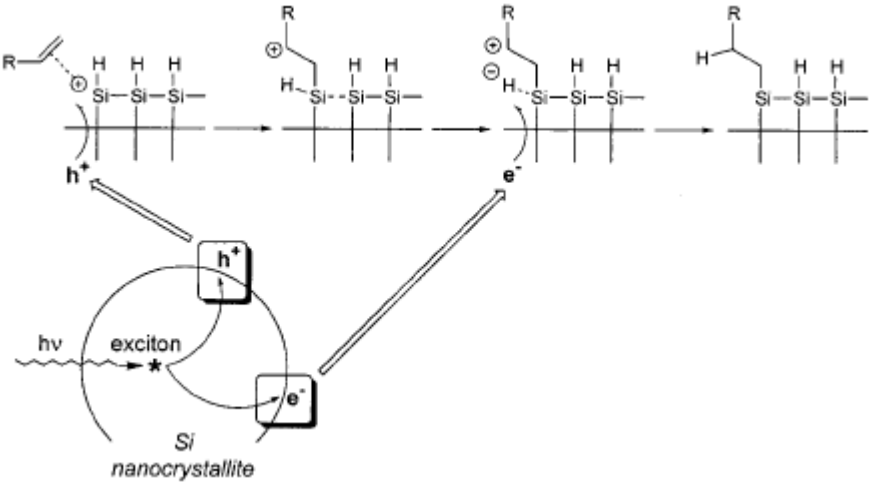

Figure 2.1.4: Proposed mechanism for the exciton-mediated hydrosilylation of porous Si.

It was thought that quantum confinement effects were crucial for this attachment reaction, which was thus thought to be limited to porous silicon. Zuilhof et al. hypothesized that this mechanism, tentatively rephrased in terms of surface plasmons, depicted in Figure 2.1.5, is

[37] M. P. Stewart, J. M. Buriak, J. Am. Chem. Soc. 2001, 123, 7821.

[38] M. R. Linford, P. E. Fenter, P. M. Eisenberger, C. E. D. Chidsey, J. Am. Chem. Soc. 1995, 117, 3145.

also active for flat H–Si and as a proof they found that the required reaction time to obtain densely packed monolayers depends on the dopant concentration, this being in line with the effects of the dopant on the band bending.[39]

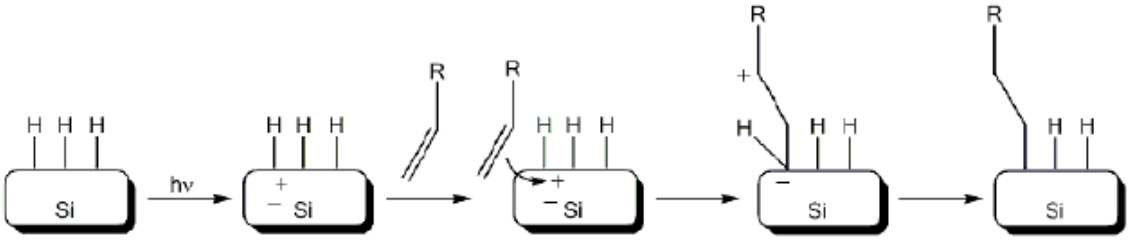

Figure 2.1.5: Mechanism proposed by Zuilhof et al. for the hydrosilylation of H–Si(100).

Our group, independently from Zuilhof and coworkers,[39] was the first to apply the visible light approach to attach organic monolayers to flat H-terminated silicon surfaces.[40]

Nevertheless, the recent results on the successfully attachment of saturated hydrocarbon chain on H-Si reported by us[17c] strongly suggests that the hydrosilylation activated by visible light proceeds through a mechanism not yet described.

2.1.2 - Copper surface and Self Assembled Monolayers

Copper is reddish metal with face-centered cubic (fcc) lattice structure. It is a good electrical conductor, second only to silver, but it obviously represents the best compromise between technological properties and costs. Copper does not react with water, but it slowly reacts with atmospheric oxygen forming a layer of copper oxide. In contrast to the oxidation of iron by wet air, this oxide layer stops the further, bulk corrosion. Copper reacts with hydrogen sulfide and sulfide-containing solutions, forming various copper sulfides on its surface. Because of its positive electrochemical potential it does not dissolve in acids except HNO_3 and H_2SO_4.

[39] (a) Q.-Y. Sun, L. C. P. M. de Smet, B. van Lagen, A. Wright, H. Zuilhof, E. J. R. Sudhölter, Angew. Chem., Int. Ed. 2004, 43, 1352. (b) Q.-Y. Sun, L. C. P. M. de Smet, B. van Lagen, M. Giesbers, P. C. Thune, J. van Engelenburg, F. A. de Wolf, H. Zuilhof, E. J. R. Sudhölter, J. Am. Chem. Soc. 2005, 127, 2514.

[40] R. Zanoni, F. Cattaruzza, C. Coluzza, E. A. Dalchiele, F. Decker, G. Di Santo, A. Flamini, L. Funari, A. G. Marrani, Surf. Sci. 2005, 575, 260.

Copper is essential and irreplaceable in many applications for its chemical, physical and mechanical properties, as heat and electrical conductivity and its corrosion resistance. Bare surfaces of metals tend to adsorb adventitious organic materials because these adsorbates lower the free energy of the interface between the metal or metal oxide and the ambient environment. These adsorbates also alter interfacial properties and can have a significant influence on the stability of nanostructures of metals.

Self-assembled monolayers are ordered molecular assemblies that form spontaneously by the adsorption of a surfactant with a specific affinity of its headgroup to a specific substrate. These layers potentially enable to tailor and to optimize the surface properties for a variety of technological applications as well as for fundamental studies of surface phenomena. Figure 2.1.4 shows the constituents of a SAM molecule (headgroup, chain or backbone, endgroup).

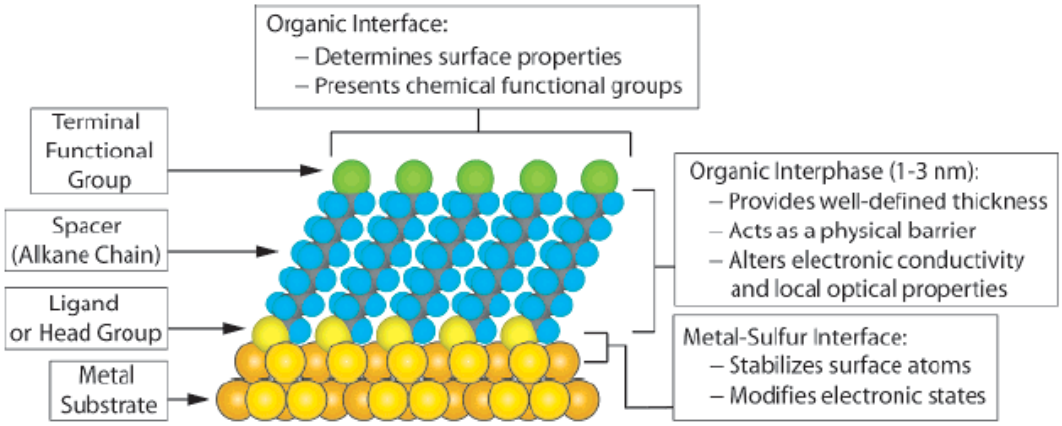

Figure 2.1.4: Schematic diagram of an ideal, single-crystalline SAM of alkanethiolates supported on a gold surface.

The headgroup shows a special affinity for the substrate. In case of coinage metals surfaces, typical headgroups are thiols. Historically[22,41] gold is the most studied substrate, then other metals have been modified, including copper. SAMs also consist of a tail with a functional group at the terminal end (endgroup). SAMs are created by the chemisorption of headgroups onto a substrate from either the vapor or liquid phase followed by a slow two-dimensional organization of chains and endgroups. As the alkyl chains become longer, the assembly becomes more ordered, since the organization is driven by van der Waals attractive forces. Areas of close-packed molecules nucleate and grow until the surface of the substrate is covered in a single monolayer. Such assemblies at solid surfaces allow the fabrication of

[41] a) R. G. Nuzzo, D. L. Allara, J. Am. Chem. Soc. 1983, 105, 4481. b) C. D. Bain, J. Evall, G. M. Whitesides, J. Am. Chem. Soc. 1989, 111, 7155.

interfaces with a well-defined composition and structure. More complex systems can be constructed by coadsorbing several thiols with different terminal functional groups or different chain length. The ability to control interfacial processes has important implications from the point of view of both fundamental and technological advances.[42]

To form an alkanethiol monolayer, a clean copper substrate, freed from organic impurities, is simply immersed into a dilute ($\sim 10^{-3}$ M) solution of the thiol molecule in an organic solvent at room temperature. The immersion time varies from a few minutes to several hours, or even days, depending on the system (for experimental procedures see Chapter 4).

Alkanethiols are strongly chemisorbed on the surface by the formation of a covalent-like bond between copper and sulfur atoms following cleavage of a sulfur−hydrogen bond. The reaction of alkanethiole on Cu may be considered formally as an oxidative addition of the SH bond to the surface, followed by a reductive elimination of the hydrogen. When a clean surface is used, the proton probably ends as a H_2 molecule. This can be deduced from the fact that monolayers can be formed from gas phase in the complete absence of oxygen:

$$R – S – H + Cu \rightarrow R – S – Cu + ½\ H_2$$

The combination of hydrogen atoms at the metal surface to yield H_2 molecules may be an important exothermic step in the overall chemisorption energetic.[43]

The fate of the hydrogen of the SH groups still has not been determined unambiguously.[44] It is widely believed that thiol adsorption is accompanied by SH bond scission.[45] It seems probable that adsorption in vacuum leads to loss of the hydrogen in the form of dihydrogen. In solution, another possibility exists. If the thiol hydrogen is not lost in the form of H_2, the presence of oxygen in the reaction medium might also lead to its oxidative conversion to water.

In the case of oxidized copper, the alkanethiols are not adsorbed directly on the $Cu^{2+}O$ surface, but reduce the oxide layer with disulfide formation by the following reaction:

[42] a) A.-S. Duwez, J. Electr. Spectr. Rel. Phenom. 2004, 134, 97. b) F. Schreiber, J. Phys.: Condens. Matter 2004, 16, R881.

[43] A. Ulman, Chem. Rev. 1996, 96, 1533.

[44] a) M. Hasan, D. Bethell, M. Brust, J. Am. Chem. Soc. 2002, 124, 1132. b) C. A. Widrig, C. Chung, M. D. Porter, J. Electroanal. Chem. Interfacial Electrochem. 1991, 310, 335. c) C.-J. Zhong, N. T. Woods, B. G. Dawson, M. D. Porter, Electrochem. Commun. 1999, 1, 17. d) J.-G. Lee, J. Lee, J. T. Jr. Yates, J. Am. Chem. Soc. 2004, 126, 440. e) W. Andreoni, A. Curioni, H. Gronbeck, Int. J. Quantum Chem. 2000, 80, 598.

[45] a) H. O. Finklea, Electrochemistry of organized monolayers of thiols and related molecules on electrods. In Electroanalytical Chemistry; Bard, A. J., Rubinstein, I., Eds.; Marcel Dekker, Inc.: New York, 1996. b) R. K. Smith, P. A. Lewis, P. S. Weiss, Prog. Surf. Sci. 2004, 75, 1.

$$2\ R-S-H + CuO \rightarrow (R-S)_2 + Cu + H_2O$$

or

$$2\ R-S-H + 2\ CuO \rightarrow (R-S)_2 + Cu_2O + H_2O$$

This reaction continues to reduce all the CuO layer, and the monolayer is formed on the reduced surface, by the following reaction:

$$R-S-H + Cu \rightarrow R-S-Cu + \tfrac{1}{2}\ H_2$$

or

$$2\ R-S-H + Cu_2O \rightarrow R-S-Cu + H_2O$$

A great amount of the thiols is changed to disulfides on the CuO surfaces. This surface reaction from thiol to disulfide may reduce the $Cu^{2+}O$ species to $Cu^{1+}{}_2O$ or Cu. On this reduced surface, the alkanethiolate monolayers are formed.

The kinetic behavior during the formation of the film consists of two distinct phases: a very fast step (adsorption of the molecules onto the substrate), which takes a few minutes, and a slower one (organization and structuration), which lasts several hours.

The detailed nature of the interface structures in alkylthiolate SAMs has been largely unknown, there has been a tendency to assume that the metal surface is a passive spectator in self-assembly process. Woodruff et al. recently evidenced that the interaction of the thiols with all metal surfaces leads to major reconstruction of the outermost layer. Copper surface reconstruction is depicted in Figure 2.1.5.

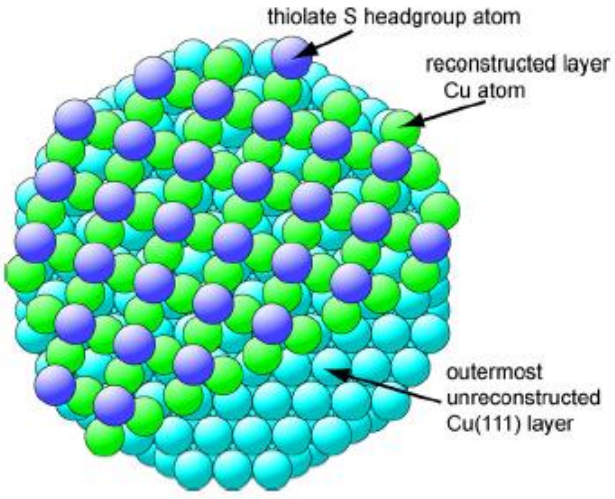

Figure 2.1.5: Schematic diagram of the pseudo-(100) reconstruction of Cu(111). The overlayer has been omitted from the lower right-hand side of the diagram to expose the underlying Cu(111) substrate. Only the S headgroup atoms of the thiolate are shown as the smallest spheres.

Cu(111) fcc substrate reconstructs in a pseudo-(100) surface, in which the S headgroup atoms occupy four-fold coordinated hollow sites within this layer. The reason for this type of reconstruction is that the four-fold coordinated site on a near-square surface structure is energetically favorite than adsorption on the unreconstructed surface, despite the strain energy associated with the interface between the outermost (111) substrate layer and the pseudo-(100) reconstructed layer.[46]

2.2 - Calixarenes in supramolecular chemistry

Among the several classes of synthetic macrocyclic compounds currently used as receptors (hosts) in supramolecular chemistry, the calix[n]arenes[47] have assumed a key role due to their synthetic accessibility and versatility. The name was introduced in 1978 by Gutsche and derives from the type of Greek vase known as *calix crater*. This "crater" or "basket" plays a very important role in shaping the entire architecture of calixarene for its function in host-guest chemistry.

Calix[n]arenes belong to the class of metacyclophanes[48] and are cyclic oligomers having para-alkylphenolic units linked by methylene bridges (Figure 2.2.1).

[46] D. P. Woodruff, App. Surf. Sci. 2007, 254, 76.

[47] a) C. D. Gutsche, Calixarenes, Monographs in Supramolecular Chemistry, Ed.: J. F. Stoddart, Royal Society of Chemistry: Cambridge, U.K., 1989. b) C. D. Gutsche, Calixarenes Revisited, Monographs in Supramolecular Chemistry, Ed.: J. F. Stoddart, Royal Society of Chemistry: Cambridge, U.K., 1998. c) Calixarenes in Action, Eds.: L. Mandolini, R. Ungaro, Imperial College Press: London, 2000. d) Calixarenes 2001, Eds.: Z. Asfari, V. Böhmer, J. Harrowfield, J. Vicens, Kluwer Academic: Dordrecht, 2001. e) C. D. Gutsche, Calixarenes, An Introduction, Monographs in Supramolecular Chemistry, Ed.: J. F. Stoddart, Royal Society of Chemistry: Cambridge, U.K., 2008.

[48] F. Diederich, Cyclophanes, Monographs in Supramolecular Chemistry, Ed.: J. F. Stoddart, Royal Society of Chemistry: Cambridge, U.K., 1991.

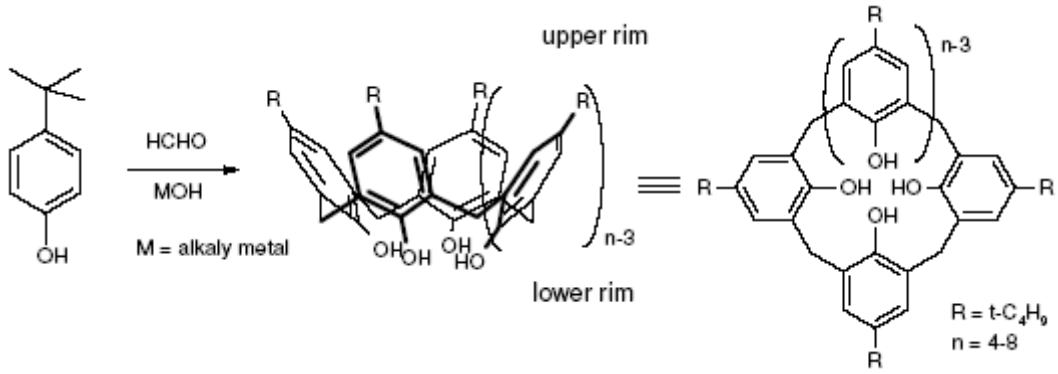

Figure 2.2.1: Synthesis of p-tert-butyl-calix[n]arene compounds (n= 4, 6 and 8).

These compounds are obtained in very high yield through a one-step condensation of formaldehyde with p-tert-butyl phenol in basic conditions. Depending on the reaction conditions (temperature and solvent media) and the nature of the base employed, it is possible to synthesize macrocycles that contain from four to eight phenol units in the ring, even though the most used ones are the calix[4]arenes and calix[6]arenes. The insertion of new functional groups on both rims (upper and lower, see Figure 2.2.1) of the macrocycle can be easily accomplished using common reactions typical of the organic chemistry. For this reason calix[n]arenes can be considered as useful building block for the synthesis of new advanced receptors.[47]

In the current nomenclature, the bracketed number (*i.e.* p-*tert*-butylcalix[4]arene) indicates the number of phenol units present in the macrocycle. The prefix "p-tert-butyl" defines the type of para-alkylated phenol used during the synthesis. The nomenclature devised by the IUPAC for this class of macrocycles is too complicated for an ordinary use (the IUPAC name for p-tert-butyl calix[4]arene is 5,11,17,23-tetakis(1,1-dimethylethyl)pentacyclo[19.3.1.1.1.1]octaosa1(25),3,5,7(28),9,11,13(27),15,17,19(26),21,23-dodecaene-25,26,27,28-tetraol) and led Gutsche to introduce an unofficial but simpler nomenclature nowadays universally accepted. With this nomenclature, the macrocyles are numbered following the schemes gathered in Figure 2.2.2.

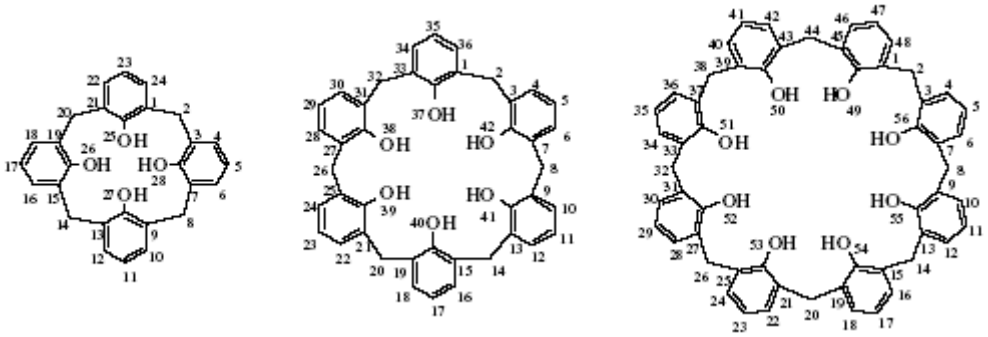

Figure 2.2.2: Conventional nomenclature of calixarenes devised by Gutsche.

Calix[n]arenes are not rigid compounds and if not properly functionalized may adopt several conformations both in solution and in the solid state. These conformations are generated by the free rotation experienced by each aromatic ring with respect to the others. The conformational behaviour of calix[4]arenes has been extensively studied. The most important conformation adopted by these compounds is called *cone* conformation. In this conformation all the phenolic units are oriented in the same direction and a π-rich aromatic cavity is well defined. The four different possible conformations have been named by Gutsche as *cone* (u, u, u, u), *partial cone* (u, u, u, d), 1,3- *alternate* (u, d, u, d) and 1,2-*alternate* (u, u, d, d) (Figure 2.2.3).

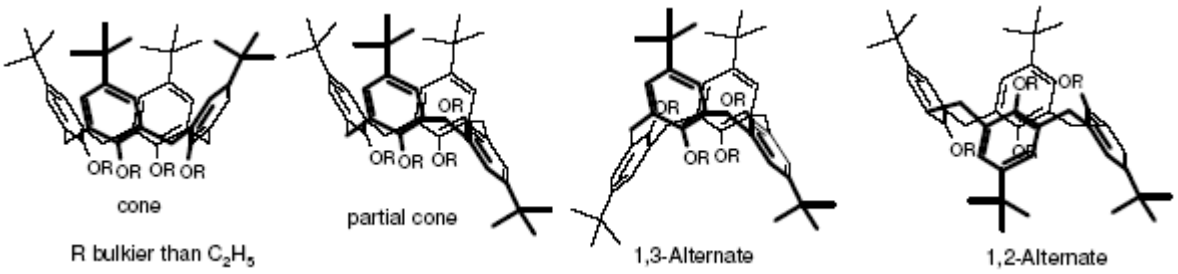

Figure 2.2.3: The four possible conformations of calix[4]arenes.

To make them cavitands it is necessary to fix them in either a cone or a partial cone conformation replacing the hydrogens of the hydroxyl functions with larger groups. In the cone-partial cone equilibrium the cone conformation is stabilized by higher polar solvents.

Historically, calix[n]arenes have played an important role in supramolecular chemistry as receptors for neutral and charged species in solution, in the gas-phase and in the solid state. Several applications of calixarenes as sensors regard their employment as a molecular platform, that is, a scaffold on which few binding sites can be arranged to specifically recognize a guest species. For example, the introduction of ester, amide or ketone functional

groups through the proper functionalization of the lower rim has generated a plethora of efficient and selective receptors for positively charged species spanning from alkaline and alkaline-earth cations to lantanides and actinides.[47c,d] In low polar solvents the organic salts are present as tight ion pairs and the π-rich aromatic cavity of calix[4]arenes and calix[6]arenes can be employed as a soft binding site for the cation by exploiting weak intramolecular interactions called cation/π interactions.[49,50]

2.3 - Rotaxanes as molecular machines

The recent developments of supramolecular chemistry[51] have extended the concept of machines and devices down to the molecular level. A *molecular machine* is defined as *an assembly of a number of molecular components that makes mechanical movements, designed to perform machine-like motions in response to appropriate external stimuli (chemical, photonics, electrochemical etc.).*[52]

Several molecular components have been successfully used to devise molecular machines. Among them, those belonging to the classes of *rotaxanes* and *pseudorotaxanes* seem to offer a wider potentiality.[53] A rotaxane is a mechanically-interlocked molecular architecture

[49] a) D. E. Gross, F. P. Schmidtchen, W. Antonius, P. A. Gale, V. M. Lynch, J. L. Sessler, Chem. Eur. J. 2008, 14, 7822. b) M. Hamon, M. Menand, S. Le Gac, M. Luhmer, V. Dalla, I. Jabin, J. Org. Chem. 2008, 73, 7067. c) M. D. Lankshear, I. M. Dudley, K. M. Chan, A. R. Cowley, S. M. Santos, V. Felix, P. D. Beer, Chem. Eur. J. 2008, 14, 2248. d) S. Le Gac, I. Jabin, Chem. Eur. J. 2008, 14, 548. e) M. D. Lankshear, N. H. Evans, S. R. Bayly, P. D. Beer, Chem. Eur. J. 2007, 13, 3861. f) M. Cametti, M. Nissinen, A. Dalla Cort, L. Mandolini, K. Rissanen, J. Am. Chem. Soc. 2007, 129, 3641. g) N. Zacarias, D. A. Dougherty, Trends Pharmacol. Sci. 2002, 23, 281. h) J. P. Gallivan, D. A. Dougherty, Proc. Natl. Acad. Sci. U.S.A., 1999, 96, 9459. i) J. C. Ma, D. A. Dougherty, Chem. Rev. 1997, 97, 1303.

[50] Luca Pescatori, Synthesis and Properties of Calix[n]arene receptors for the preparation of "active" organic-inorganic hybrid materials, PhD thesis, Parma 2010.

[51] J. W. Steed, D. R. Turner, K. J. Wallace, Core Concepts in Supramolecular Chemistry and Nanochemistry, John Wiley & Sons, Chichester, 2007.

[52] V. Balzani, A. Credi, M. Venturi, Molecular devices and machines - A journey into the nanoworld, Wiley-VCH, Germany, 2003.

[53] a) P. R. Ashton, I. Baxter, M. C. T. Fyles, F. M. Raymo, J. F. Stoddart, A. J. P. White, D. J. Williams, J. Am. Chem. Soc. 1988, 120, 2297. b) M. Asakawa, P. R. Ashton. R. Ballardini, V. Balzani, M. Belohradsky, M. T. Gandolfi, O. Kocian, L. Prodi, F. M. Raymo, J. F. Stoddart, M. Venturi, J. Am. Chem. Soc. 1997, 119, 302. c) F.

consisting of a dumbbell-shaped axle that is threaded through a macrocycle or a ring-like component (Figure 2.3.1).

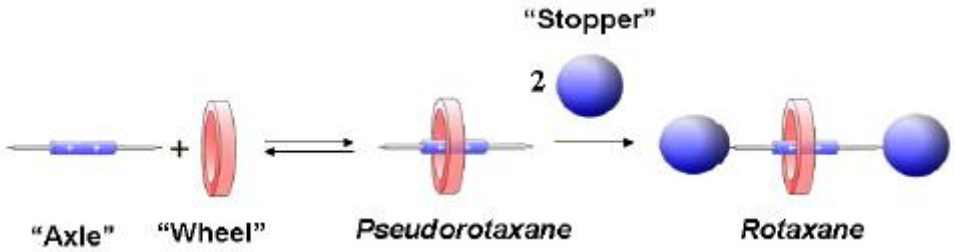

Figure 2.3.1: Schematic representation of pseudorotaxane and rotaxane.

The name is derived from the Latin for wheel (*rota*) and axle (*axis*). The two end-groups of the dumbbell (the stoppers) are larger than the internal diameter of the ring, thus preventing the dethreading of the components since this would require significant distortion or cleavage of covalent bonds. When the axle bears only one or no stopper, the system is termed pseudorotaxane.[52]

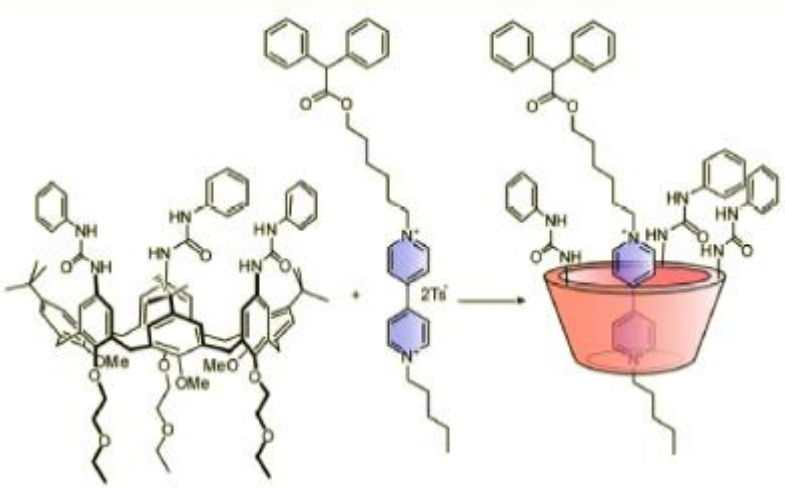

Figure 2.3.2: Formation of pseudorotaxanes form triphenylureido calix[6]arene-based wheel and monostoppered viologen-based axle.

Different rings and axles can be employed to form a rotaxane. In the recent years the research group of Prof. Pochini (University of Parma) has extensively used a triphenylureido

M. Raymo, J. F. Stoddart, Chem. Rev. 1999, 99, 1643. d) J.-P. Sauvage, C. O. Dietrich-Buchecker, Molecular Catenanes, Rotaxanes and Knots, Wiley-VCH, Weinheim, 1999.

calix[6]arene derivative as a wheel for the synthesis of rotaxanes and pseudorotaxanes[54] (Figure 2.3.2) with axles based on derivatives of 4,4'-bipyridinium salt (viologens).

Calix[6]arene derivatives such as the one depicted in Figure 2.3.2 have, as important peculiarity, a truncated cone structure where an axle could, in principle, enter form the narrower or wider side, giving rise to oriented pseudorotaxanes or rotaxanes characterized by the univocal orientation of the wheel side with respect to the two termini of the axial component. It is possible to govern the threading process from the macrocycle upper rim using monostoppered asymmetrical axle to yield oriented pseudorotaxanes and rotaxanes.[53b] In low polar media the access of the axle into the cavity from the lower rim is prevented for sterical reasons by the inward orientation of the three methoxy groups present on the rim, but the access of the axle from the upper rim is favoured by the presence of three hydrogen bond donor ureido groups that are able to separate the ion-pair, thus pivoting the entrance of the bipyridinium axle into the cavity. The access to the cavity can be also controlled varying the polarity of the media where the threading process is carried out. In more polar media like acetonitrile, the threading process occurs also from the lower rim and it is thus possible to obtained almost equimolar mixture of the two different oriented pseudorotaxanes that can than be converted after the stopping reaction in the respectively mixture of the two oriented rotaxanes.[55]

These pseudorotaxanes are capable of complexing the counteranions[56] of the bipyridinium guest through hydrogen-bonding interactions with the NH ureido groups. Such an anion complexation has been clearly evidenced by X-ray crystallography in the solid state[53c] and by ^{1}H-NMR spectroscopy in solution[53b] for the pseudorotaxane. It can be expected that the counteranions of the dicationic guest play an important role in the formation of the pseudorotaxane, from both a thermodynamic and a kinetic viewpoint, for the following reasons: (i) in the apolar solvents employed for the self-assembly process, the bipyridinium species can form tight ion pairs with their anions, and (ii) the size and binding properties of the wheel cavity are suitable for the inclusion of only the dicationic portion of the axle. Therefore, it is reasonable to assume that separation of the dicationic thread from its

[54] a) A. Credi, S. Dumas, S. Silvi, M. Venturi, A. Arduini, A. Pochini, A. Secchi, J. Org. Chem. 2004, 69, 5881. b) A. Arduini, F. Calzavacca, A. Pochini, A. Secchi, Chem. Eur. J. 2003, 9, 793. c) A. Arduini, R. Ferdani, A. Pochini, A. Secchi, F. Ugozzoli, Angew. Chem. Int. Ed. 2000, 39, 3453.

[55] A. Arduini, F. Ciesa, M. Fragassi, A. Pochini, A. Secchi, Angew. Chem. Int. Ed. 2005, 44, 278.

[56] a) T. S. Snowden, E. V. Anslyn, Curr. Opin. Chem. Biol. 1999, 3, 740. b) P. D. Beer, P. A. Gale, Angew. Chem. Int. Ed. 2001, 40, 486. c) V. Amendola, L. Fabbrizzi, C. Mangano, P. Pallavicini, A. Poggi, A. Taglietti, Coord. Chem. Rev. 2001, 219, 821.

counteranions has to take place before insertion into the cavity of the calixarene wheel. The simultaneous recognition of cations and anions[57] is crucial to achieve an efficient threading process in low-polarity solvents[58] and can provide an additional means for controlling self-assembly.[50,59]

2.4 - Gold nanoparticles

Monolayer Protected Clusters (MPCs),[22,28] also known as 3D Self-Assembled Monolayers (3D-SAMs), represent an emerging class of organic–inorganic hybrid materials. Differently from colloids, MPCs are constituted by a discrete aggregate of metal atoms (called inorganic core) stabilized by a shell of organic molecules (arranged like a monolayer around the metal surface), that maintain them stable in solution and prevent aggregation phenomena (Figure 2.4.1).

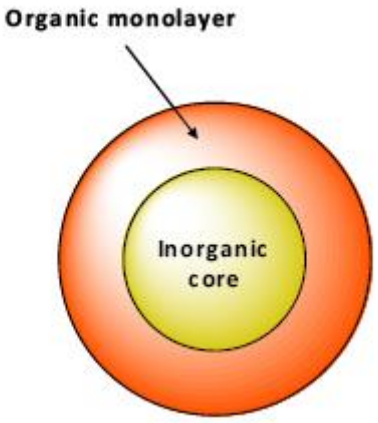

Figure 2.4.1: Schematic representation of a monolayer protected cluster (MPC).

[57] a) P. A. Gale, Coord. Chem. Rev. 2003, 240, 191. b) Jones, J. W.; Zakharov, L. N.; Rheingold, A. L.; Gibson, H. W. J. Am. Chem. Soc. 2002, 124, 13378. c) A. P. de Silva, G. D. McClean, S. Pagliari, Chem. Commun. 2003, 2010. d) Tobey, S. L.; Anslyn, E. V. J. Am. Chem. Soc. 2003, 125, 10963.

[58] a) J. A. Wisner, P. D. Beer, N. G. Berry, B. Tomapatanaget, Proc. Natl. Acad. Sci. U.S.A. 2002, 99, 4983. b) J. W. Jones, H. W. Gibson, H. W., J. Am. Chem. Soc. 2003, 125, 7001.

[59] M. Montalti, L. Prodi, Chem. Commun. 1998, 1461.

Among the plethora of MPCs synthesized so far, those characterized by a core of gold atoms (AuMPCs) and stabilized with a layer of thiolated ligands have attracted the largest interest of the scientific community because of their facile preparation, stability, and solubility in both aprotic and protic solvents.[28]

A very attractive topological property of MPCs is the possibility to anchor onto the metallic core a discrete number of suitable receptors in a radial tri-dimensional arrangement.[14] AuMPCs stabilized with thiolated calix[4]arene derivatives can be successfully employed as multivalent hosts for the recognition of organic salts both in organic[60] and aqueous media,[61] when the calix[4]arene aromatic cavities, which represent potential recognition units, are exposed to the bulk and not toward the surface (Figure 2.4.2).

Another aspect of potentially great importance is associated with quantum size effects arising from the confinement of electrons in very small nanoclusters (< 1 nm).

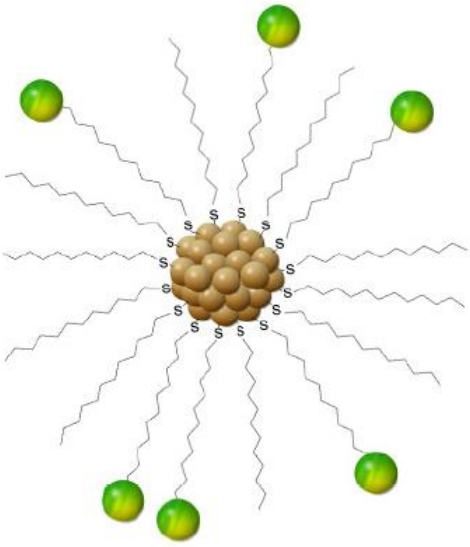

Figure 2.4.2: AuMPCs stabilized with thiolated ligands.

The important role assumed nowadays by AuMPCs is, however, strictly derived from the more ancient studies on gold colloids. The first study dates back to 1857, when Faraday reported on the formation of deep red solutions of colloidal gold by reduction of an aqueous solution of chloroaurate ($AuCl_4^-$) using phosphorus in CS.[28,62] The reduction of $HAuCl_4$ with

[60] A. Arduini, D. Demuru, A. Pochini, A. Secchi, Chem. Commun. 2005, 645-647.

[61] T. R. Tshikhudo, D. Demuru, Z. X. Wang, M. Brust, A. Secchi, A. Arduini, A. Pochini, Angew. Chem. Int. Ed. 2005, 44, 2913-2916.

[62] M. Faraday, Philos. Trans. 1857, 147, 145.

sodium citrate has been for the long time the most used method to prepare water soluble nanoparticles. The first versatile and reproducible method for the synthesis of lipophilic AuMPCs was reported by Brust and Schiffrin in 1994.[63]

This method allowed for the synthesis of gold nanoparticles (ranging in diameter between 1.5 and 5 nm) stabilized with n-dodecanthiol chains, which were thermally and air-stable. The AuMPC prepared with this method could be repeatedly isolated and redissolved in most organic solvents without irreversible aggregation or decomposition. This new materials could be easily handled and functionalized just as stable organic and molecular compounds. The method is inspired by the Faraday's two-phase system[61] and it employs thiolated ligands as stabilizers of the gold surface due to the soft Lewis character of both Au and S.

$AuCl_4^-$ (aq) + $N(C_8H_{17})_4$ + (org) → $N(C_8H_{17})_4$ + $AuCl_4^-$ (org),

$AuCl_4^-$ (org) + $nC_{12}H_{25}SH$ (org) + 3m e^- → 4m Cl^- (aq) + $[Au_m(C_{12}H_{25}SH)_n]$ (org).

The aurate $AuCl_4^-$ is initially transferred to the toluene phase using tetraoctylammonium bromide as phase-transfer catalyst and reduced in situ by $NaBH_4$, previously dissolved in water, in the presence of dodecanethiol. During this step the organic phase changes its colour from orange to deep brown within a few seconds upon addition of $NaBH_4$.

Murray et al. have later shown that large thiol/gold molar ratios give smaller average core sizes.[64] Following this author, indeed, the MPC synthesis reaction in the organic phase (toluene) is a two-step process here summarized:

$AuCl_4^-$ (toluene) + RSH →$(-Au^ISR-)_n$ (polymer),

$(-Au^ISR-)_n + BH_4^- \rightarrow Au_x(SR)_y$.

In the first step, the aurate is reduced to Au^I by the thiols and inserted in a polymeric structure where the Au^I species are coordinated by two sulphur groups. During the second step, this polymeric structure is reduced by the hydride with the formation of the nanocluster. The two steps are consistent with a "nucleation–growth–passivation process" and large thiol/gold mole ratios, fast addition of $NaBH_4$ and short reaction times produce AuMPCs characterized by very small core sizes (< 2 nm). The same authors have shown that a high

[63] M. Brust, M. Walker, D. Bethell, D. J. Schiffrin, R, Whyman, J. Chem. Soc., Chem. Commun. 1994, 801.

[64] a) M. J. Hostetler, J. E. Wingate, C.-J. Zhong, J. E. Harris, R. W. Vachet, M. R. Clark, J. D. Londono, S. J. Green, J. J. Stokes, G. D. Wignall, G. L. Glish, M. D. Porter, N. D. Evans, R. W. Murray, Langmuir 1998, 14, 17. b) W. P. Wuelfing, A. C. Templeton, J. F. Hicks, R. W. Murray, Anal. Chem. 1999, 71, 4069. c) W. Chen, A. C. Templeton, R. W. Murray, Langmuir 2000, 16, 3543.

abundance of very small clusters is obtained also using bulky ligands.[65] A series of monolayer-protected clusters gold (MPCs) stabilized by monodentate and multidentate thiolated calix[n]arene derivatives was prepared by using the Brust-Schiffrin synthesis and characterized with transmission electron microscopy (TEM) and X-ray Photoelectron Spectroscopy (XPS).[50]

[65] S. Chen, R. W. Murray, Langmuir 1999, 15, 682.

Chapter 3

Experimental methods

3.1 – X-ray Photoemission Spectroscopy

Photoemission spectroscopy was first developed by the Nobel Prize in Physics Kai Siegbahn, starting in 1957. When a material is irradiated by a source of sufficient energy, the emission of electrons is observed, with a kinetic (KE) energy determined by the Einstein relation:

$$KE = hv - BE, \qquad (3.1)$$

where hv is the photon energy and BE the characteristic binding energy.

In case of UV irradiation, only valence electrons can be ejected (UPS, Ultraviolet Photoelectron Spectroscopy), but to ionize more tightly bound (or "core") electrons X-rays are required (XPS, X-ray Photoelectron Spectroscopy). The structures observed in a photoemission spectrum relates to the ionized state. According to the Koopmans rule: $IE = -\varepsilon_k$, where the ionization energy IE (*i.e* the energy difference between the final and the initial state) can be identified with the negative orbital energy $-\varepsilon_k$, neglecting orbital relaxation (the "final state effect") and relativistic effects. The photoemission process is extremely rapid (10^{-16} s).

The variations observed in the binding energy provide chemical information, since they are associated with bonds between atoms. This change is called "chemical shifts".

Photoemission technique is sensitive to the outermost 10 nm of a surface: while photons typically penetrate the solid for hundreds of Å, obviously depending on the material type and photon wavelength, the thickness of the surface layer investigated by XPS is given

by λcosθ, where θ is the angle between the surface normal and the analyzer (polar angle or *take-off angle*), as depicted in Figure 3.1.1.

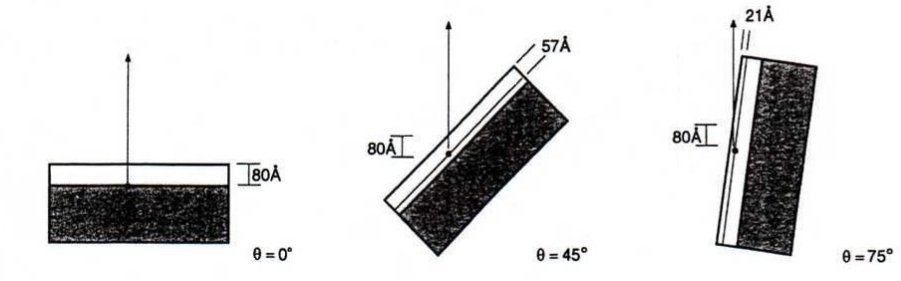

Figure 3.1.1: Different thickness surface layers at varying the take-off angle.

The value of λ (IMFP, Inelastic Mean Free Path) is limited by electron-electron scattering, *i.e.*, the excitation of collective modes (plasmons), and by recombination processes (Auger), while the electrons escape into vacuum from the solid. Thus, a fraction of photoelectrons (primary electrons) escapes into vacuum without suffering scattering and energy losses, while a large part of photoexcited electrons (secondary electrons) scatter and suffer various energy losses. The escape depth of electrons depends on their kinetic energy. There is a decrease in λ with a rather flat minimum in the 50-500 eV range, and finally a progressive increase beyond about 1000 eV ($\lambda = aE^{-2} + bE^{0.5}$).

There are analytical functions derived for different materials, as shown in Figure 3.1.2. Seah and Dench[66] in their analysis of attenuation lengths provide a set of relations for different classes of materials over the energy range 1 eV-6 keV. These relations can be written as

$$\lambda = aE^{-2} + bE^{0.5} \qquad (3.2)$$

where a and b are constant factors depending on the type of material (elements, inorganic compounds, organic compounds).

The photoelectron spectrum provides qualitative and quantitative information on all the elements present in the investigated sample.

[66] M. P. Seah, W. A. Dench, Surf. Interface Anal. 1979, 1, 2.

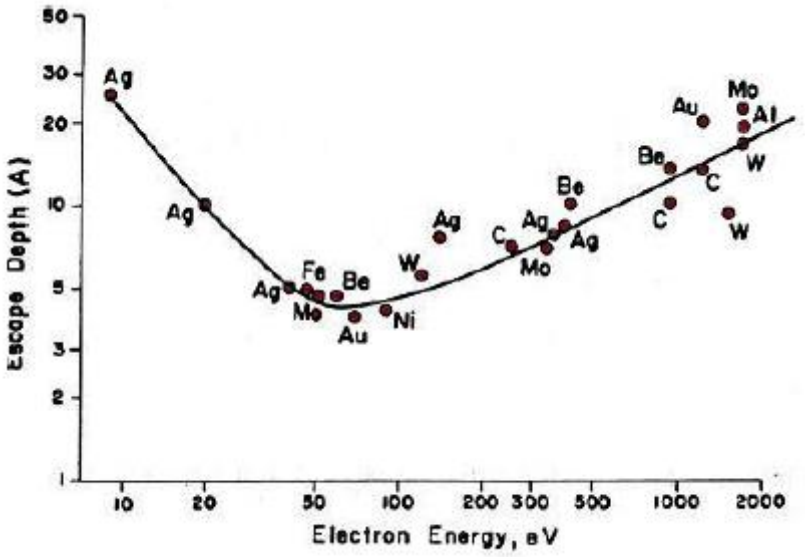

Figure 3.1.2: Inelastic mean free path in a solid, as a function of electron energy.

The intensity of transition due to ionization of level *x* of a sample is:

$$I_x = I(hv)\, N_i\, \sigma_{n,l}(hv)\, \lambda_s(E_k)\, F(E_k,E_a)\, T(E_k,E_a)\, D(E)\, G, \qquad (3.3)$$

where I(hv) is the flux of incident photons with energy hv, N_i is the atomic density of the *i* species, $\sigma_{n,l}$ is the ionization cross-section for the level *n,l*, λ is the IMFP for electrons with kinetic energy E_k, $F(E_k,E_a)$, $T(E_k,E_a)$, D(E) and G are factors depending from the experimental configuration and spectrometer. E_a and E are characteristic energies for the spectrometer. Typically, relative atomic ratios are determined, not the absolute values.[67]

Surface coverage on Copper - Surface coverage on Cu substrate has been estimated by making use of the model for quantitative interpretation of XPS data.[68]

The intensity I_{Cu} from a solid support covered by an overlayer of thickness t:

$$I_{Cu} = R(\theta)_{Cu}\, \rho_{Cu}\, X_{Cu}\, \Lambda_{Cu}^{S}\, \exp[-t / \Lambda^{\circ}_{Cu} \sin\theta] \qquad (3.4)$$

Intensity I_S from a monolayer of atoms covered by an overlayer of thickness t:

$$I_S = R(\theta)_S\, r\sigma_S\, X_S \exp[-t / \Lambda^{\circ}_S \sin\theta] / \sin\theta \qquad (3.5)$$

In the above expressions, $R(\theta)_k$ is the instrument response function at take-off angle θ, F_k is the number density of atoms that emit into line k, σ_k is the surface density of emitting atoms (atoms/area), r is a roughness factor. The product $r\sigma_k$ represents the effective surface density of atoms as seen by the instrument's analyzer. X_k is the photoionization cross section, Λ_{Cu}^{S},

[67] D. Briggs, M. P. Seah, Practical Surface Analysis, vol. 1, 2nd ed., J. Wiley & Sons, Chichester, 1990.

[68] R. Levicky, A. Johnson, Langmuir 2004, 20, 9621.

Λ^{O}_{Cu} and Λ^{O}_{S} are Inelastic Mean Free Paths (IMFPs) for photoelectrons in the solid support and overlayer, respectively, and t is the overlayer thickness. The electron IMFP values for the compounds investigated are absent in the literature, thus we calculated it according to the eq. 3.2. SAM $r\sigma_S$ values were obtained from experimental I_{S2p}/I_{Cu2p} ratios, using eq. (3.5) divided by eq. (3.4).

Surface coverage on Silicon - The coverage ratio Φ related to the molecular moiety has been calculated according to the following equation:[69]

$$\Phi = (I_{ml} / \sigma_{ml})* (\sigma_{Si2p} / I_{Si2p}) *(AF_{ml} / IF_{Si(100)}), \qquad (3.6)$$

where I_{ml} and I_{Si2p} are measured intensities (areas) of XPS peaks of a characteristic atom of the organic monolayer and of the Si 2p region, respectively. σ_{ml} and σ_{Si2p} are their corresponding cross-section values or their relative sensitivity factors (RSF). The parameter AF_{ml} is the attenuation factor of the intensity of the photoelectrons emitted from the monolayer due to the monolayer itself, and is given by:

$$AF_{ml} = \exp[(-d_{ml}/ \lambda_{ml} \cos\theta)], \qquad (3.7)$$

where d_{ml} is the thickness of the molecular monolayer and λ_{ml} is the IMFP of electrons emitted from the monolayer passing through the monolayer itself. The electron IMFP values for the compounds investigated are absent in the literature, thus we have calculated it according to the eq. 3.2. The parameter $IF_{Si(100)}$ is the intensity ratio which takes into account the attenuation of electrons emitted from Si both due to the monolayer and to the Si itself. It is given by:

$$IF_{Si(100)} = 1 - \exp[(-d_{Si(100)}/ \lambda_{Si} \cos\theta)], \qquad (3.8)$$

where $d_{Si(100)}$ is the thickness of the first monolayer of the oriented Si(100) surface, that is 0.136 nm,[70] while λ_{Si} is the IMFP of Si 2p electrons through Si, that is 2.5 nm for Al kα monochromated X-ray source. Due to the approximation in the λ_{ml} and d_{ml} values the eq. 3.6 is affected by a large error. Hence, Φ values are only indicative and they should not be read as "absolute" values but used only for comparisons.

X-ray photoelectron spectroscopy results have been obtained on an experimental apparatus in UHV consisting of a modified Omicron NanoTechnology MXPS system with an

[69] Y. Liu, S. Yamahazi, S. Yamabe, Y. Nakato, J. Mater. Chem. 2005, 15, 4906.

[70] F. J. Himpsel, F. R. McFeely, A. Taleb-Ibrahimi, J. A. Yarmoff, Phys. Rev. B 1988, 38, 6084.

XPS chamber equipped with a monochromatic X-ray source (Omicron XM-1000) and an Omicron EA-127 energy analyzer. Samples were transferred between the various experimental areas by means of linear magnetic transfer rods or manipulators. X-ray sources employed were Al Kα (1486.6 eV) and its monochromatic emission (1487.7 eV) and Mg Kα (1253.6 eV), emitted by aluminum or magnesium target, generated operating the anode at 14-15 kV, 10-20 mA. All measurements have been conducted in the least possible time after sample preparation. Samples were transferred to the XPS facility in Schlenk tubes under vacuum, and introduced in the XPS chamber. No sizable sign of sample degradation after extended acquisition times under the X-rays was observed for the samples. XPS atomic ratios for the functionalized hybrids have been estimated from experimentally determined area ratios of the relevant core lines, corrected for the corresponding theoretical atomic cross-sections and for a square-root dependence of the photoelectrons kinetic energies. The effects on quantitative analysis possibly due to photoelectron diffraction at preferential directions of electron collection were minimized by mounting the sample always with the same orientation with respect to the analyzer axis. The sampling depth has been varied by collecting spectra at 11° (sampling depth 2.37 nm) and 81° (1.17 nm) with respect to the sample surface normal.

3.1.1 - XPS of small nanoparticles

Photoemission from non-conducting solids, as small nanoparticles passivated by an organic layer, is affected by charging. This charging effect leads to a general shifting of the spectrum on the energy scale, leading to difficulties in interpreting chemical states. In case of static charging the overall spectrum is rigidly shifted. A differential charging in different regions may cause a broadening or a splitting of peaks. The first situation is easy to control: photoemission leaves a positive static charge potential (C) on the non-conducting sample, so the apparent binding energy BE' is related to the true binding energy BE by the relationship BE=BE'- C.[67]

Although static charging can significantly shift the binding energy of the photoelectron peaks, it does not necessarily preclude the determination of the true binding energy, provided that the value of C can be established from a calibration peak. We used C 1s of the organic mojety referenced at 285 eV (see Chapter 5).

For nanoparticles of dimension < 10 nm a shift towards a higher binding energy and a broadening of FWHM are observed with decreasing particle size.[71] A small metal particle exhibits a positive core-level binding energy with respect to the bulk material. The origin of this effect has been debated.[72] Most widely accepted is the interpretation by Wertheim et al,[73] in which the final state Coulomb charge is responsible for the shift. In more detail, in order to screen the core hole created by the photoemission process, conduction electrons are pulled towards the hole. This will produce a charge of +e on the surface of the cluster. If this charge is not neutralized by the substrate within the core-hole lifetime (10^{-15} s), the binding energy of the entire spectrum is raised by an amount of $e^2/2r$, with r the cluster radius. For large particles the screening is very effective. Only at the smallest diameters of the particles, the screening efficiency should decrease to the limit of no-conduction electron.

3.2 – Atomic Force Microscopy

Atomic Force Microscopy (AFM) or Scanning Force Microscopy (SFM) is a very high-resolution type of scanning probe microscopy. The AFM utilizes a sharp probe moving over the surface of a sample in a raster scan, which bends in response to the force between the tip and the sample. Since the tip obeys Hooke's law for small displacements, the interaction force between the tip and the sample can be found. The movement of the tip or sample is performed by an extremely precise positioning device made from piezoelectric ceramics.

The three main classes of interaction are *contact mode*, *tapping mode* and *non-contact mode*. As the name suggests, in the contact mode the tip and sample remain in close contact as the scanning proceeds. When operated in tapping mode the cantilever is oscillated at its resonant frequency and positioned above the surface so that it only taps the surface for a very small fraction of its oscillation period. This is still contact with the sample in the sense defined earlier, but the very short time over which this contact occurs means that lateral forces are dramatically reduced as the tip scans over the surface. In non-contact method the

[71] D. van der Putten, R. Zanoni, C. Coluzza, G, Schmid, J. Chem. Soc. Dalton Trans. 1996, 1721.

[72] D. van der Putten, R. Zanoni, J. Electr. Spectr. Rel. Phenom. 1995, 76, 741 and references therein.

[73] G. K. Wherteim, S. B. DiCenzo, D. N. E. Buchanan, Phys. Rev. 1986, 33,5384.

cantilever must be oscillated above the surface of the sample at such a distance that it is no longer in the repulsive regime of the inter-molecular force curve.

A needle-sensor atomic force microscope (VT-AFM, Omicron NanoTechnology) was used, which is attached to a UHV chamber where XPS measurements were also run. The silicon nitride microfabricated tip had a nominal curvature radius < 10 nm and a resonance frequency of 997,500 kHz. The values of average z-height and root mean square (rms) roughness (defined as the standard deviation from the average z-height values), were determined by Scala Pro software (Omicron NanoTechnology).

3.3 - Electrochemical measurements

In this thesis, electrochemistry has been applied mainly for the determination of reduction potentials by means of cyclic voltammetry.

Cyclic voltammetry (cv) is a type of potentiodynamic electrochemical measurement.

In a three-electrode cell, the controlling electronic is designed to adjust the potential between the reference and the working electrodes, but the big impedance between these two electrodes forces the resulting current to flow through the counter electrode. During a cyclic voltammetry experiment, the potential is scanned back and forth linearly with time between two extreme values (V_1 and V_2), the switching potentials. When the potential of the working electrode is more positive than that of the redox couple, the corresponding species may be oxidized and produce an *anodic* current (i_a). Similarly, if the redox couple is reversible, on the return scan, as the working electrode potential becomes more negative than the reduction potential of the redox couple, the reduction may occur to produce a *cathodic* current (i_c). As a result, information about the redox potential and electrochemical reaction rates of the compounds can be obtained.

A typical cyclic voltammogram recorded for a reversible single electrode transfer reaction is shown in Figure 3.1.1.

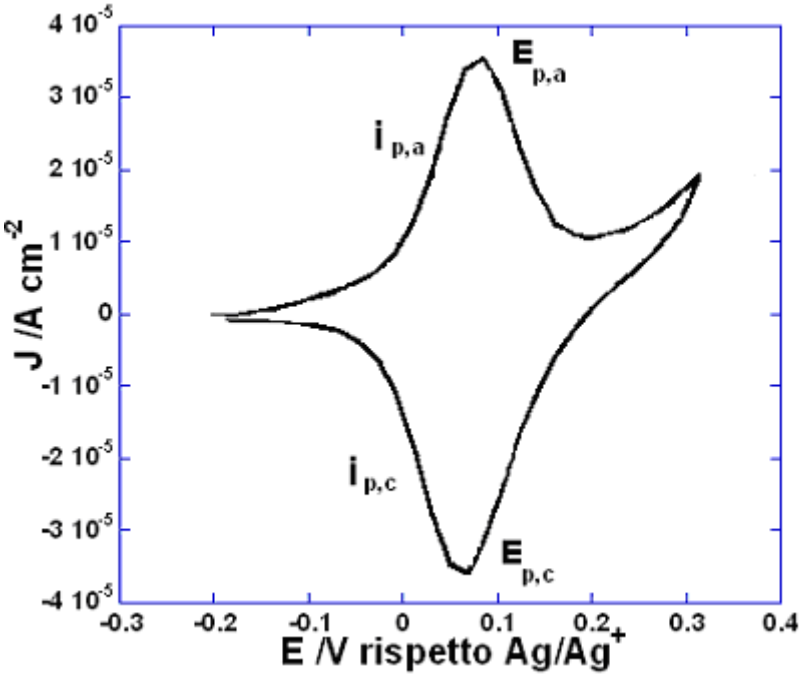

Figure 3.3.1: Current as a function of voltage in a typical CV.

Reversible couples will display a ratio of the peak currents passed at reduction ($i_{p,c}$) and oxidation ($i_{p,a}$) that is near unity ($1 = i_{p,a}/i_{p,c}$). When such reversible peaks are observed thermodynamic information in the form of half cell potential $E°_{1/2}$ can be determined from the reduction ($E_{p,c}$) and oxidation peak ($E_{p,a}$): $E°_{1/2} = (E_{p,c} + E_{p,a})/2$.

All electrochemical measurements were performed with a three-electrode cell using an Autolab Electrochemical Analyzer (model PGSTAT 12, Eco Chemie BV, The Netherlands). The counter electrode was a platinum coil wire, and a silver wire immersed in 0.01 M $AgNO_3$/0.1 M TBAP in CH_3CN, separated from the main solution by a porous fritted glass + agar plug, served as a reference electrode. All potentials reported will be henceforth referred to this reference.

Chapter 4
Production and characterization of organic-inorganic hybrids based on calixarene derivatives on copper

The following are the first reported examples of calixarene-based hybrids on Cu. SAMs of calixarene and rotaxane derivatives have been produced in solution and characterized by means of XPS and electrochemistry.

4.1 - Adsorption of thiols on copper

The preliminary step of cleaning the polycrystalline copper plates (Cu 99.99%) (18x15x1 mm^3) was performed through this recipe:

i. 15 min sonication in acetone, to eliminate organic contaminants;

ii. 30 sec immersion in HNO_3 (32.5%), to oxidize the surface and remove adsorbed species;

iii. 2x5 sec rinsing in distilled water;

iv. 30 min immersion in HCl (3.7%), to dissolve oxides;

v. 3 min 30 sec rinsing in distilled water;

vi. 30 sec rinsing in acetone.

Successively, a weighted amount of the selected calixarene or rotaxane was dissolved in toluene. We used a 0.2 mM solution for calixarenes, 0.4 mM for rotaxane, in order to maintain the same concentration of sulfur.

A Cu plate was dipped in the molecular solution at room temperature for controlled time (typically 4 hours). The functionalized sample was rinsed with toluene for 2x5 min to eliminate physisorbed molecules, and dried under a stream of dry N_2. Concentration and immersion time were optimized in order to obtain a monolayer coverage and to limit physisorption and Cu oxidation at the same time.

As a reference, a Cu plate was covered with undecanethiol (45 mM solution for 17 hr, to form a self-assembled monolayer). A mixed film was prepared by ligand exchange: the Cu substrate functionalized with calix[4]arene was immersed in the undecanethiol solution for 4 hr. XPS analysis was accomplished to evaluate the monolayer composition.

Calix[6]arene wheel and viologen axle were previously assembled in toluene and dichloromethane to form rotaxane. An equimolar quantity of the desired axle was added to a calixarene solution under stirring. In few min the colour of solution changed to orange. The mixture was stirred at room temperature for 30 min and then filtered off to remove the excess of solid axle.

The reactivity of the rotaxane and pseudorotaxane was investigated in toluene and dichloromethane, in order to possibly evidence the influence of a different polarity of the solvent on the threading of the adducts and their assembling on Cu surface. The kinetics of formation of the adducts is favoured in a dichloromethane solution,[54a] but the larger solubility of the charged axle may favour the anchoring of the bare axle directly to the surface.

Calix[4]arene complexation **–** We tested the reactivity on Cu of the anchored calix[4]arene which bring on the upper rim a phenylureido group (Figure 4.1.1) in a series of experiments. The hybrids were obtained after a first cycle of immersion of Cu in a solution of N-methylpyridinium iodide, followed by rinsing in CH_3OH acidified with HCl and by a second immersion of the same Cu plate in the solution of the same salt.

In Figure 4.1.1 calixarenes and rotaxanes anchored on polycrystalline Cu are shown. The introduction of calix[n]arenes on polycrystalline Cu surfaces requires the functionalization of the calixarene macrocycle with appropriate anchoring points. The high

affinity of sulfur for Cu has been largely documented,[74] therefore we chosen calix[n]arene derivatives that are characterized by the presence of two or three ω-thiolated chains on their lower rim (Figure 4.1.1). A monostoppered axle (Figure 4.1.1e) and an unstoppered axle (Figure 4.1.1f) were used for the formation of rotaxane and pseudorotaxanes, respectively, by threading reactions with the calix[6]arene wheel (Figure 4.1.1d). Thanks to the thiol groups present on one ending of the axles, the corresponding rotaxanes can be covalently anchored on the polycrystalline Cu surface.

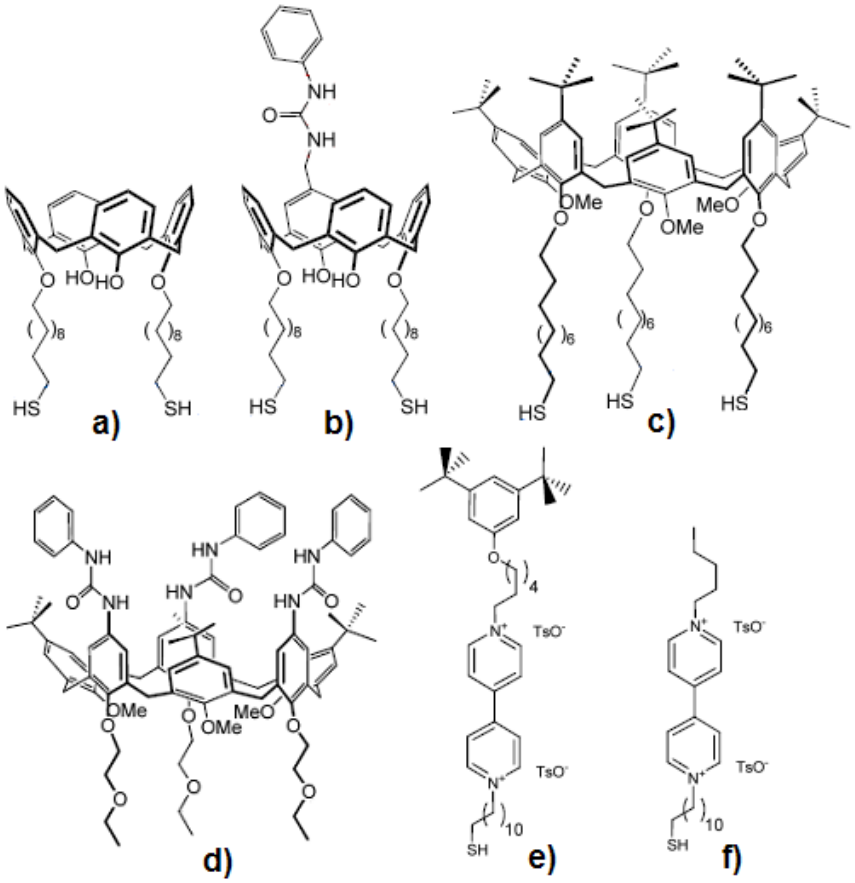

Figure 4.1.1: Calixarene and rotaxane derivatives for the functionalization of polycrystalline Cu surfaces: a) calix[4]arene, b) calix[4]arenePhenylUrea, c) calix[6]arene, d) calix[6]arenePhenylurea, e) N,N′-dialkylviologen (monostoppered axle), f) N,N′-dialkylviologen (not stoppered axle). Rotaxane results from the assembling of d) and e), while pseudorotaxane from d) and f).

[74] H. Sellers, A. Ulman, Y. Shnidman, J. E. Eilers, J. Am. Chem. Soc. 1993, 115, 9389.

4.2 - Results and discussion: XPS investigation

X-ray Photoemission Spectroscopy (XPS) is a well established tool for the characterization of the molecular structure and atomic composition of organic films. XPS survey spectra can be used to-check for the presence of the desired elements in the film and to evaluate its relative atomic composition. Relative atomic ratios have to be interpreted with the help of a quantitative model, since photoelectrons arising from atoms underneath others on the substrate are attenuated by the overlying material.

4.2.1 - Characterization of calix[4,6]arenes on copper

The chemisorption experiments have been systematically conducted on polycrystalline Cu surfaces, which have been preliminarily characterized by XPS. The relevant region of adsorbed calixarenes is S 2p, which is reported in Figure 4.2.1, together with the spectrum of undecanthiol ($C_{11}SH$), which we took as the reference compound for the present investigation, since it is known to form a nearly ideal SAM on Cu.[75]

	S 2p/eV	S-Cu/Cu	σ (nm^{-2})	SH/S-Cu	C/S (theor.)
calix[4]arene	162.7 163.9	0.45	3.1	0.12	28 (25)
calix[6]arene	162.2 163.3	0.47	3.2	0.10	34 (34)
undecanethiol	162.2 163.3	0.51	3.8	0.03	12 (11)
Mixed calix[4]arene + undecanethiol	162.3 163.3	0.49	3.4	0.12	17

Table 4.2.1: XPS peak positions and quantitative ratios (± 10%), and values of the surface coverage (σ) for Cu/calixarene, Cu/$C_{11}SH$ and mixed film.

[75] P. E. Laibinis, G. M. Whitesides, D. L. Allara, Y.-T. Tao, A. N. Parikh, R. G. Nuzzo, J. Am. Chem. Soc. 1991, 113, 7152.

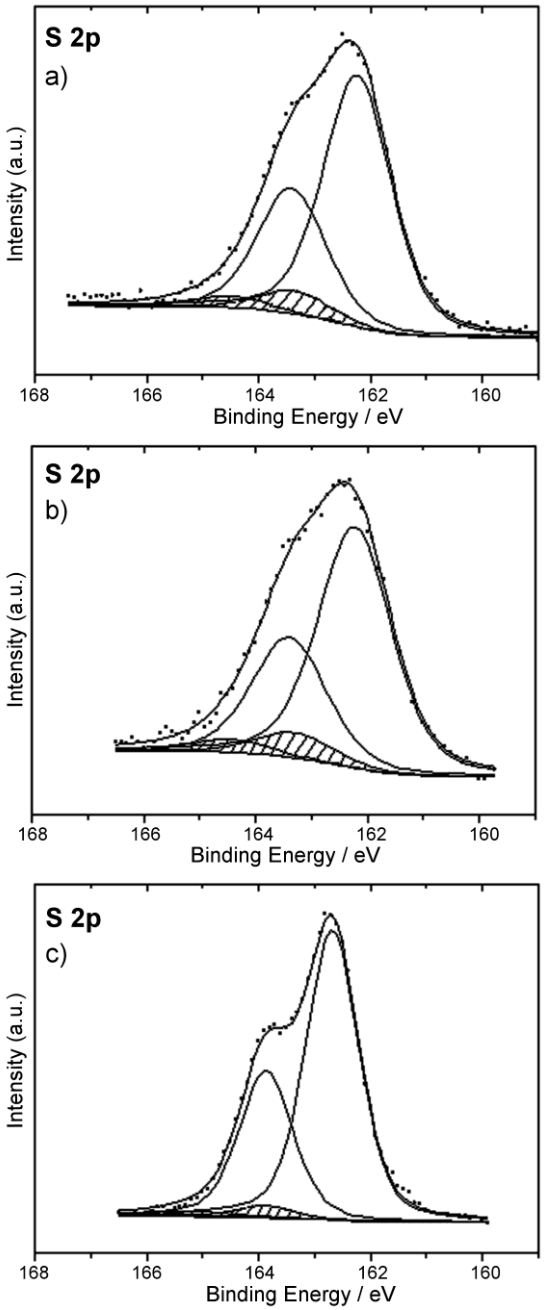

Figure 4.2.1: S 2p XPS spectra taken at 11° from the surface normal of Cu/thiolate ligand. The main spin-orbit split component is due to thiolate. The cross-hatched areas identify the component due to SH. a) calix[4]arene, b) calix[6]arene and c) undecanthiol.

Two S 2p spin-orbit split doublets are always evident, which refer to the formation of thiolate and, at an higher binding energy (BE), to the presence of residual thiol groups. These last could belong to calixarenes chemisorbed via a different thiol group and/or to purely

physisorbed molecules. The relative amount of this component does not exceed ~10% for calixarenes, and it is much smaller in the case of $C_{11}SH$ (3%).

The surface coverage, σ, was estimated by means of a literature model,[68] by making use of the SCu(thiolate)/Cu ratio (Table 4.2.1). The Inelastic Mean Free Paths (IMFPs) were calculated according to Seah and Dench (see Paragraph 3.1).[76] The atomic ratios of calixarenes are, within the experimental error, closely similar to the case of $C_{11}SH$. The coverages fall in the same range, hinting at a close-to-ideal monolayer coverage. These results are consistent with the passivation of Cu surfaces. In fact, only Cu(0) and Cu(I) components are present in the Cu LMM Auger spectra, while a Cu(II) component was never found in the Cu 2p spectrum (Figure 4.2.2).

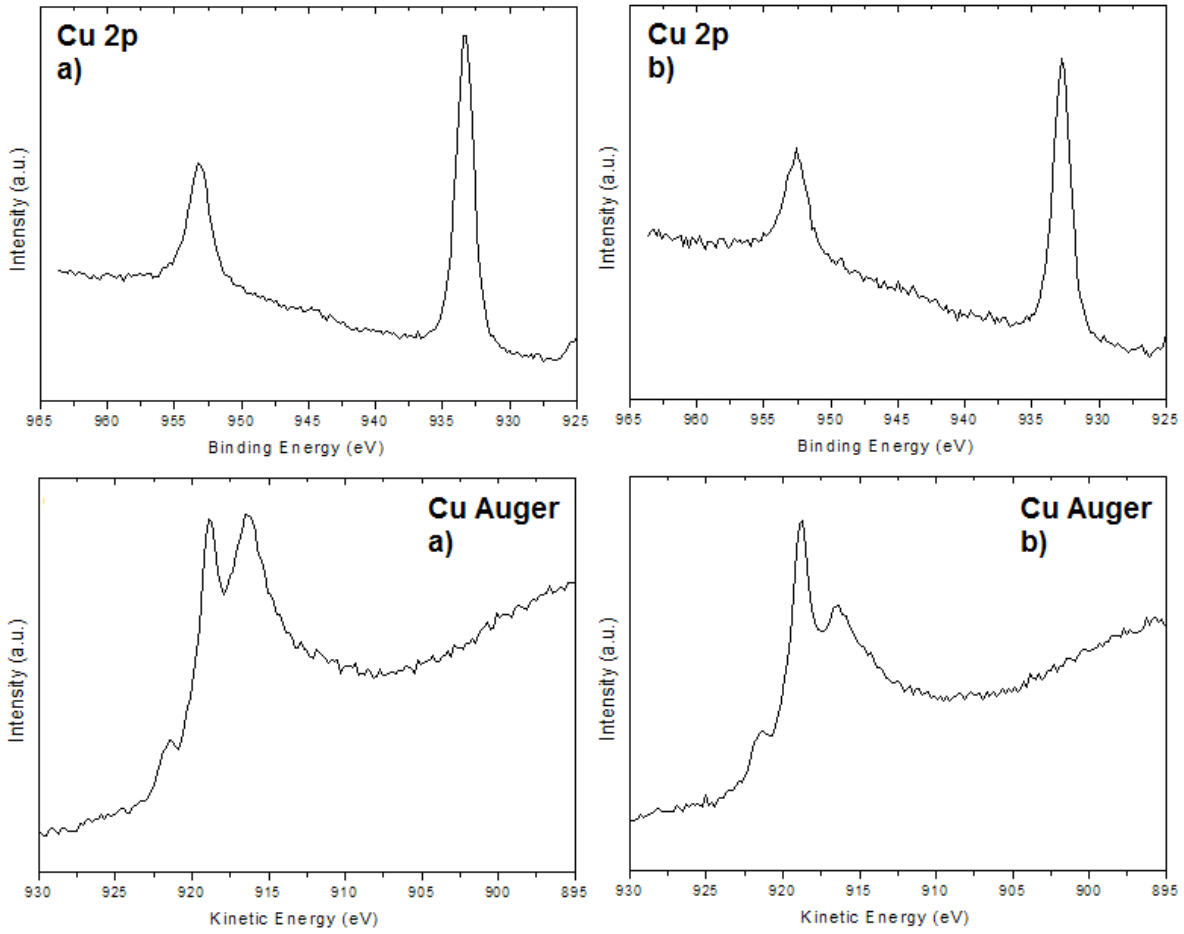

Figure 4.2.2: Cu 2p and Cu LMM Auger lines of Cu/calixarene: a) calix[4]arene and b) calix[6]arene.

[76] M. P. Seah, W. A. Dench, Surf. Interf. Anal. 1979, 1, 2.

A clear indication that molecules adsorb intact on the surface with no added contamination comes from inspection of Table 4.2.1, where a perfect match can be seen between theoretical and experimental C/S ratios. We took this encouraging result as a reference in the study of a mixed monolayer, which was produced in order to demonstrate the feasibility of a double functionalization. Such monolayer was obtained by ligand exchange, starting from a calix[4]arene/Cu surface, which was eventually contacted with $C_{11}SH$. The experimental C/S value is 17, right in between calix[4]arene and $C_{11}SH$, which hints at a 1:1 monolayer on Cu.

4.2.2 - Recognition reactions of N-methylpyridinium ion-pairs towards anchored heteroditopic calix[4]arene receptors

We tested the reactivity of heteroditopic calixarenes anchored on Cu with a series of experiments. To this aim, we selected calix[4]arenePhenylUrea in order to extend to surfaces the solution studies on its reactivity towards N-methylpyridinium and salt.[77] This previous study evidenced how a phenyluerido group in the upper rim of a calixarene macrocycle allows for a combined effect (a cooperative heteroditopic effect) on the recognition reaction of a salt.[78] The combination of a hard H-bond, which can be established by the urea group with an anion, with a soft calix-cation π-bond,[79] through the methyl group of the pyridinium, reduces the ionic interaction in the salt, as testified, *e.g.*, by the fact that N-methylpyridinium chloride (NMPCl), when it acts as a guest, is a ligand-separated ion pair, in the solid state.[79b] By testing a series of NMP salts with different anions, such as tosylate, Cl^-, I^-, trifluoroacetate, the binding constants at RT for the formation of 1:1 adducts in $CHCl_3$ were determined, which evidenced that the phenylurea group increases the affinity for the NMPX salt by up to two orders of magnitude with respect the monotopic receptor.[79a]

[77] a) L. Pescatori, A. Arduini, A. Pochini, A. Secchi, C. Massera, F. Ugozzoli, Org. & Biomol. Chem. 2009, 7, 3698. b) L. Pescatori, A. Arduini, A. Pochini, A. Secchi, C. Massera, F. Ugozzoli, CrystEngComm 2009, 11, 239.

[78] A. Arduini, E. Brindani, G. Giorgi, A. Pochini, A. Secchi, J. Org. Chem. 2002, 67, 6188.

[79] a) K. Zhu, S. Li, F. Wang, F. Huang, J. Org. Chem. 2009, 74, 1322. b) C. M. G. dos Santos, T. McCabe, G. W. Watson, P. E. Kruger, T. Gunnlaugsson, J. Org. Chem. 2008, 73, 9235. c) L. Kovbasyuk, R. Kramer, Chem. Rev. 2004, 104, 3161.

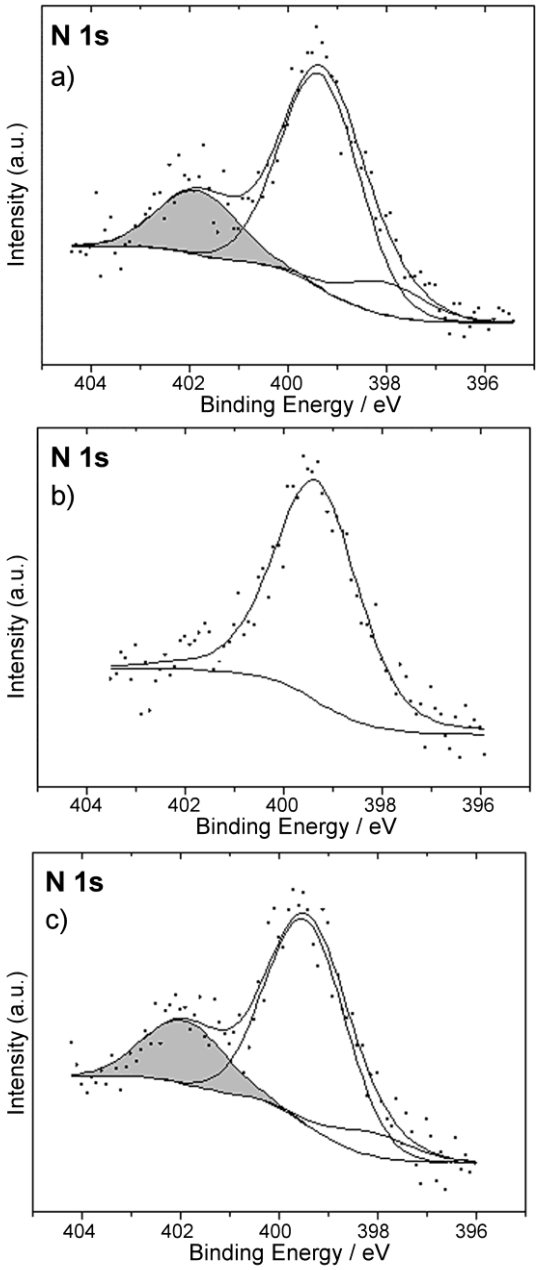

Figure 4.2.3: Sequence of N 1s XPS spectra taken at 11° from the surface normal of Cu/calix[4]arenePhenylUrea, after immersion in a CH_2Cl_2 solution of NMPI (a), after subsequent rinsing in a CH_3OH solution, acidified with HCl (b), after a new immersion in the above solution (c) (the gray areas identify the component due to N^+).

A sequence of N 1s XPS spectra of Cu/calix[4]arenePhenylUrea is reported in Figure 4.2.3. They have been obtained after a first cycle of immersion in a CH_2Cl_2 solution of N-methylpyridinium iodide (NMPI), followed by rinsing in CH_3OH acidified with HCl and by a second immersion in the solution of the pyridinium salt.

Each N 1s spectrum of this sequence is complex, and three components result from curve fitting. The main component, also present in the initial sample, before complexation, is assigned to the NH of the calixarene phenylureido group, on the basis of the literature.[80] A second peak component at a higher BE, characteristic for N^+,[81] appears after each immersion cycle, while it is absent upon rinsing with acidified CH_3OH. Such component necessarily relates to the coordination of pyridinium cation by the calix[4]arene (Figure 4.2.3a,c). The minor component at ~398 eV is assigned to a direct coordination to the Cu surface of neutral pyridine molecules,[82] an impurity which may accompany the synthesis of methylpyridinium. This assignment of the component is further supported by its disappearance upon acid rinsing in CH_3OH.

The N 1s XPS spectra for Cu/calix[4]arenePhenylUrea before and after immersion in the pyridine solution are closely similar, as a result of the presence of ammonium (coming from the synthesis) in the former. In this sample, the rinsing procedure applied to the sequence of samples in Figure 4.2.3 was not effective in removing ammonium, because of the poor solubility of this cation in CH_3OH. We recall here that water rinsing cannot be applied. Notice that the N^+ component in the two cases comes from distinct species, ammonium and pyridinium, respectively.

We have established the extent of such recognition reaction by taking the experimental relative atomic ratios between the two N 1s components, reported in Table 4.2.2. Such ratios differ from the value expected from stoichiometry, indicating that the filling of the calix sites by the pyridinium amounted to 60-70%. The establishment of the recognition reaction and the molecular integrity are confirmed by the close match, within the experimental error, of experimental and theoretical C/N values (Table 4.2.2).

The S 2p spectrum of Cu/calix[4]arenePhenylUrea is reported in Figure 4.2.4, where the two spin-orbit split doublets, already assigned above, are present in a SH/SCu 0.27 ratio. The larger amount of physisorbed molecules, with respect to the simpler calix[4]arene, is expected because of the presence of phenylureido group. A coverage of 0.43 nm^{-2} can be calculated from the SCu/Cu ratio.[68,76] The reduction in surface coverage with respect to the case of calix[4]arene could result from a larger surface disorder, due to the combined effects of polarity and flexibility of the phenylureido group.

[80] R. J. J. Jansens, H. Van Bekum, Carbon 1995, 33, 1021.

[81] D. Schulze, K. H. Hallmeier, D. Wett, R. Szargan, J. Electron. Spectros. Rel. Phenom. 2006, 151, 204.

[82] I. Gallardo, J. Pinson, N. Vilà, J. Phys. Chem. B 2006, 110, 19521.

	S 2p/eV	N 1s/eV	NH/N^+	C/N
Cu/calix[4]arenePhenylUrea + NMP (1st cycle)	161.9 163.2	398.0 399.3 401.8	3.0 (2)	21.2 (21.3)
After rinsing	161.9 163.2	398.0 399.3 401.8	-	27.4 (29)
Cu/calix[4]arenePhenylUrea + NMPI (2nd cycle)	161.9 163.2	398.0 399.3 401.8	2.6 (2)	24.1 (21.3)

Table 4.2.2: XPS peak positions and NH/N^+ quantitative ratios (± 10%) for Cu/calix[4]arenePhenylUrea as prepared and as a function of progressive NMP^+ uptake from a solution and rinsing.

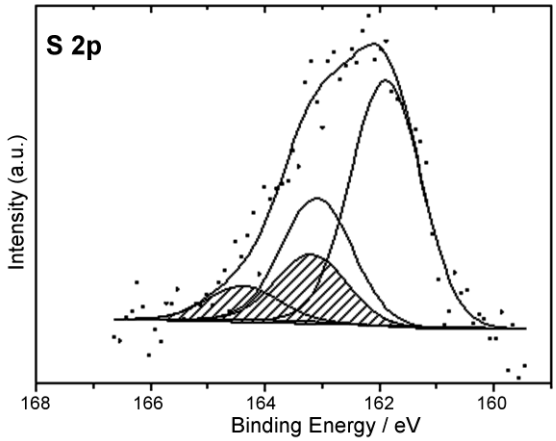

Figure 4.2.4: S 2p XPS spectrum taken at 11° from the surface normal of Cu/calix[4]arenePhenylUrea. The main spin-orbit split component is due to thiolate. The cross-hatched areas identify the component due to SH.

As for the I^- anion, its quantitative ratio to N^+ was lower than expected for the anchored calix[4]arenePhenylUrea. The N^+/I^- ratio further diminished after rinsing, and a Cl^- peak became visible in the XPS spectrum. We interpret this as a result of the anion exchange, which takes place during the rinsing cycle in a CH_3OH solution acidified with HCl to free the aromatic cavity of calix[4]arenePhenylUrea (Figure 4.2.5).

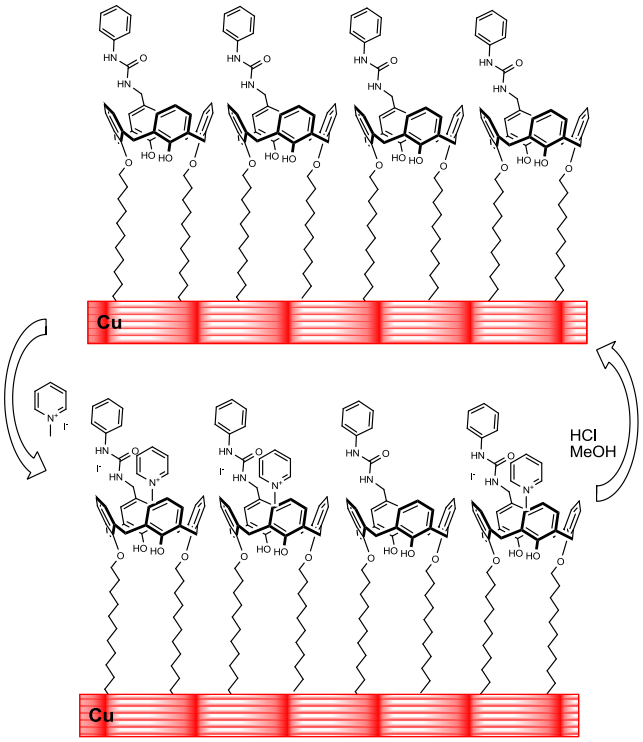

Figure 4.2.5: Schematic representation of the recognition process occurring between calix[4]arene heteroditopic receptors anchored on Cu surface and N-methylpyridinium cation (NMP^+).

4.2.3 - Self-assembling of rotaxane and pseudorotaxane species on copper

The recognition reaction in solution of N,N'-dialkylviologen-based axles with triphenylureidocalix[6]arene-based wheel,[54b] followed by immersion of Cu in the above solution, resulted in the first reported example of rotaxane and pseudorotaxane species self-assembled on Cu. To this aim, two similar though conceptually different pre-formed systems were used. As shown in previous solution studies[17b,54a] the rotaxane that originates by threading the wheel with the mono-stoppered axle in low polar solvent such as toluene, is an oriented pseudorotaxane bearing the phenyl stopper and the -SH function at the upper and lower rim, respectively (Figure 4.2.6). In these same conditions, the threading reaction carried out by using the axle that lacks the stopper, yields the pseudorotaxanes which has the SH function oriented toward the macrocycle upper rim. This means that the anchoring of these

two different systems yields in one case an oriented rotaxane, in which the Cu surface acts as a stopper, and a reversely oriented pseudorotaxane in the other (Figure 4.2.6).

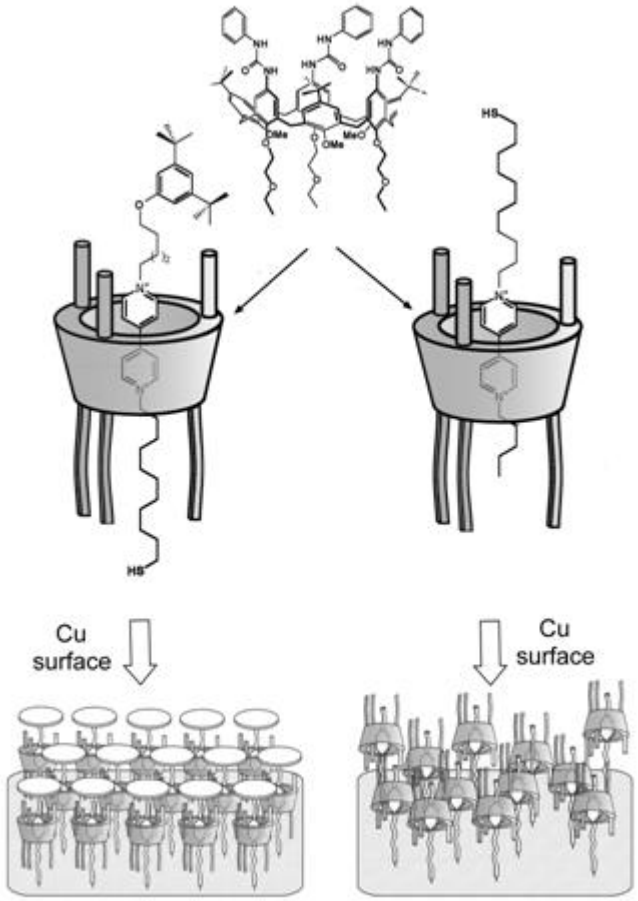

Figure 4.2.6: Schematic representation of the threading reaction between calix[6]arene-based wheel and viologen-based axles. In toluene solution, the mono-stoppered axle gives rise to oriented rotaxane and pseudorotaxanes.

The assembling on Cu of preformed pseudorotaxanes was preferred to a 2-step reaction (adsorption of axles on Cu followed by threading of the calix, by progressively reacting Cu with each of the two solutions) because of the poor adsorption of N,N'-dialkylviologen on the surface, likely due to repulsive interactions between the positive charge of the axle.

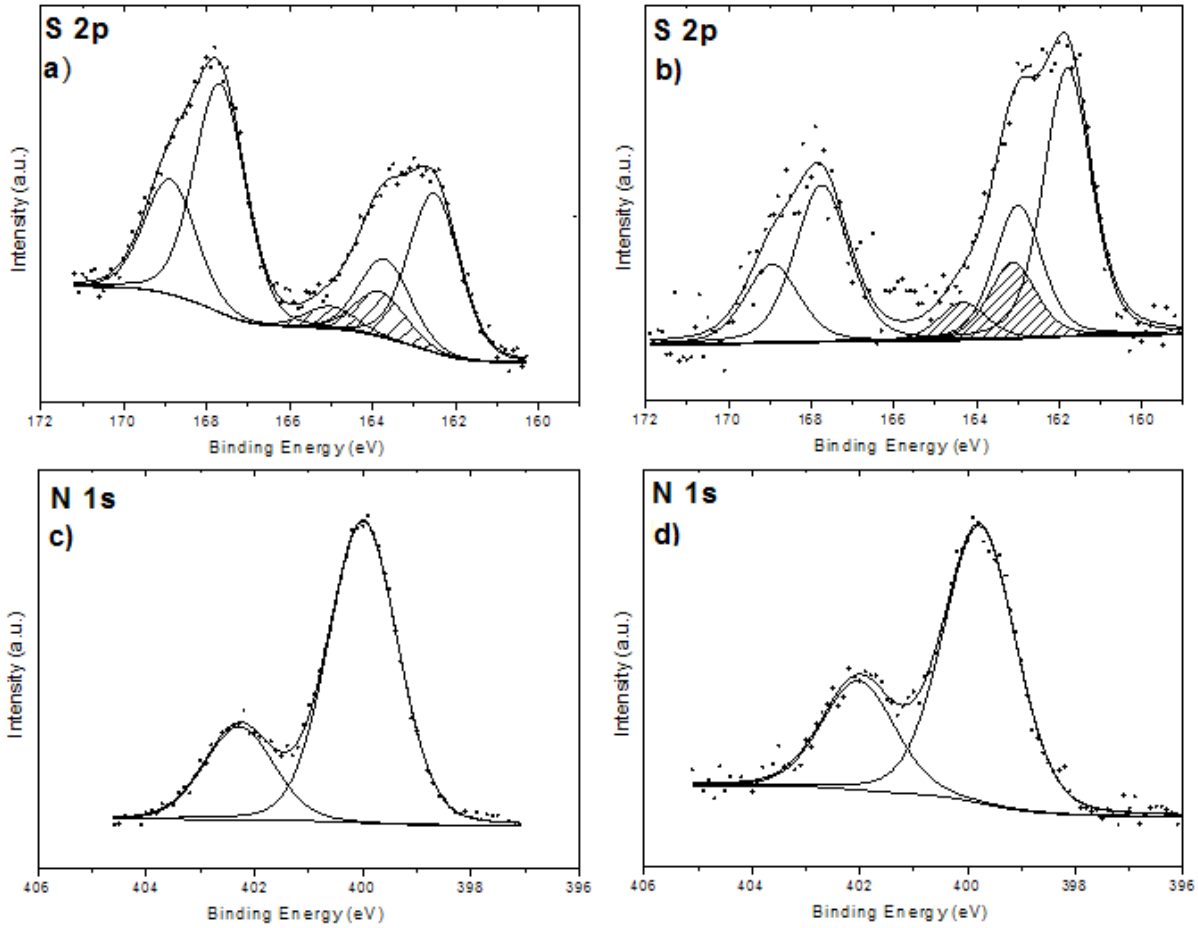

Figure 4.2.7: S 2p XPS spectra taken at 11° from the surface normal of a) rotaxane and b) pseudorotaxane on Cu. The main spin-orbit split component is due to thiolate. The cross-hatched areas identify the component due to SH. The doublet at high BE is assigned to tosylate. N 1s XPS spectra of c) rotaxane and d) pseudorotaxane on Cu. The experimental curve is displayed as dotted line, with the NH and N^+ peak components, resulting from curve-fitting, as solid lines.

Figure 4.2.7 reports the N 1s and S 2p peaks of the rotaxane and pseudorotaxane adducts, respectively. NH and N^+ peak components are again present, indicating the anchoring of these species at the Cu surface. The NH/N^+ ratio is in the range of 3, as expected from the stoichiometric value in the absence of dethreading (Table 4.2.3).

We also found no sizeable dethreading of the pseudorotaxanes by inspection of the values of the NH/N^+ and C/N ratios, which fall in the range expected for intact chemisorbed rotaxanes. The S 2p photoemission region displays the two couples of spin-orbit components with the same meaning and assignment reported above, apart from the presence at high BE of the peak component related to the tosylate counterion. The relative intensity of this last peak to the rest of the S 2p signal follows the stoichiometry of the salt.

	S 2p/eV	N 1s/eV	NH/N^+	C/N	S-Cu/Cu	θ (nm^{-2})
Cu/rotaxane	162.5 163.8 167.7	400.0 402.3	2.8 (3)	15.3 (18.1)	0.32	1.6
Cu/pseudorotaxane	161.8 163.1 167.7	399.8 402.0	3.4 (3)	16.4 (16.2)	0.44	2.8

Table 4.2.3: XPS peak positions and experimental and theoretical (reported in brackets) quantitative ratios (± 10%) and surface coverage for rotaxane and pseudorotaxane on Cu.

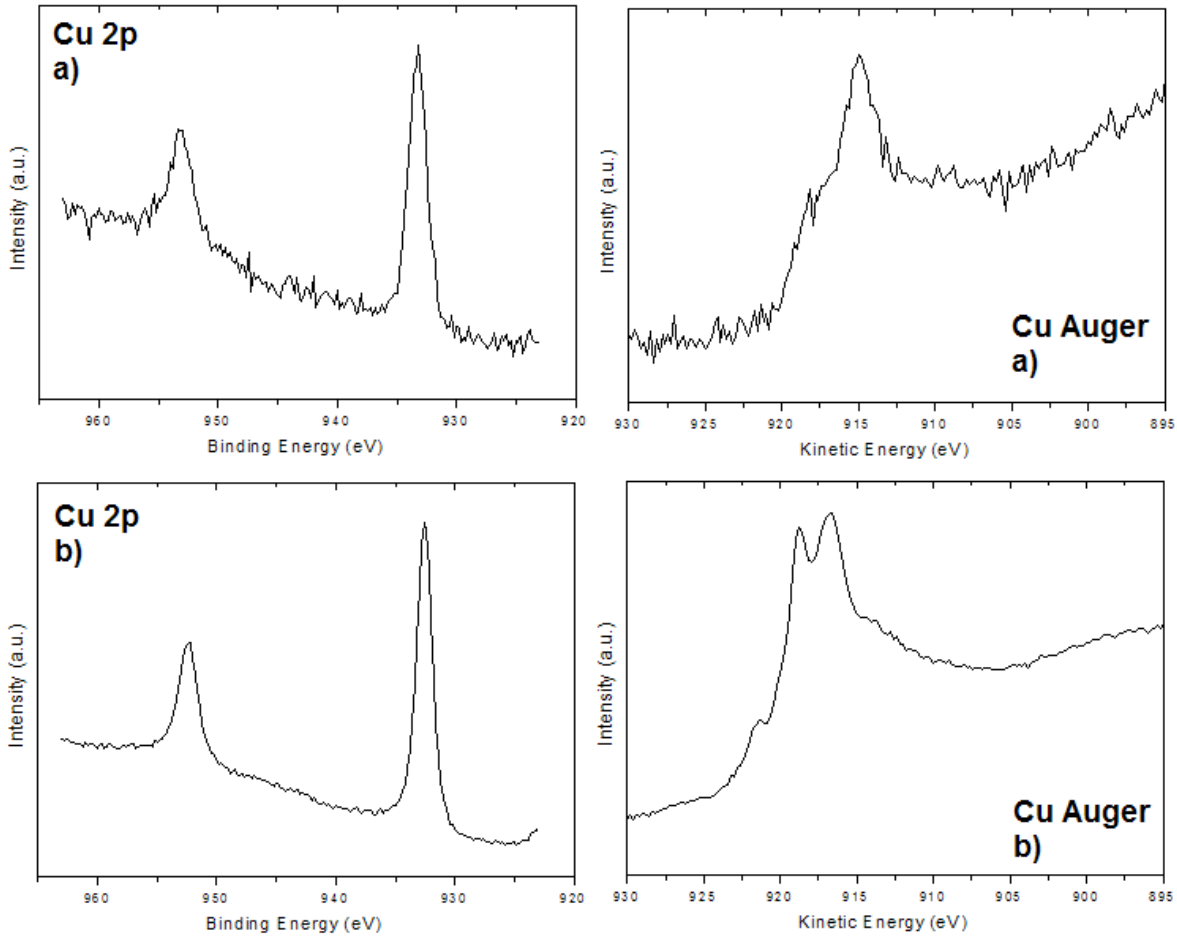

Figure 4.2.8: Cu 2p and Cu LMM Auger lines of Cu/rotaxane(a) and Cu/pseudorotaxane (b).

The Cu 2p spectra in Figure 4.2.8 evidence the absence of Cu(II). In the Cu LMM Auger spectra only Cu(0) and Cu(I) components are present, with a different amount of the two states because of the different surface coverage and arrangement of the systems on Cu.

The surface coverage, calculated from the S-Cu/Cu ratio,[68,76] is comparable to that of calixarenes and consistent with the increased complexity of the molecular system.

4.3 – Electrochemical study

Electrochemical polarization represents a valuable tool for triggering host-guest interactions, since it can change the oxidation state of the guest or the host, a parameter which can be crucial for bonding. In fact, in such host-guest systems it could be present an electroactive unit which exhibits reversible redox processes, and the other component could be sensitive and answer to the electrochemical tate of the the electroactive unit. This second property allows for the investigation of the complexation/decomplexation process by means, for example, of voltammetric techniques.

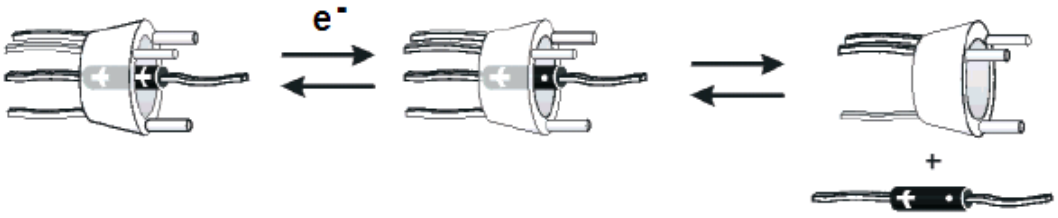

Figure 4.3.1: one-electron reduction and subsequent dethreading of pseudorotaxane.

Pseudorotaxanes in which the threading/dethreading of the axle and wheel components can be controlled by appropriate stimuli constitute basic prototypes of molecular machines. The valuable redox properties of the viologen unit can be exploited to trigger the assembly/disassembly of the corresponding pseudorotaxanes.

In a previous study, Credi et al. demonstrated the possibility to electrochemically switch the threading-dethreading process in solution of viologen-calix[6]arene pseudorotaxane systems by means of cyclic voltammetry (Figure 4.3.2).[83]

[83] A. Credi, S. Dumas, S. Silvi, M. Venturi, A. Arduini, A. Pochini, A. Secchi, J. Org. Chem. 2004, 69, 5881.

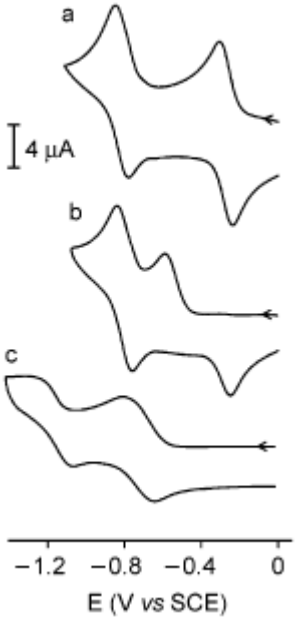

Figure 4.3.2: Cyclic voltammetry of a) viologen, b) pseudorotaxane and c) rotaxane (from ref. 83).

The axles exhibited two monoelectronic and reversible reduction processes ($E_{1/2}°$ = -0.29 V, $E_{1/2}°$ = -0.81 V *vs.* SCE) of the viologen unit, and no oxidation process. The inclusion into the cavity caused a large negative shift of the first reduction potential of the viologen unit of the axle (Figure 4.3.2). In other words, the axle became more difficult to reduce, reflecting the stabilization offered by the wheel. The second reduction process occurred at the same potential as for the free axle in the pseudorotaxane (Figure 4.3.2), whereas it was shifted to more negative values in the rotaxane ($E_{1/2}°$ = -1.18 V).

These results show that one-electron reduction of the axle promotes its dethreading in case of the pseudorotaxane. The examined pseudorotaxanes can be disassembled in a fast and reversible manner by one-electron reduction of their axle components.

On the basis of this study, we investigated in detail the controlled release of rotaxanes and pseudorotaxanes anchored on Cu by application of a suitable potential. It is known that the reduction of the bypiridinium N^+ center induces the dethreading of the wheel from the viologen axle in pseudorotaxanes.[83]

We first measured the reduction potentials of pseudorotaxane chemisorbed on Au microelectrode via cyclic voltammetry (Figure 4.3.3). Au microelectrode was preferred to Cu because of the high reduction current displayed by the latter. We found two well separated

peaks at -0.7 and -1.2 V (*vs*. Ag/Ag^+ in acetonitrile), which we assigned, on the basis of the literature,[83,84] to the two N^+ reductions of the viologen-based axle.

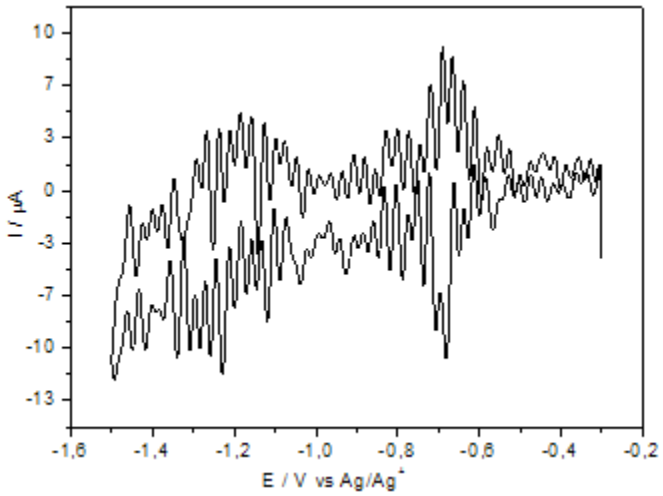

Figure 4.3.3: Cyclic voltammetry of pseudorotaxane on Au microelectrode (scan rate: 500 mV/s).

We compared the behaviour of rotaxane and pseudorotaxane on Cu by keeping the two samples biased at -1.7 V (*vs*. Ag/Ag^+ in acetonitrile) for 1 min. XPS results before and after polarization can be compared in Table 4.3.1. The diminishing of the thiolate component of S 2p in case of rotaxane (Figure 4.3.4) is a clear indication of the release of approximately half of the rotaxanes, induced by the breaking of Cu-S bonds. This is accompanied by the drastic fall of intensity displayed by the tosylate anion, likely due to its reduction, in addition to the loss of rotaxane. The reduction of the viologen N^+ appears in the N 1s spectrum as a new component at ~398.9 eV (Figure 4.3.4). Its energy separation with respect to triphenylureido N is consistent with the electron-withdrawing effect exerted on N by the C=O group in the latter.

The nearly constant ratio between the NH group from the triphenylurea and the S of the anchored species, NH/(SH + S-Cu) in Table 4.3.1 indicates the residual presence of intact rotaxanes at the surface.

[84] K. Nikitin, E. Lestini, M. Lazzari, S. Altobello, D. Fitzmaurice, Langmuir 2007, 23, 12147.

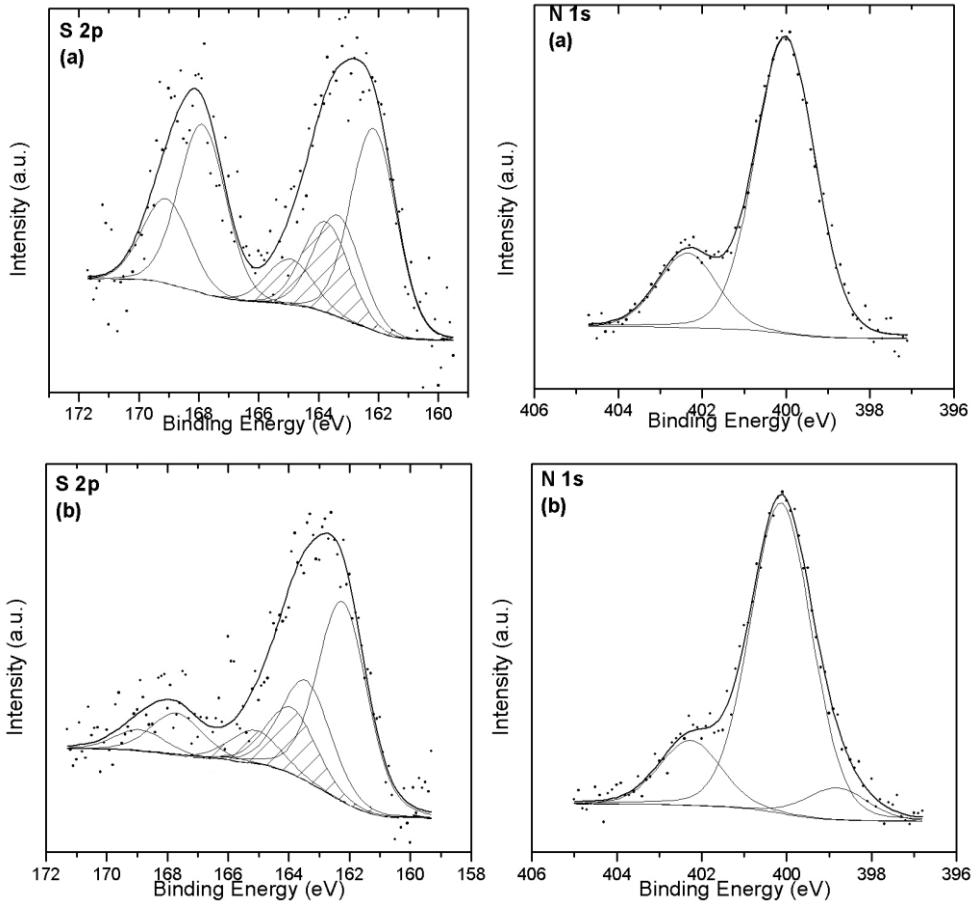

Figure 4.3.4: N 1s and S 2p XPS spectra of Cu/rotaxane before (a) and after (b) after 1 min biasing. The main spin-orbit split S 2p component in is due to thiolate and the cross-hatched areas identify the component due to SH.

	OTs^-/Cu	S-Cu/Cu	NH/(SH + SCu)	N^+/(SH + SCu)
Cu/rotaxane	0.17	0.18	3.8	0.89
Cu/rotaxane[a]	0.03	0.11	3.0	0.74
Cu/pseudorotaxane	1.1	0.44	4.5	1.3
Cu/ pseudorotaxane[a]	0.10	0.43	1.9	0.57
Cu/ pseudorotaxane	0.96	0.40	5.3	1.5
Cu/ pseudorotaxane[b]	0.10	0.38	2.8	0.64

[a] 1 min bias; [b] 3 min bias.

Table 4.3.1: XPS quantitative ratios (± 10%) for rotaxane Cu/rotaxane and Cu/pseudorotaxane before and after biasing.

In the more complex case represented by pseudorotaxane, a clear evidence for dethreading of the wheel as the largely prevailing effect of biasing comes from the sizeable lowering of the ratio NH/(SH + S-Cu) in Table 4.3.1. Notice the constancy in the S-Cu/Cu atomic ratio, which excludes loss of the whole pseudorotaxane. We still notice the drastic loss of tosylate anion, with the same meaning as above (Figure 4.3.5).

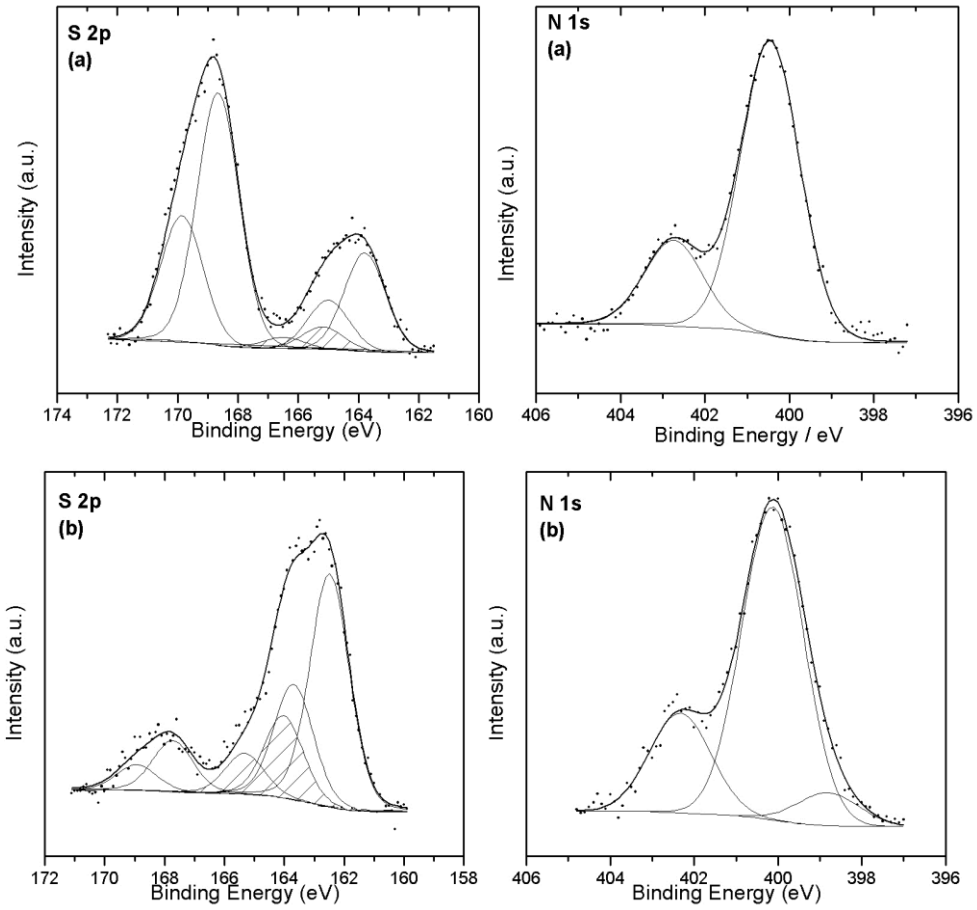

Figure 4.3.5: N 1s and S 2p XPS spectra of Cu/pseudorotaxane before (a) and after (b) after 1 min biasing. The main spin-orbit split S 2p component in is due to thiolate and the cross-hatched areas identify the component due to SH.

This general trend is further confirmed by extending the biasing to 3 min. The low BE component in the N 1s spectrum increases with respect to 1 min biasing (Figure 4.3.6 and Table 4.3.1).

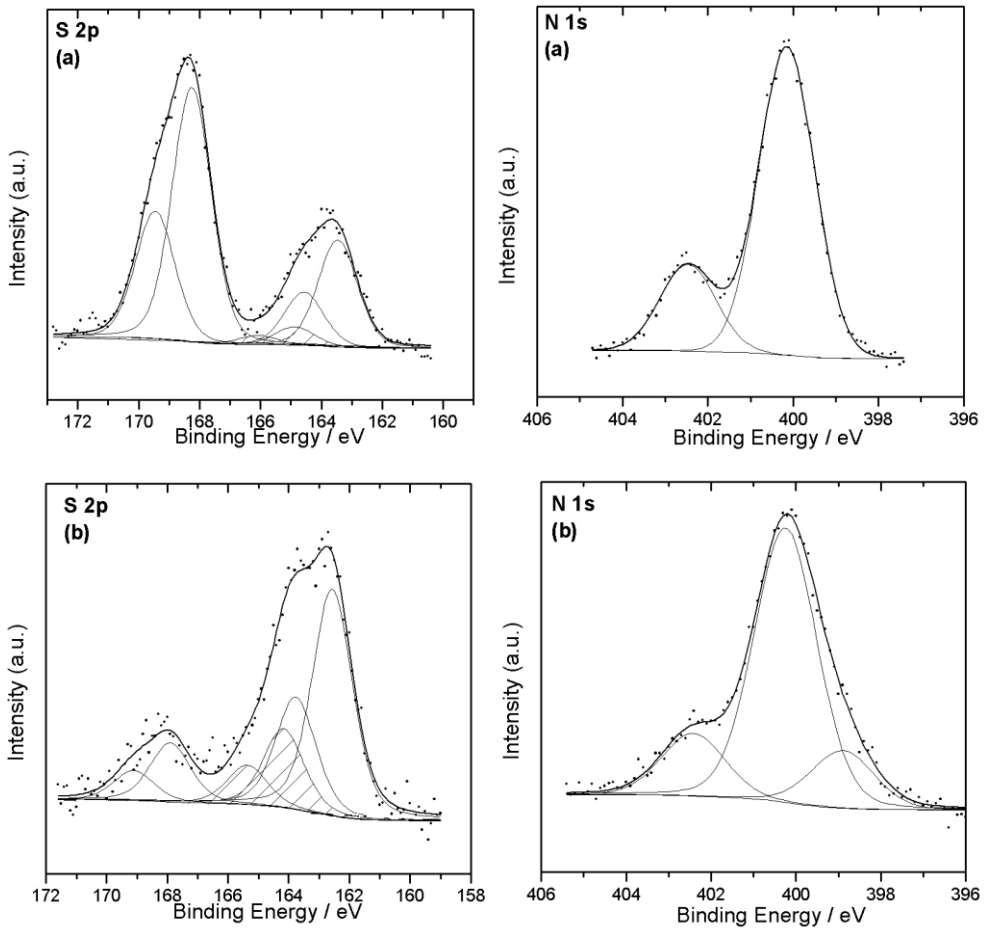

Figure 4.3.6: N 1s and S 2p XPS spectra of Cu/pseudorotaxane before (a) and after (b) after 3 min biasing. The main spin-orbit split S 2p component in (b) and (d) is due to thiolate and the cross-hatched areas identify the component due to SH.

The absence of any further dethreading of the wheel comes from the comparable decrease of the NH/(SH + S-Cu) ratio after 1 and 3 min. We interpret this last result as due to the second reduction of the radical cation axle, from which the wheel has departed after the first reduction.[83]

4.3 – Conclusions

We have prepared and studied by means of XPS the first examples of calixarenes, rotaxanes and pseudorotaxanes supramolecular systems self-assembled on polycrystalline Cu surfaces. Covalent functionalization of calix[4,6]arenes on Cu was reached using a dip-coating procedure which allowed for good surface coverages and Cu passivation. Molecular adhesion has been demonstrated by the presence and relative quantitation of XPS signals from specific elements in the molecules. We have successfully tested the combination of different functionalities by producing a mixed film, prepared by ligand exchange of calix[4]arene with undecanethiol. The availability of the calix[4]arene cavity to reversibly host further species after anchoring on Cu has been demonstrated by a sequence of uptake and release cycles with pyridinium salts. Pseudorotaxane species, composed of a calix[6]arene wheel derivatized with N-phenylureido groups on the upper rim, and viologen-containing axle, have been anchored on Cu via the SH-termination of the axle. XPS demonstrated the successful self-assembling of fully threaded rotaxanes and pseudorotaxanes and the effectiveness of controlled release upon biasing of full rotaxanes and of the pseudorotaxane wheel.

Chapter 5
Production and characterization of organic-inorganic hybrids based on calixarene derivatives and H-Si(100)

5.1 - Hydrogenation of Si(100)

H-terminated Si(100) can be prepared via either ultra-high vacuum methods, requiring a careful cleaning of the substrate and exposure to atomic hydrogen, or following wet-chemistry procedures. We have applied the latter approach, which lends itself to a much more versatile use with different, even complex chemicals presenting low volatility or even unsuitable to exposure in a vacuum because of decomposition.

Si(100) wafers of ~ 400 μm thickness, p-doped (boron-doped, single-side polished, 1^{-10} Ω × cm resistivity) with areas of ~ 1 cm^2 have first been washed in boiling 1,1,2-trichlorethane for 10 min and subsequently in ethanol at room temperature, with sonication for 5 min. They were oxidized in H_2O_2/HCl/H_2O (2:1:8) at 353 K for 15 min and rinsed copiously with ultra-pure de-ionized water (Water Plus). These solutions cleaned the surface from organic and metallic contaminations. The resulting surfaces were hydrogenated by etching with 10% aqueous HF for 10 min, rinsed with ultra-pure water again, dried under a stream of N_2 and immediately used in the functionalization process.

Considering the nature of the molecular systems to be anchored, which could suffer from exposure to UV radiation, all hybrid systems were produced via an extra-mild, visible-light induced photochemical functionalization, described in its general aspects in Chapter 2.

In the following, the details of the methods as it applies to the molecules here investigated are exposed.

5.2 - An extra-mild photochemical functionalization for the establishment of a Si-C covalent anchoring bond

The photochemical approach is considered to be the mildest route to the functionalization of H-terminated Si surfaces, and it has generally been applied via hydrosilylation reactions of terminal alkenes and alkynes (Paragraph 2.1).

Freshly etched Si samples were always used as the substrates for anchoring. The functionalization experiments on the surface-activated samples were carried out using standard preparative Schlenk-line procedures (Figure 5.2.1).

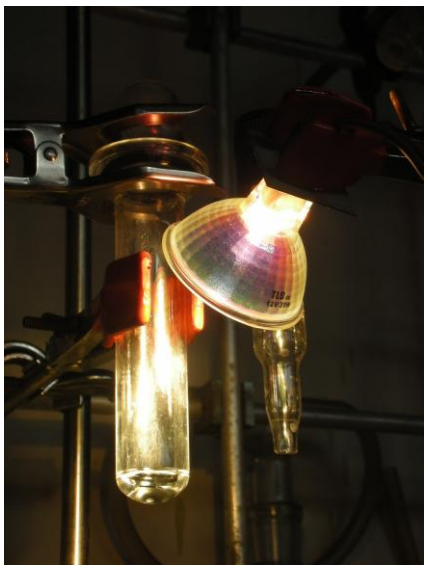

Figure 5.2.1: Photochemical functionalization of Si wafers in a Schlenk-line.

The suitable calixarene or pseudorotaxane was dissolved in toluene (10 mM concentration or calixarene, 5 mM concentration for pseudorotaxane instead). H-Si was

dipped in the preventively deoxygenated molecular solution through 3 freezing-pumping-annealing cycles, and kept under N_2, to preserve silicon from surface oxidation. The sample was subjected to a 35 mW/cm^2 visible irradiation for 4 h from a quartz-iodine lamp. After functionalization, all samples were subjected to the same cleaning procedure, consisting of two sonication cycles, 5 min each, with dichloromethane, and drying in a stream of N_2, to eliminate physisorbed molecules. Care was taken in order to reduce all sources of O_2 and H_2O contamination in preparation steps.

The pseudorotaxane was prepared by adding equimolar amounts of calixarene wheel and viologen axle to a toluene solution under stirring. In few min the colour of the solution changed to orange. The mixture was stirred at room temperature for 30 min and then filtered off to remove the excess of solid axle.[54b,c]

Calix[4]arene complexation – We tested the availability of the calix[4]arene substituted with a phenylureido group to further reactions, once anchored on Si (Figure 5.2.2). The tests were performed after a first cycle of immersion of a Si(100) wafer in a solution of N-methypyridinium iodide, followed by rinsing in CH_3OH acidified with HCl (to remove species from the cavity) and by a second immersion in the solution of the same salt, which was requested for the reaction to be completed (see infra). Iodide was chosen as the anion because, in addition to its high binding constant for the formation of the adduct with N-methylpyridinium,[77a] its characteristic XPS signals do not interfere with those from Si peaks, thus allowing for an easier quantitation.

Pseudorotaxane threading from solution – After the functionalization reaction, H-Si(100)-pseudorotaxane samples were dipped in the calixarene-wheel solution in toluene for 15 min.

In Figure 5.2.2 the investigated calixarenes and rotaxanes anchored on H-Si(100) are shown.

In order to evaluate the feasibility of the Si surface functionalization with calixarene derivatives, we tested compounds which present on their lower rim suitable anchoring terminations. In particular, calix[4]arene and calix[6]arene are characterized by the presence of two and three ω-alkenyl chains on their lower rim, respectively. Moreover, the two macrocycles present some heteroatoms in their structure. XPS signals due to heteroatoms are

diagnostic for the characterization of the functionalized surface. Calix[4]arene is characterized by the presence of two bromine atoms (Figure 5.2.2a) or phenylureido groups (Figure 5.2.2b), and calix[6]arene possesses three nitro groups on its upper rim (Figure 5.2.2c).

From solution studies it is known that calix[6]arenePhenylUrea wheel (Figure 5.2.2d) plus N,N′-dialkylviologen (bearing a ω-alkenyl anchoring group) (Figure 5.2.2e) axle give rise to the formation of stable pseudorotaxanes in apolar solvents (log$K$ > 6).[17d,54a]

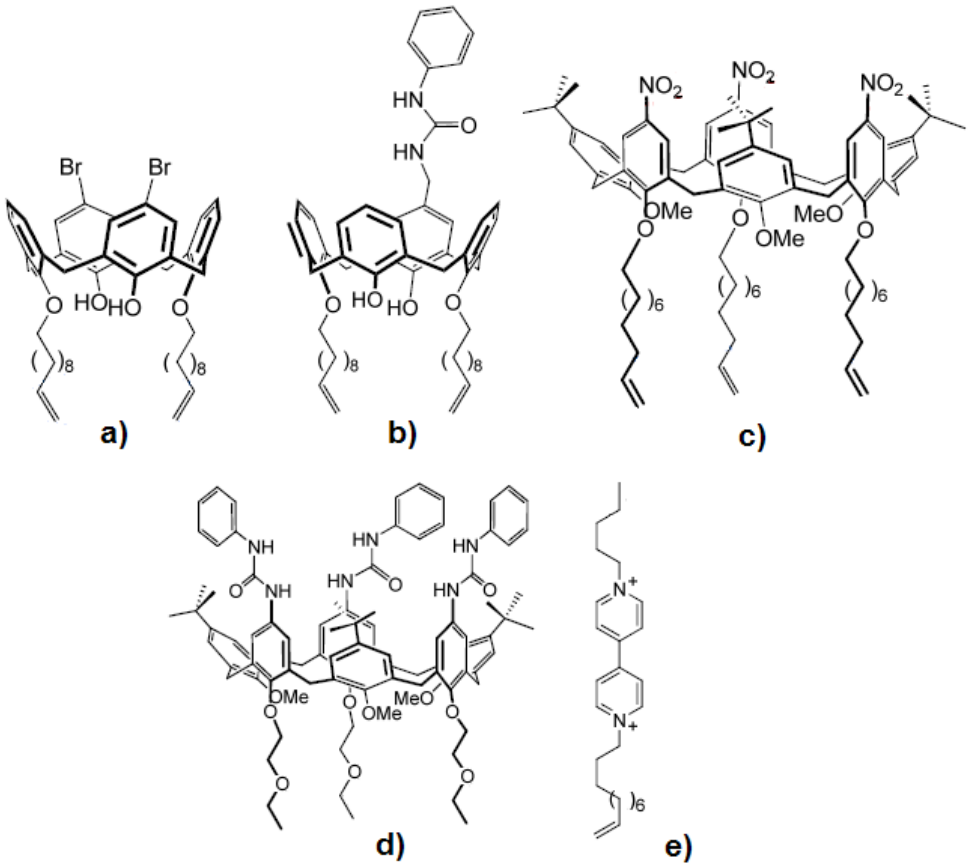

Figure 5.2.2: Calixarenes derivatives and pseudorotaxane for the functionalization of H-Si(100) surfaces: a) calix[4]areneBr_2, b) calix[4]arenePhenylUrea, c) calix[6]areneNO_2, d) calix[6]arenePhenylUrea, e) N,N′-dialkylviologen. Pseudorotaxane results from the assembling of d) and e).

5.3 - XPS investigation: Results and discussion

5.3.1 - Characterization of calix[4,6]arenes on Si(100)

The initial H-Si(100) surfaces were routinely checked via XPS, in order to control their quality and reproducibility.

We first investigated the behaviour of calix[6]areneNO_2 on Si(100). Curve-fitting of the Si 2p peak shows separated signals for bulk silicon (cross hatched areas) and for its surface contributions (white areas). The absence of signals possibly related to Si oxides shows that we produced a functional hybrid with preservation of the surface (Figure 5.3.1a). The distinctive XPS region of the organic moiety is N 1s. The spectrum is complex and contains the typical signal of aromatic -NO_2 group (principal peak and its shake up)[85] to the high binding energy side (Figure 5.3.1b). The surface coverage, estimated from substrate attenuation by making use of the NO_2/Si ratio (Table 5.3.1), is 27%,[69] which may be considered as good, once we consider that only the methyl group is able to form a full monolayer on Si.[86]

	N 1s/eV	NO_2/Si	Φ (%)
Calix[6]areneNO_2	407.0 408.5	0.032	27

Table 5.3.1: XPS peak positions and quantitative ratios (± 10%), and values of surface coverage (Φ) for Si/calix[6]areneNO_2.

[85] G. Distefano, M. Guerra, D. Jones, A. Modelli, F. P. Colonna, Chem Phys. 1980, 52, 389.

[86] E.J. Nemanick, P.T. Hurley, L.J. Webb, D.W. Knapp, D.J. Michalak, B.S. Brunschwig, N.S. Lewis, J. Phys. Chem. B 2006 110, 14770.

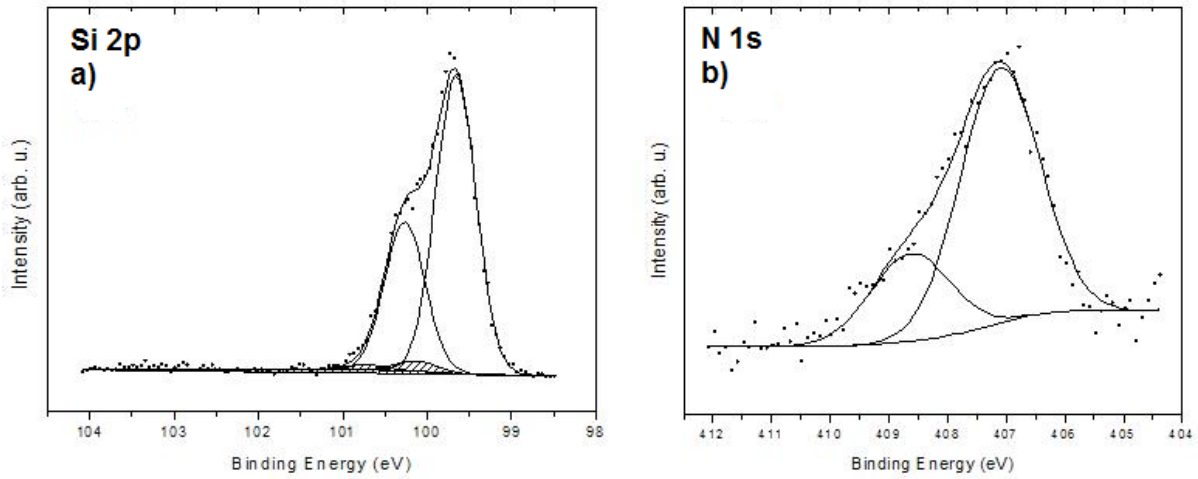

Figure 5.3.1: Si 2p (a) and N 1s (b) XPS spectra of Si(100)/calix[6]areneNO_2 taken at 11° from the surface normal. The cross-hatched areas in a) identify the component due to reacted Si.

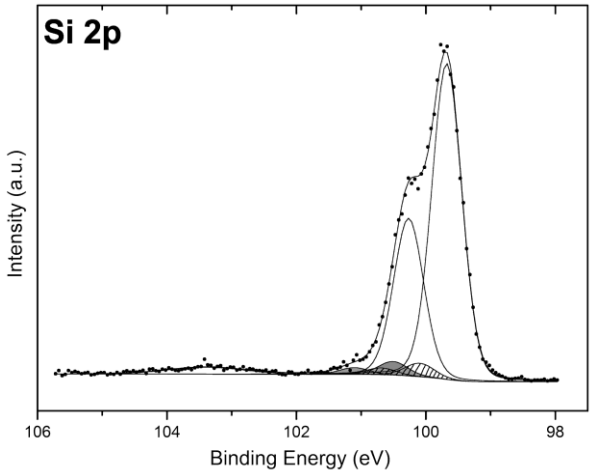

Figure 5.3.2: Si 2p XPS spectra taken at 11° from the surface normal of Si(100)/calix[4]areneBr_2. The main spin-orbit split component is due to bulk Si. The cross-hatched and grey areas respectively identify the components due to C-Si and Br-Si bonds.

Figure 5.3.2, where the XPS spectrum of the Si 2p region of the most reactive molecule in the investigated series, calix[4]areneBr_2, is displayed, shows only a small amount of Si oxide. This last could have resulted from the short exposure to air, which was unavoidable when introducing the samples from a Schlenk tube, where the preparation has been conducted, to the UHV apparatus. In the same spectrum, in addition to the main $2p_{3/2,1/2}$ peaks due to bulk Si, two couples of spin-orbit split peaks are present, at 100.1 and 100.5 eV,

which are assigned, on the basis of the literature, to Si-C and Si-Br bound components, respectively.[87]

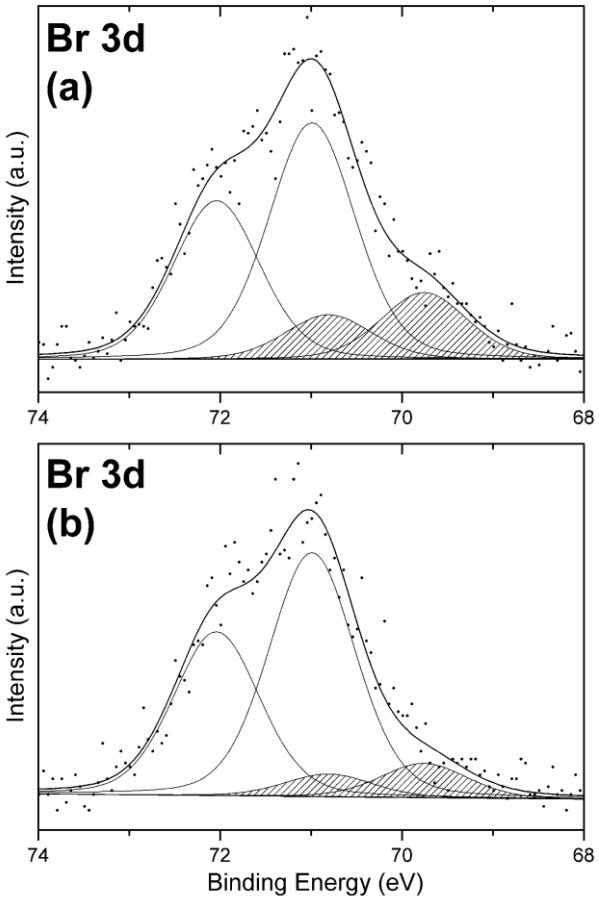

Figure 5.3.3: Br 3d XPS spectra taken at 11° (a) and 81° (b) from the surface normal of Si(100)/calix[4]areneBr_2. Notice the relative enhancement of the Br-C component at a more grazing (*i.e.*, more surf. sensitive) angle.

	Br 3d/eV	Br/Si	Φ (%)
Calix[4]areneBr_2	69.8 71.0	0.018	16

Table 5.3.2: XPS peak positions and quantitative ratios (± 10%), and values of surface coverage (Φ) for Si/calix[6]areneBr_2.

[87] J. Terry, R. Mo, C. Wigren, R. Cao, G. Mount, P. Pianetta, M. R. Linford, C. E. D. Chidsey, Nucl. Instrum. Methods Phys. Res. Sect. B 1997, 133, 94.

The corresponding Br 3d peak for the same sample (Figure 5.3.3b) is the sum of two spin-orbit split components, which were resolved via curve-fitting with the same peak constraints (ΔE = 1.05 eV, 2:3 peak area ratio). The two components are assigned to Br-Si (spin doublet at 69.7 and 70.8 eV, shadowed in the graph) and Br-C (spin doublet at 71.0 and 72.0 eV), on the basis of the literature.[17a,88] The assignment is further confirmed by the dependence of the relative intensity of the two peaks upon the photoelectron collection angle (Figure 5.3.3a,b). In fact, at a more grazing angle (*i.e.*, in more surface-sensitive conditions) the Br-C component is relatively enhanced, as expected for the species located at a further distance with respect to the surface.

The surface coverage was estimated from substrate attenuation by making use of the Br/Si ratio (Table 5.3.2), as in the previous case.[69]

A Br-Si component indicates that some decomposition of the calixarene ligands has occurred during the functionalization, with abstraction of bromine from the calixarene rim. Decomposition of the molecular substrate was not unexpected, since we found similar results in the case of Br-undecene.[17a] More quantitatively, a Br-Si/Br-C ratio of 0.28 is obtained at 11° photoelectron collection angle (0.14 at 81°). Interestingly, NMR analysis of the residual solution of calix[4]areneBr_2 resulting from the anchoring reaction excluded the presence of de-brominated calixarenes, suggesting that the fraction of calixarenes which has lost bromine is anyhow present on the Si surface, after reaction.

These findings have two major implications. First, in order to reduce decomposition of the organic moiety, a milder route to hydrosilylation of organics, obtained by us via white-light exposure, can be more effective than UV-photostimulation, applied before.[15a,15e,89] Secondly, bromine abstraction could result in direct bonding of the calix through its upper rim to the Si surface[89] which would hamper host-guest reactions. We checked for the surface orientation of the calix, and found them standing up, which again hints at different photoassisted reactivity when using white-light *vs.* UV.

To this aim, we made use of two series of calix[4]arenes, the mono- and di-bromo substituted, and tested their reactivity towards Cs^+ picrate.

[88] H. Jin, C. R. Kinser, P. A. Bertin, D. E. Kramer, J. A. Libera, M. C. Hersam, S. T. Nguyen, M. J. Bedzyk, Langmuir 2004, 20, 6252.

[89] G. Condorelli, A. Motta, M. Favazza, I. L. Fragalà, M. Busi, E. Menozzi, E. Dalcanale, L. Cristofolini, Langmuir 2006, 22, 11126.

In solution, the partial-cone and 1,3-alternate conformers of calix[4]arenes show remarkable selectivity in the complexation of cesium ion[90] and, for this reason, are promising in the ^{135}Cs removal from radioactive waste (Figure 5.3.4).

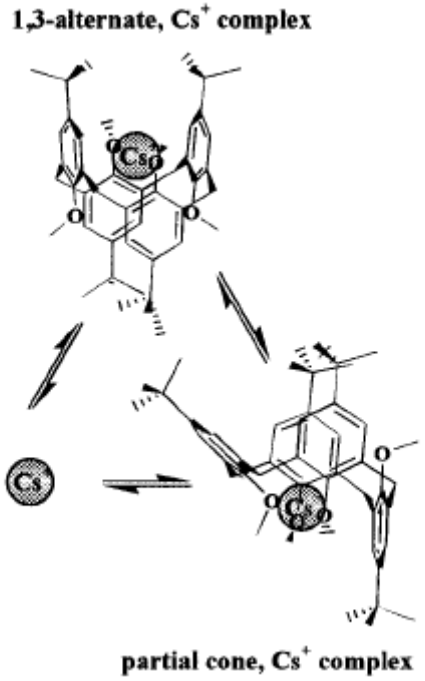

Figure 5.3.4: Complexation of the cesium cation by calix[4]arene in the 1,3-alternate and partial cone interconverted conformations.

The calculated Cs/Br atomic ratios matches, within the ± 10% experimental uncertainty associated to XPS semiquantitative measurements, the values expected from stoichiometric ratios, respectively 0.43 (theor.: 0.5) and 0.93 (theor.: 1.0) (Figure 5.3.5).

These results unequivocally show that the chemisorbed calix[4]arenes are available to guest species. In fact, the small difference between theoretical and experimental couples of values here above is not compatible with the Br-Si/Br-C ratio of 0.28.

[90] U. C. Meier, C. Detellier., J. Phys. Chem. A 1998, 102, 1888.

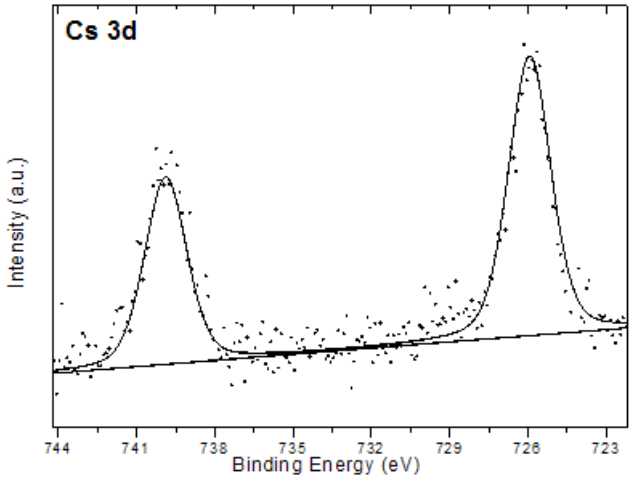

Figure 5.3.5: Cs^+ XPS spectra of Si(100)/calix[4]areneBr_2 after complexation with cesium picrate.

5.3.2 - Recognition reactions of N-methylpyridinium ion-pairs towards anchored heteroditopic calix[4]arene receptors

We tested the reactivity on Si(100) of anchored heteroditopic calixarene-based receptors[49] with a series of experiments. To this aim, we selected the calix[4]arenePhenylUrea systems (Figure 5.2.2), in order to study their reactivity towards N-methylpyridinium[77] (NMP) salt. The availability of a phenyluerido group in the upper rim of a calix allows for a combined effect on the recognition reaction of a salt (a cooperative heteroditopic effect).[79] In fact, the ionic interaction in the salt is reduced by the proper combination of a hard H-bond, which can be established by the amido group of the phenylurea unit with an anion, with a soft calix-cation π-bond, through the methyl group of the pyridinium. Testing a series of NMP salts with different anions evidenced that the phenyl-urea increases the affinity for the NMPX salt by up to two orders of magnitude.[77a]

	NH/N^+
Si(100)/calix[4]arenePhenylUrea	7.4
Si(100)/calix[4]arenePhenylUrea + NMPI (1st cycle)	4.8
Si(100)/calix[4]arenePhenylUrea after rinsing	8.5
Si(100)/calix[4]arenePhenylUrea + NMPI (2nd cycle)	2.1
Si(100)/calix[4]arenePhenylUrea + NMPI (theor.)	2

Table 5.3.3: XPS NH/N^+ quantitative ratios for Si(100)/calix[4]arenePhenylUrea as prepared and as a function of progressive NMP^+ uptake from a solution and rinsing.

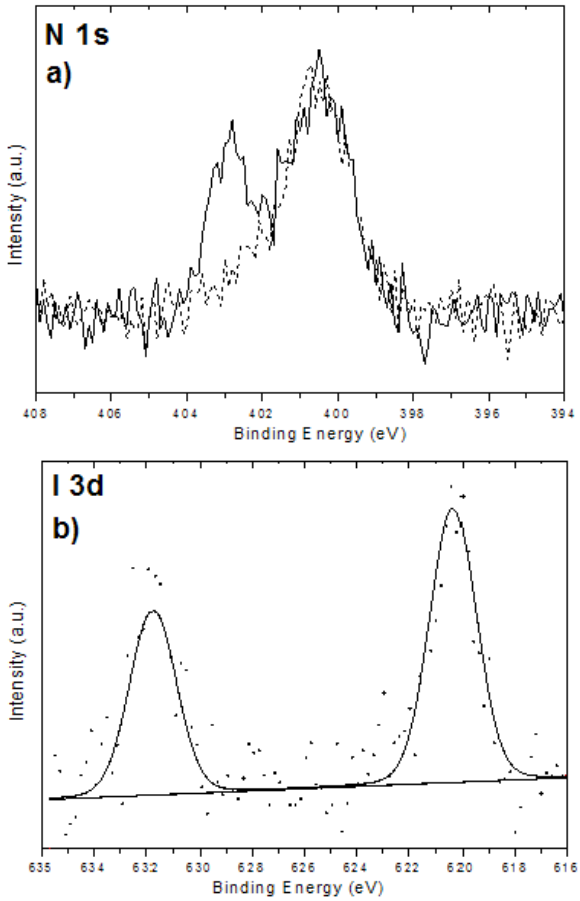

Figure 5.3.6: a) N 1s XPS spectra of a Si(100)/calix[4]arenePhenylUrea sample as such (dotted line) and after immersion in a solution of NMP^+I^- (solid line). Notice the relative enhancement of the N^+ component at higher binding energies; b) I 3d XPS spectrum from the same sample.

The contemporary presence in the N 1s region of two peak components, shown in Figure 5.3.6a, due to both the NH group and the N^+ from the pyridine ring (NMP^+), calls for the establishment of the recognition reaction between these reactants, to an extent which was quantified by taking the experimental relative atomic ratios between the two N 1s components.

As reported in Table 5.3.3, a small amount of N^+ was already present in the anchored calix[4]arene before contacting with NMPI, which was likely due to the surface anchoring process on H-Si. The ratio matched the value expected from stoichiometry already at the second cycle of filling-depleting of the calix.

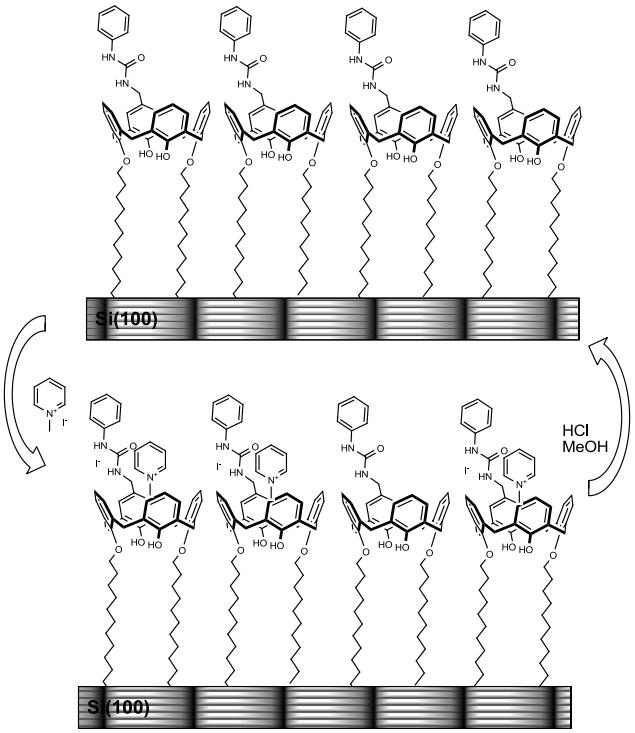

Figure 5.3.7: Schematic representation of the recognition process occurring between calix[4]arene heteroditopic receptors anchored on silicon surface and N-methylpyridinium cation (NMP^+).

As for the I^- anion (Figure 5.3.6b), its quantitative ratio to N^+ was lower than expected from stoichiometric ratios for the anchored calix[4]arene. The ascertained presence, in this sample, of deprotonated surface SiO^- groups, which can substitute for the anion in the ion-pair

interactions with NMP^+, offers a likely explanation of this effect.[40,91] The N^+/I^- ratio further diminished after rinsing, and a Cl^- peak became visible in the XPS spectrum. We interpret this as a result of the anion exchange, which takes place during the rinsing cycle to free the calix[4]arene cavity, operated with a CH_3OH solution acidified with HCl (Figure 5.3.7).

5.3.3 - Self-assembling of pseudorotaxane species on Si(100)

A further recognition reaction was successfully tested by producing the first example of a pseudorotaxane species on Si(100). The species obtained is based on an N,N′-dialkylviologen-calix[6]arenePhenylUrea adduct. We explored two approaches. We first started by reacting (via a photoassisted recipe strictly analogous to the one reported above) the N,N′-dialkylviologen axle, carrying a terminal C=C group and synthesized in high yield, with H-Si(100) (Figure 5.2.2).

The result was, however, poor, as testified by the low N/Si atomic ratio from XPS measurements. No silicon oxidation was detected. A likely explanation for the poor adhesion is because of the charge present on each axle, which does not allow for a compact monolayer to form on Si, thus exposing Si to further reactions.

We then started directly from the pseudorotaxane in a toluene solution, by reacting the same calix[6]arene wheel and the viologen-based axle. H-Si(100) was reacted with the above solution under the usual photoassisted conditions (Figure 5.3.8). This two-step reaction successfully produced a threaded rotaxane covalently bound on Si, as shown by the XPS results (Figure 5.3.9).

[91] a) R. Zanoni, M. Cossi, M. F. Iozzi, F. Cattaruzza, E. A. Dalchiele, F. Decker, A. G. Marrani, M. Valori, Superlattices and Microstructures 2008, 44, 542. b) E. A. Dalchiele, A. Aurora, G. Bernardini, F. Cattaruzza, A. Flamini, P. Pallavicini, R. Zanoni, F. Decker, J. Electroanal. Chem. 2005, 579, 133.

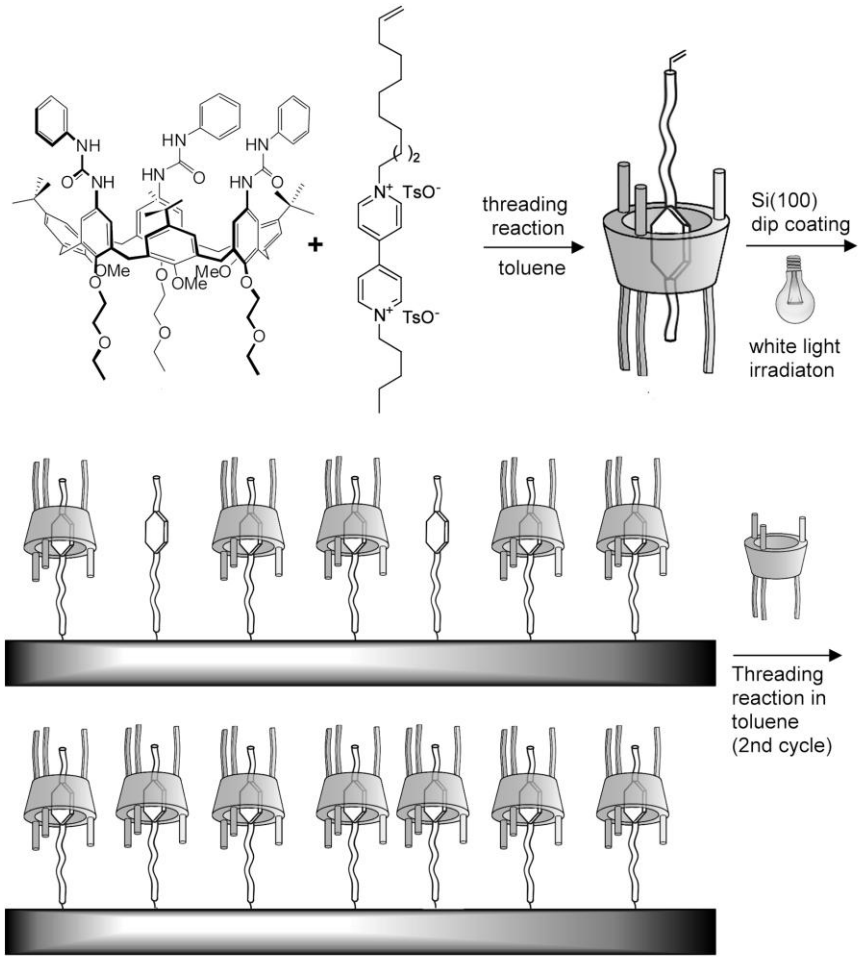

Figure 5.3.8: Threading reaction in toluene between viologen axle and calix[6]arene wheel. The resulting pseudorotaxane was anchored on Si(100) surface in a two-step process.

Figure 5.3.9 reports the N 1s peak, where NH and N^+ peak components are again present, indicating the anchoring of the pseudorotaxane at the Si surface. The NH/N^+ ratio is 2, which should be compared with an expected stoichiometric value of 3 in the absence of dethreading. Since we are aware that UV light can induce viologen reduction and affect dethreading,[92] we tested different experimental conditions, in order to obtain a monolayer of pseudorotaxane on Si(100). In order to identify the role of visible light in affecting dethreading, we performed a parallel experiment on H-Si(100) and on a polycrystalline Cu surface at RT, with the same contact time (see Chapter 4). Both surfaces were contacted with a preformed adduct of a calix[6]arene with a suitable axle (a C=C or SH-terminated C_{11} chain). The reaction was photoassisted for Si(100), while no illumination was necessary for the reaction to be completed on Cu. In the latter case, we found no sizeable dethreading of the

[92] P. M. S. Monk, The Viologens, John Wiley & Sons, Chichester, 1998.

pseudorotaxanes. This was inferred from the NH/N^+ ratio, equal to 3.0, the value expected from stoichiometry. On Si(100), a value of 2.0 was, instead, found. We then further operated the anchoring reaction on Si(100) under the same illumination conditions, but at a solution temperature closer to the experimentally determined value for dethreading of the pure adduct in a solution. This resulted in a drop to 1.5 of the NH/N^+ ratio. In Figure 5.3.8, the XPS spectrum of the Si 2p region, is displayed, showing the presence of Si oxide. This last could have resulted from the short exposure to air during preparation and from the lower passivation of the surface due to the pseudorotaxane size.

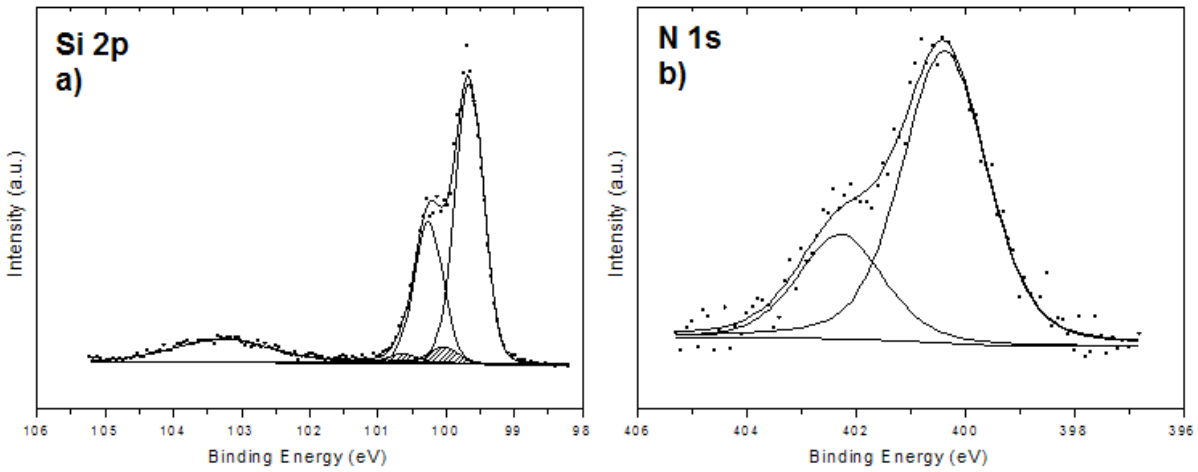

Figure 5.3.9: Si 2p (a) and N 1s (b) XPS spectra of a Si(100)/pseudorotaxane. The cross-hatched areas in a) identify the component due to reacted Si. In b) the experimental curve is displayed as dotted line, with the NH and N^+ peak components, resulting from curve-fitting, as solid lines.

In order to overcome the limitations inherent to the experimental conditions needed for surface anchoring of the pseudorotaxane, we post-reacted the Si(100) surface covered with a mixed layer of pseudorotaxane and axle with a solution only containing the calix[6]arene wheel. The NH/N^+ ratio increased to 2.8, which indicates that the mixed monolayer reacts to produce a nearly full threading of the residual axles. Notice that, following this recipe, we came to the same conditions obtained on Cu of a full monolayer of anchored pseudorotaxane.

A mixed monolayer on Si(100), composed of pseudorotaxanes and axles, can further uptake free calixarenes from a solution, resulting in a self-assembled monolayer of rotaxane.

5.4 – AFM investigation: Results and discussion

Application of in situ AFM allowed assessing the surface morphology of the reacted Si surfaces. Here are reported the AFM image recorded from the hybrid H-Si(100)/calix[4]areneBr_2, for which the XPS Si 2p and Br 3d spectra are displayed in Figures 5.3.2 and 5.3.3.

The image is representative of the total area explored. The surface revealed a homogeneous morphology, consisting of globular assemblies. The rms roughness value obtained from the image is 0.13 nm. Linear cross-section profiles as the one evident in Figure 5.4.1, taken from a measured area of 0.82 x 0.86 μm^2, reveal sub-micrometric grains with an average height equal to ~2.3 nm, which closely compares with the length for a calix[4]arene molecule, ~2.2 nm.

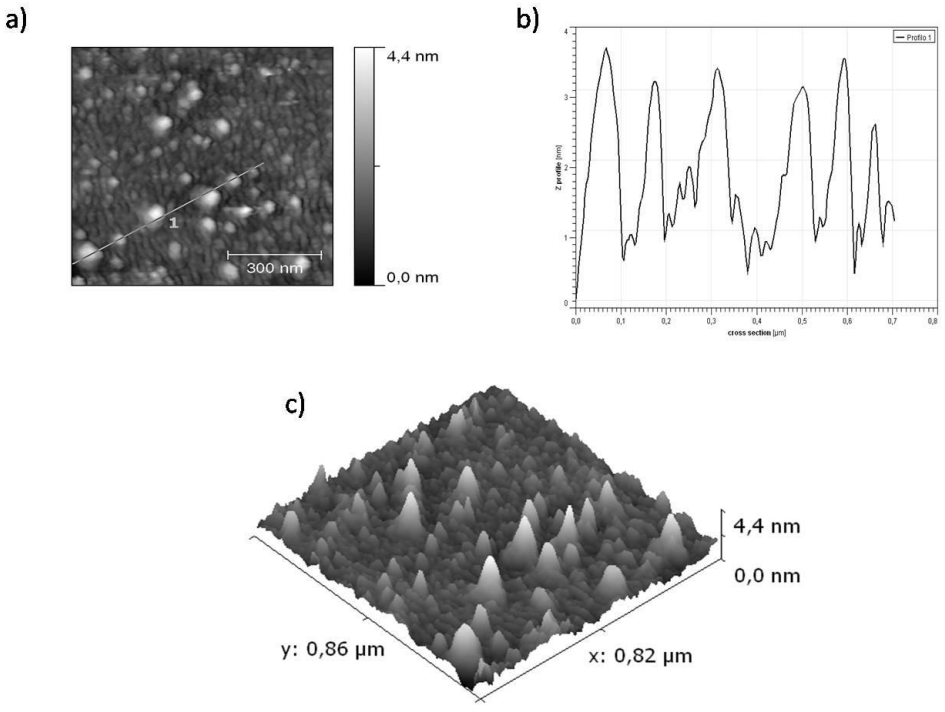

Figure 5.4.1: AFM results on H-Si(100)/calix[4]areneBr_2. AFM image from a 0.82 × 0.86 μm^2 area is reported at (a), with the corresponding analysis of a linear cross-section profile, (b), taken along the marked segment. A 3D image from the same area is reported in (c).

5.5 – Cross-exchanging of surfaces

We also checked for the extent to which the anchoring process of thiols (and alkene) terminal groups is selectively realized on Cu (or Si, respectively) surface sites. We separately contacted a Cu polycrystalline surface with calix[4]areneBr_2 (C=C termination), and a Si(100) wafer with calix[4]arene (-SH termination). The results are reported in Figure 5.5.1. No molecular uptake was observed in both cases, from the absence of the characteristic peak in the relevant photoemission regions (Br 3d and S 2p). The result is significative for possible extension of our approach to the patterning of Si(100) surfaces containing Cu vias.

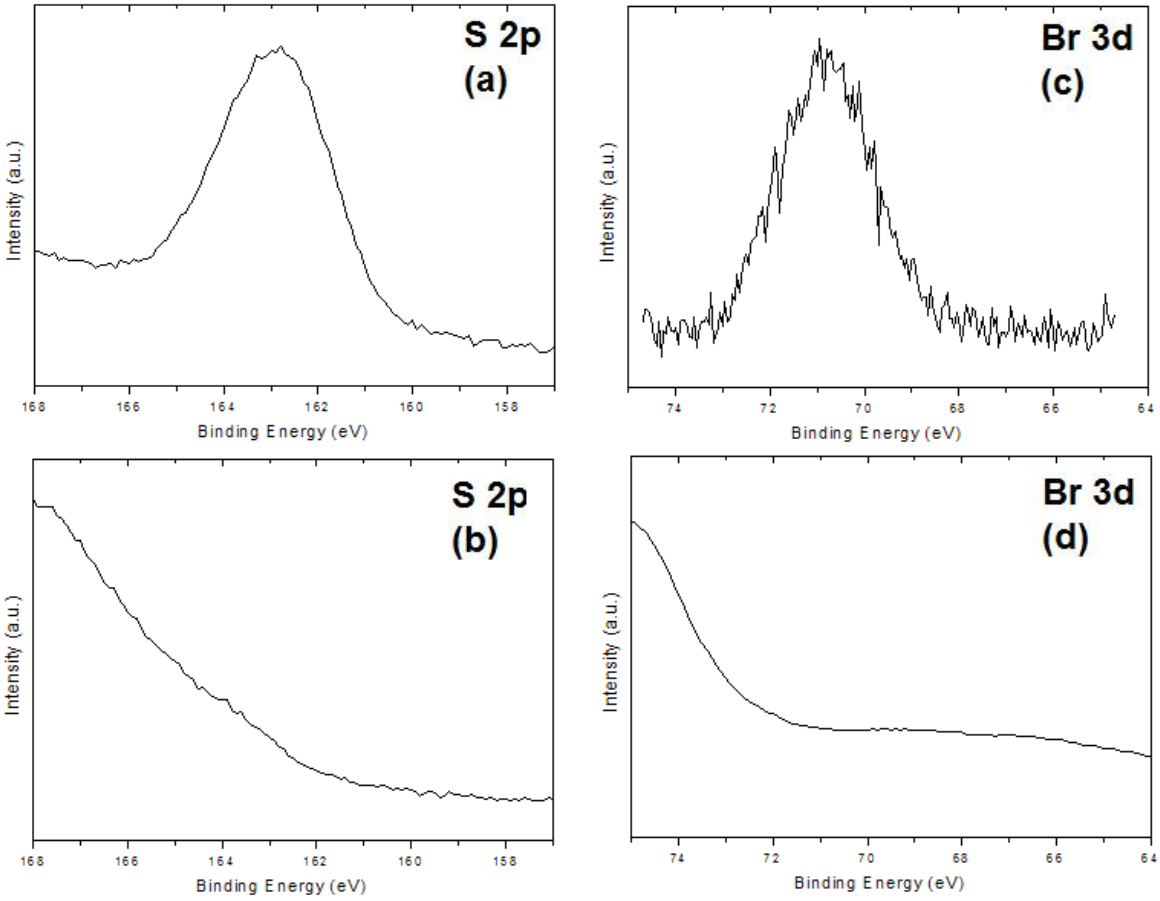

Figure 5.5.1: XPS S 2p spectra Cu/calix[4]arene (a) and Si/calix[4]arene (b), Br 3d spectra of Si/calix[4]areneBr_2 (c) and Cu/ calix[4]areneBr_2 (d). The features in (b) and (d) are due the raising background.

5.6 – Conclusions

We have studied the covalent functionalization of Si(100) with calix[4]arenes and pseudorotaxane-based calix[6]arene, which were obtained through a wet chemistry recipe. We made use of an extra-mild photochemical activation, which makes use of photoassisted anchoring via visible light of C=C terminated anchoring arms. Our recipe largely preserves the integrity of the molecular substrate, as verified by XPS, also allowing for a full monolayer of pseudorotaxane to be formed on Si(100), along a two-step reaction. Molecular adhesion has been tested and the recipes improved by the feedback assistance of XPS, through assignment and relative quantitation of signals from specific elements in the molecules, and by AFM results. Mixed monolayer on Si(100), composed of pseudorotaxanes and axles, can further uptake free calixarenes from a solution. This result opens up to the realization of more complex mixed monolayer, by employing suitably substituted calixarenes.

A covalent functionalization on both Si and Cu surfaces requires the molecules to be differently modified: a thiol (-SH) or C=C termination is respectively suitable for Cu or H-Si(100). We cross checked the reactivity of the different anchoring group on the Cu and Si surfaces. No molecular uptake was observed when each of the two surfaces was exposed to the molecular system suitable for the other. Each calixarene only chemisorbed on the expectedly right surface.

Chapter 6
XPS characterization of nanometric and subnanometric calixarene protected gold nanoparticles

6.1 – Introduction

6.1.1 - Synthesis

Gold nanoparticles (AuNPs) were synthesized at the Università di Parma by the group of Prof. Pochini. Taking advantage of the two-phase synthetic procedure reported by Brust (see Paragraph 2.4),[63] the reduction of the aurate was accomplished with $NaBH_4$ in a toluene solution containing the thiolated calixarene ligand. Nanoclusters were prepared for each ligand using different S:Au molar ratios of 3:1, 1:3 and 1:6. In these ratios S expresses the equivalents of thiolated alkyl chains present in the solution regardless the nature of the multidentate ligand. In this way, the outcomes of the synthesis carried out using the same S:Au ratio become independent by the absolute amount of the calixarene employed and, most important, directly comparable with the literature data relative to monodentate thiolated ligands.

The ratio of alkanethiol to Au controls the size of the resulting nanoparticles by adjusting the relative rates of particle nucleation and growth (higher ratios yield smaller particles). AuNPs protected with multipodand thiolated calix[n]arene ligands bearing one,

two, three or four convergent ω-undecanthiol chains on their lower rim were produced and characterized (Figure 6.1.1).

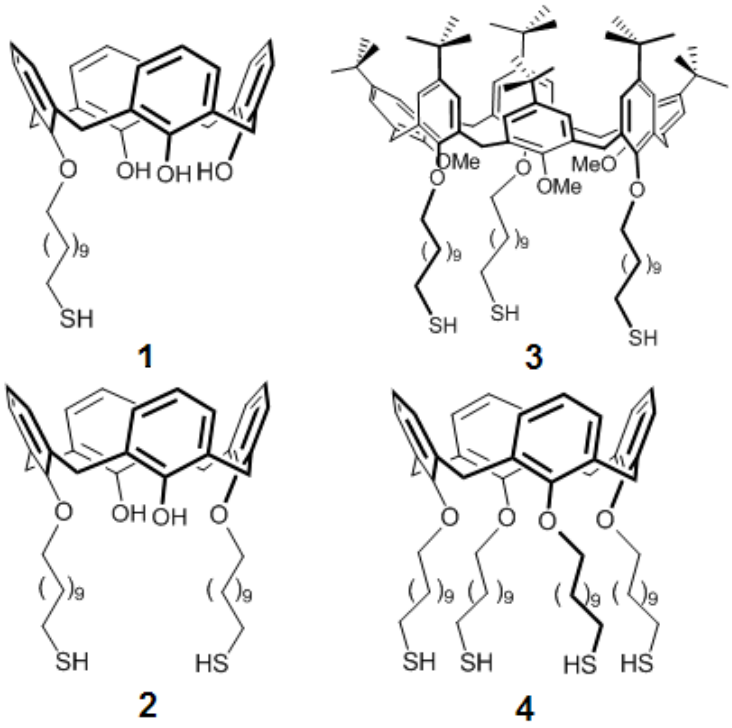

Figure 6.1.1: Structural formulae of monodentate (1), bidentate (2), tridentate (3) and tetradentate (4) thiolated calix[n]arenes.

The investigation tool used in this thesis for the characterization of NPs was X-ray Photoelectron Spectroscopy (XPS). A more detailed characterization (Transmission Electron Microscopy (TEM), UV-Vis Spectroscopy, Dinamic Light Scattering, Elemental Analysis and ^{13}C-NMR) has been accomplished by the research group of Prof. Pochini at Università di Parma, but only the results from TEM are discussed here, for their relevance in the interpretation of XPS results.[93]

Each set of NPs was designated as $Cx_m(RS)_n$-Au, where *m* (4 or 6) and *n* (1 to 4) identify the calixarene macrocycle and its denticity, respectively. To distinguish among nanoparticles stabilized with the same ligand but prepared using different S:Au ratios, the index s, m or l was used. This index would represent the relative core size (s = small, m = medium and l = large), of the nanoparticles with respect the 3:1, 1:3 and 1:6 S:Au molar ratio used for their synthesis (Table 6.1.1).

[93] L. Pescatori, A. Boccia, F. Ciesa, F. Rossi, V. Grillo, A. Arduini, A. Pochini, R. Zanoni, A. Secchi, Chem. Eur. J. 2010, 16, 11089.

6.1.2 - TEM measurements

We report in the following on the TEM results because of their primary use as reference to the outcomes of XPS. The core size distribution of the synthesized AuNPs was determined through TEM measurements. This analysis showed that for each ligand used, the mean core size (*d*TEM) of the corresponding nanoclusters is inversely proportional to the S:Au ratio employed during the synthesis (Table 6.1.1). This was an expected result since the effect of the ligand concentration on the size of the resulting nanoclusters has been already verified.[64]

NP	Ligand	Designation	S:Au[a]	*d*TEM (nm)
$[Cx_4(RS)\text{-}Au]$	1	1s	3:1	1.5 ± 0.3
$[Cx_4(RS)_2\text{-}Au]$	2	2s	3:1	0.8[b] ± 0.2
$[Cx_4(RS)_2\text{-}Au]$	2	2m	1:3	1.6 ± 0.4
$[Cx_4(RS)_2\text{-}Au]$	2	2l	1:6	2.5 ± 0.7
$[Cx_6(RS)_3\text{-}Au]$	3	3s	3:1	1.0 ± 0.2
$[Cx_6(RS)_3\text{-}Au]$	3	3m	1:3	2.0 ± 0.5
$[Cx_6(RS)_3\text{-}Au]$	3	3l	1:6	2.6 ± 0.5
$[Cx_4(RS)_4\text{-}Au]$	4	4s	3:1	1.0 ± 0.2

[a] equivalents of alkylthiol chains per aurate.

[b] HAADF-STEM measurements.

Table 6.1.1: Designation, composition and mean core size of the calix[n]arene-protected AuNPs.

The effect of the ligand denticity on the size of the nanocluster is well evidenced by comparing the *d*TEM and the size distribution diagrams (Figure 6.1.2) determined for 1s, 2s and 3s samples obtained using the same S:Au molar ratios.

Interesting results were obtained by comparing the TEM images taken from the three sets of nanoparticles 1s, 2s and 3s, which were prepared using an identical S:Au ratio of 3:1, but having the monodentate 1, the bidentate 2 and the tridentate 3 calixarene as protecting thiolate ligand, respectively (Figure 6.1.1). The core size distribution diagrams corresponding

to each TEM image clearly evidence that the nanoparticles present in the samples 2s and 3s are endowed with a mean core size (*d*TEM < 1 nm) smaller than those present in 1s (*d*TEM ~ 1.5 nm, Figure 6.1.2). The latter nanoclusters were characterized by *d*TEM comparable to those reported for n-dodecanthiol-protected NPs prepared using the identical S:Au ratios.[64c] The *d*TEM of 4s sample resulted equal to that of 2s and 3s (Table 6.1.1).

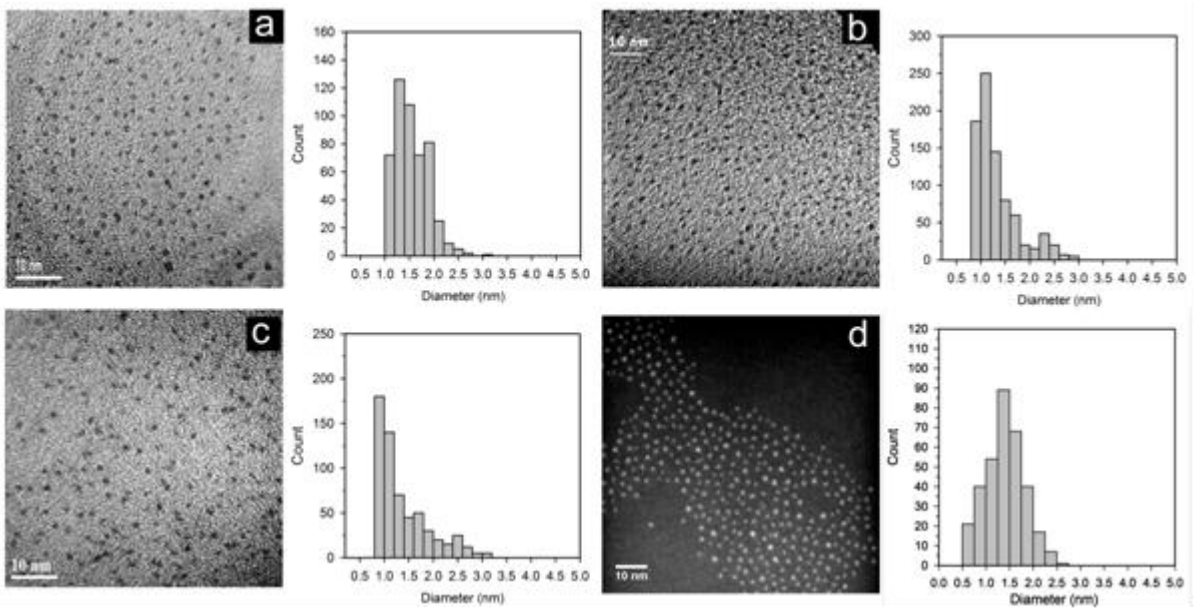

Figure 6.1.2: TEM images and core size distribution diagrams of calixarene-protected AuNPs prepared using a S:Au = 3:1. a) 1s (*d*TEM = 1.5 ± 0.3 nm), b) 2s (*d*TEM = 1.0 ± 0.3 nm,), c) 3s (*d*TEM = 1.0 ± 0.2 nm); d) HAADF-STEM image and core size distribution diagram of 2s (*d*STEM = 1.2 ± 0.3 nm).

Most important, the distribution analysis revealed that the use of a threefold excess of alkylthiol chains per aurate (S:Au = 3:1) for the multidentate ligands induces the formation of very small clusters. HAADF-STEM analysis evidenced the presence of subnanometric icosahedral Au_{13} NPs (d ~ 0.8 nm) (Figure 6.1.2). These results support the hypothesis that the size distribution of the calix[n]arene protected AuNPs is affected by the denticity of the ligand.

We propose that the observed reduction in the core size of the nanoparticles stabilized with the multidentate ligands 2, 3 and 4 is due to the convergent arrangement and the elevated effective molarity of the (two, three or four, respectively for 2, 3 or 4) thiolate chains to the growing gold core, after the formation of the first Au-S bond, which increases the passivation rate. In fact, a constant S:Au stoichiometric ratio 3:1 was chosen in the synthesis of the full

series of 1s, 2s, 3s, in order to keep the number of thiol chains constant, by adding the proper amount of the ligand.

6.2 - Results and discussion: XPS investigation

The XPS analysis has been conducted on the series of s, m, l NPs in Table 6.1.1 and on the ligand exchanged Au_{11} NPs (2ex). The latter nanoparticles were obtained through ligand-place exchange reaction by reacting $Au_{11}(PPh_3)_7Cl_3$ undecagold clusters with an excess of thiolate calix[4]arene 2 (Figure 6.1.1). These solid compounds were spread over a graphite tip attached to the XPS sample holder and analyzed.

The relevant XPS regions for the investigated systems are those of Au 4f and S 2p, which appear as complex peaks and required curve-fitting procedures (Figures 6.2.1-Figure 6.2.6).

As evidenced by a rigid energy shift of the overall spectrum, the nanoclusters experienced static charging under X-rays to different amounts, which were quantified and corrected by referencing the C 1s signal of the calixarene at 285.0 eV (see Paragraph 3.1). Such static charging only affected m and s NPs, to comparable extents.

XPS measurements have shown that gold is present in the core in different chemical states. Theoretically reconstructed Au 4f peaks invariably show three spin-orbit split components (Table 6.2.1), while two main components were expected, one due to the Au-S bonds and the second to Au-Au (both central and surface atoms) (Figure 6.2.1-Figure 6.2.3). Their assignment is further complicated by the fact that the three Au components happen to follow at different BEs, depending on the cluster size. We assign the Au electronic states for l, m and s NPs by first considering the typical energy separation between Au $4f_{7/2}$ components, as extracted from the relevant literature:[94] Au-Au(I) (1.4 ± 0.4 eV) and Au(I)-Au(III) (1.7 ± 0.4 eV). These values are consistently reproduced by peaks Au(a), (b) and (c) (Table 6.2.1), which are present with different relative ratios in the series, depending on the mean dimension

[94] a) F. Demoisson, M. Mullet, B. J. Humbert, J. Colloid Interface Sci. 2007, 316, 531. b) M. C. Bourg, A. Badia, R. B. Lennox, J. Phys. Chem. B 2000, 104, 6562. c) D. G. Castner, K. Hinds, D. W. Grainger, Langmuir 1996, 12, 5083.

of NPs. The minor Au(c) component can be assigned to Au(III) species likely deriving from $AuCl_4^-$.

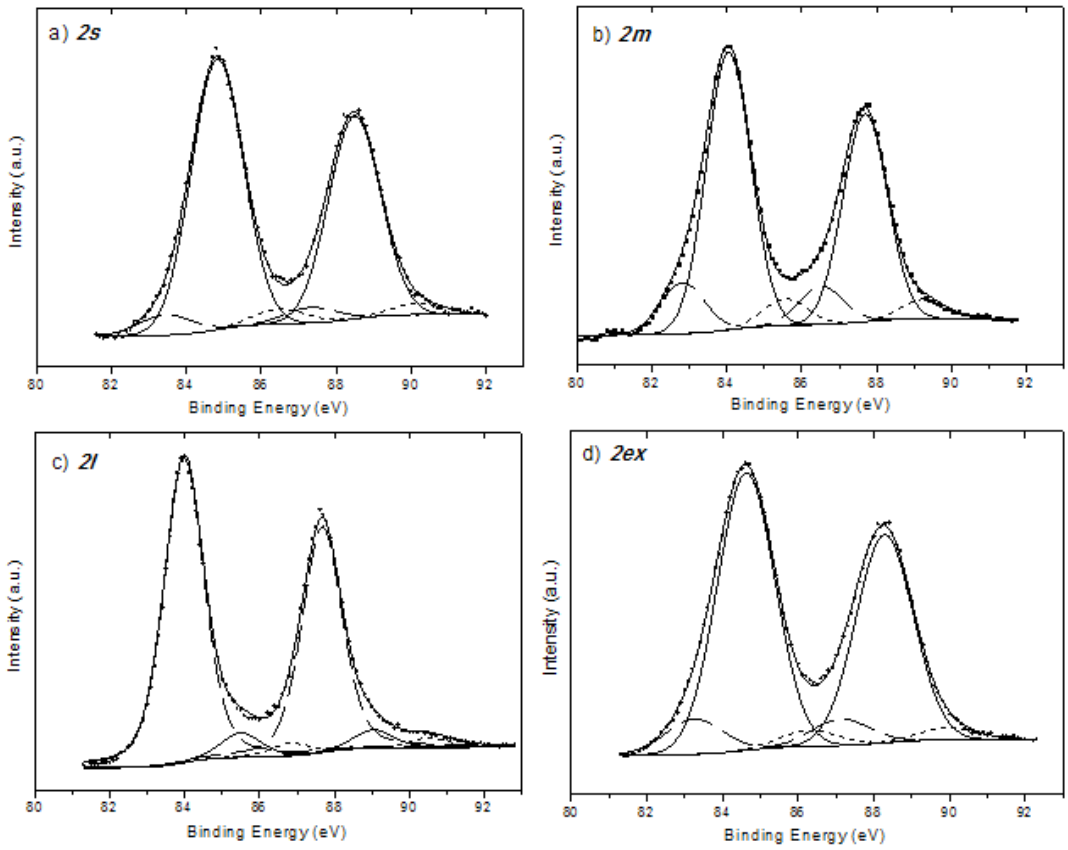

Figure 6.2.1: Au 4f XPS spectral regions of a) 2s, b) 2m, c) 2l and d) 2ex. Experimental curve (dots) and Au $4f_{7/2,5/2}$ curve-fitted components: Au(a) (dash line), Au(b) (solid line), and Au(c) (dot line).

In the 3l sample, Au(III) species is predominant, resulting in a different spectrum profile (Figure 6.2.2c). The Au(c) component experienced a differential charging under X-rays and its position was not stable during the measurement. So the correct binding energies of Au(b) and Au(c) determined from the fit are not reliable. The depth profile analysis revealed that the Au(III) species lies at the surface of the NP, as its signal increases at grazing take-off angle (81°) (see Paragraph 3.1) (Figure 6.2.2d).

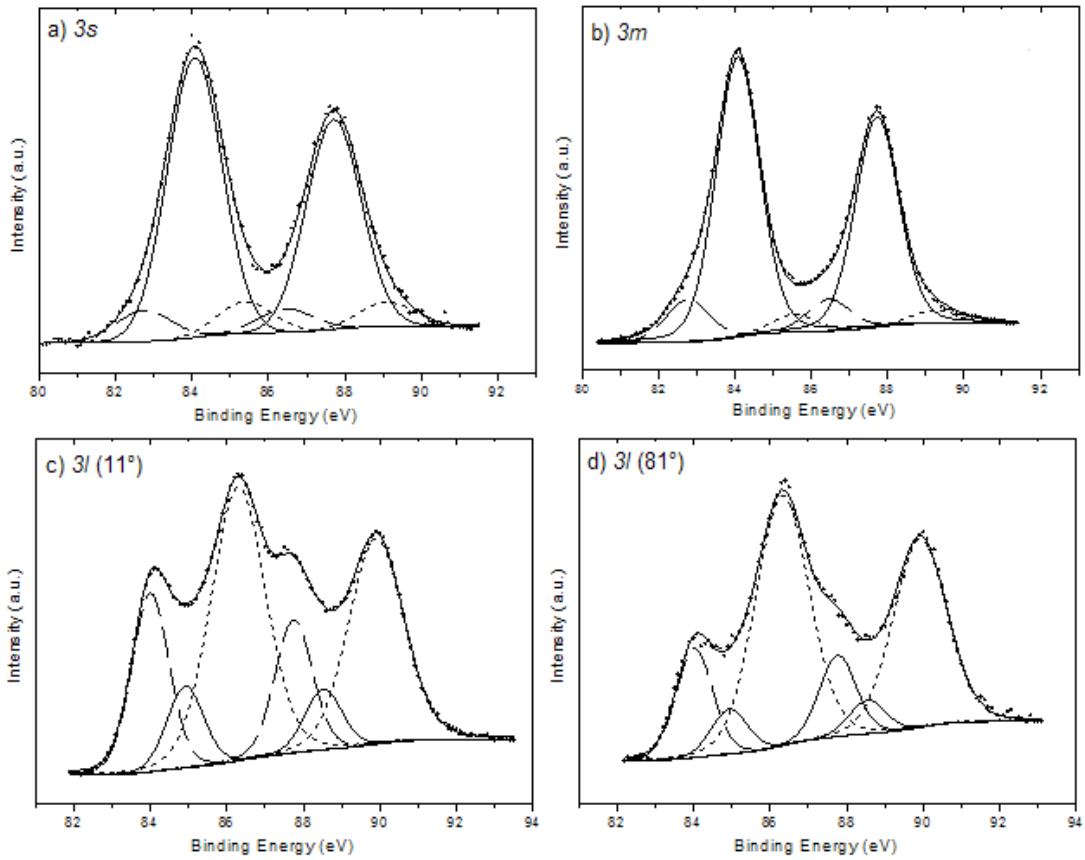

Figure 6.2.2: Au 4f XPS spectral regions of a) 3s, b) 3m, c) 3l (11°), d) 3l (81°). Experimental curve (dots) and Au $4f_{7/2,5/2}$ curve-fitted components: Au(a) (dash line), Au(b) (solid line), and Au(c) (dot line).

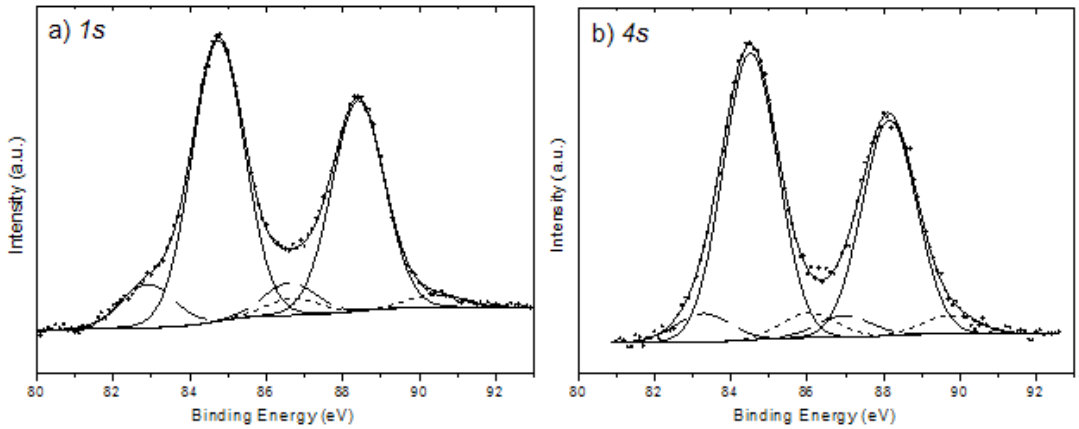

Figure 6.2.3: Au 4f XPS spectral regions of a) 1s and b) 4s. Experimental curve (dots) and Au $4f_{7/2,5/2}$ curve-fitted components: Au(a) (dash line), Au(b) (solid line), and Au(c) (dot line).

	Au 4f			S 2p			*d*TEM
	label	BE	Au(b)/Au(a)	label	BE	S/Au	
1s	Au(a) Au(b) Au(c)	82.9 84.7 86.7	6	Au-S	162.9	0.7	1.5
2s	Au(a) Au(b) Au(c)	83.5 84.8 86.5	10	Au-S S-S	163.2 165.3	1.0	1.0
2m	Au(a) Au(b) Au(c)	82.8 84.1 85.6	5	Au-S	162.4	0.6	1.6
2l	Au(a) Au(b) Au(c)	84.0 85.5 86.8	0.1	Au-S	162.3	0.3	2.5
2ex	Au(a) Au(b) Au(c)	83.3 84.6 87.1	8	Au-S	163.0	1.0	1.0
3s	Au(a) Au(b) Au(c)	82.8 84.1 85.4	9	Au-S S-S	162.3 163.6	1.5	1.0
3m	Au(a) Au(b) Au(c)	82.8 84.1 85.5	7	Au-S S-S	162.4 163.7	0.4	2.0
3l	Au(a) Au(b) Au(c)	84.0 84.9 86.3	0.4	Au-S S-S	163.0 164.1	0.3	2.6
4s	Au(a) Au(b) Au(c)	83.3 84.5 86.1	10	Au-S	163.2	1.8	1.0

Table 6.2.1: XPS binding energies for Au 4f and S 2p and relative quantitative ratios (± 10%) for different series of calixarene-stabilized AuNPs.

It is expected on the simple basis of the decreasing trend of surface/bulk atomic ratio in a cluster as a function of its increasing nuclearity that the Au(a)/Au(b) ratio is the largest for l and the smallest for s NPs, as indeed found, with the m ones lying definitely closer to the latter.

The main $Au4f_{7/2}$ component in all the spectra is invariably associated with a relative shift to the main S $2p_{3/2}$ component equal to 78.3 ± 0.1 eV in almost all cases, a value found in the literature as characteristic for S-bound Au atoms.[93] The S 2p spectra present a major component due to thiolate-Au bond, accompanied in the case of 2s, 3s, 3m and 3l NPs by a small contribution from distinct sulphur species (Figure 6.2.4-Figure 6.2.6). We assign this minor component to disulphide bridges connecting distinct calixarenes,[95] since NMR analysis excludes the alternative assignment in terms of free thiols, because of the absence of SH groups in the NPs. Relevant quantitative results [S:Au and Au(b):Au(a)] are reported in Table 6.2.1.

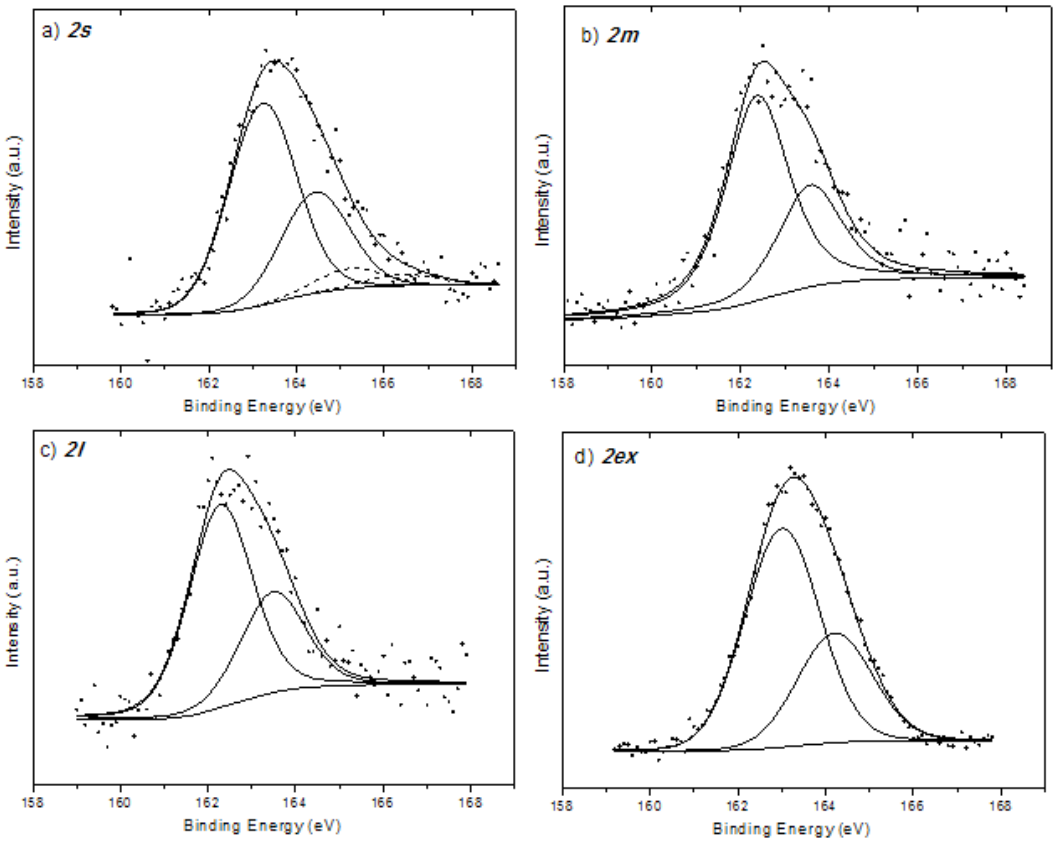

Figure 6.2.4: S 2p XPS spectrum of a) 2s, b) 2m, c) 2l and d) 2ex. Experimental curve (dots) and S $2p_{3/2,1/2}$ curve-fitted components: S-Au major components (solid line), disulphide bridges (dot line).

[95] a) S. W. Joo, S. W. Han, K. Kim, J. Colloid Interface Sci. 2001, 240, 391. b) S. W. Joo, S. W. Han, K. Kim, J. Phys. Chem. B 2000, 104, 6218. c) S. W. Joo, S. W. Han, K. Kim, Langmuir 2000, 16, 5391. d) S. W. Joo, S. W. Han, K. Kim, J. Phys. Chem. B 1999, 103, 10831.

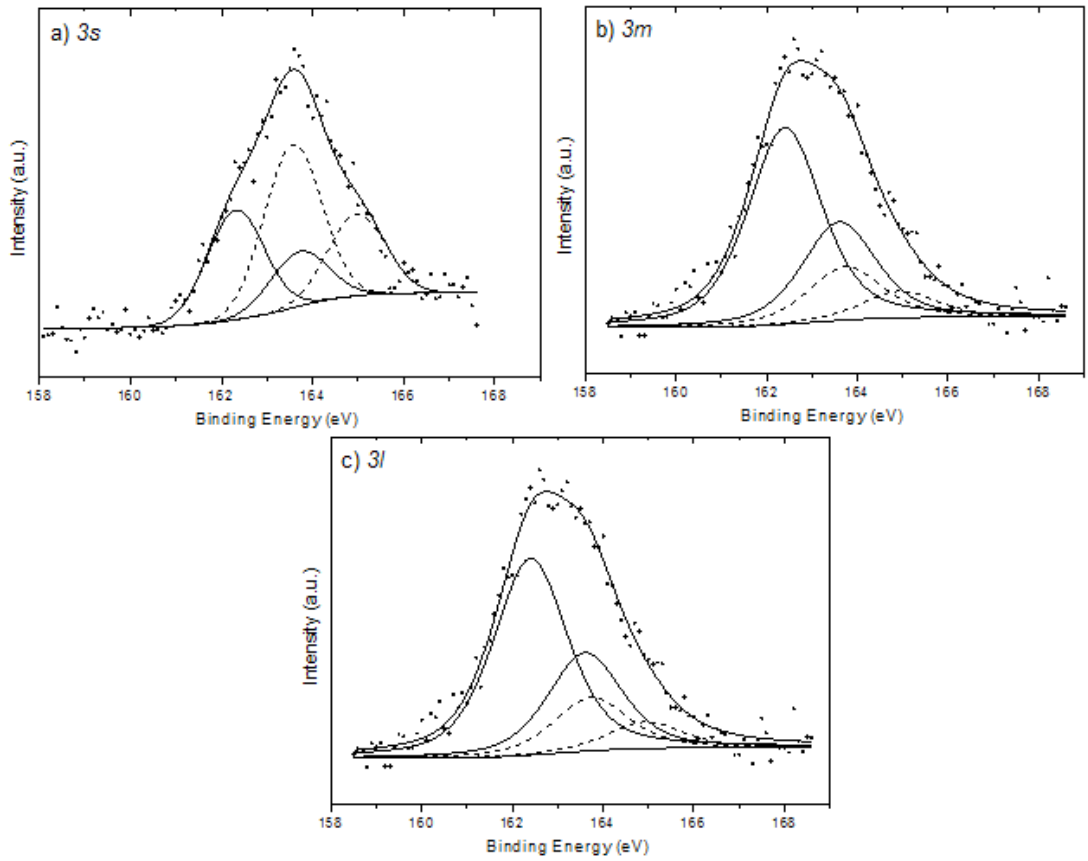

Figure 6.2.5: S 2p XPS spectrum of a) 3s, b) 3m and c) 3l. Experimental curve (dots) and S $2p_{3/2,1/2}$ curve-fitted components: S-Au major components (solid line), disulphide bridges (dot line).

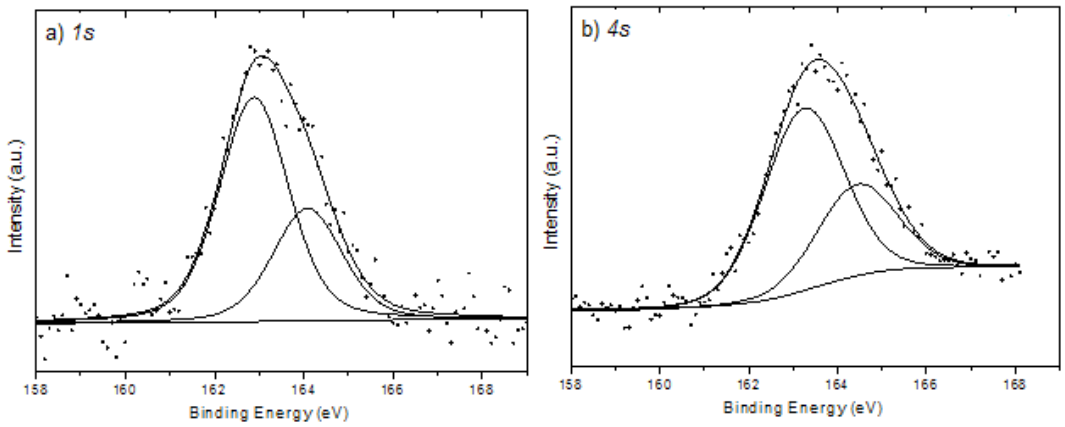

Figure 6.2.6: S 2p XPS spectrum of a) 1s and b) 4s.

The S 2p spectra of 3s in Figure 6.2.5a showed an excess of disulphide with S-S/S-Au ratios of 4.6. This implies an excess of calixarenes not bound to gold, resulting from a not successful purification.

The S 2p major component due to thiolate-Au bond is also fully compatible with the structural motif (*staple*) first seen in the external organic shell of the X-ray structure of the

Au_{25} nanoclusters protected with phenylethanthiolate groups reported by Murray,[96] and confirmed in subsequent reports.[97] The staple motif can be described as Au-thiolate moieties in the form of –SR-Au-SR-. We note that Au BEs and relative quantitative ratios for 2ex are closely comparable to 2s, 3s and 4s, and distinct from the m, l series and 1s. More in detail, the S:Au and A(b):Au(a) ratios obtained for 2ex, and expected for a Au_{11} cluster, are only reproduced in the cases of 2s, 3s and 4s, within the typical experimental error (± 10%). The S:Au ratios of 3s and 4s are also affected by a not effective purification (S:Au > 1 points out an excess of sulphur). A value equal to 1 means that all the gold atoms of the core are involved in Au-S bonds.

As for BEs, Au(a) $4f_{7/2}$ values for s and m NPs fall in the range of 82.8-83.5 eV, *i.e.* at consistently negative BE shift with respect to bulk Au (84.0 eV). Their interpretation in terms of a negatively charged Au central atom is supported by previous literature reports.[98]

We can take the relative abundance of Au(a) together with S:Au ratios as an indirect measure of the cluster nuclearity, allowing for a distinction to be made between s, m and l. In fact, the experimental S:Au and Au(b):Au(a) ratios are inversely proportional to the size of the nanoclusters. This trend is consistent with the observation that the smaller is the core size of the NPs, the larger the percentage of surface Au atoms bound to S. In addition to that, we could tentatively infer the NPs nuclearity by comparing the present results with the expected values in the notable cases of previously reported Au_{11}, Au_{13}, $Au_{25}(SR)_{18}^{-}$, Au_{38}/Au_{40}, Au_{55}, Au_{68}, Au_{102}, and Au_{144} clusters.[96]

On the basis of the S:Au and Au(b):Au(a) ratios data in Table 6.2.1 (~ 1 and ~ 10:1, respectively), the nuclearities of 2s, 3s and 4s are likely assigned to Au_{11} or Au_{13} (which can be hardly distinguished by XPS only), furthermore their *d*TEMs show a subnanometric core, while m NPs belong to higher nuclearity species. As regards to l, the S:Au and Au(b):Au(a) ratios are too small to find a correspondence with the above range of Au nuclearity, thus hinting at a larger range of cluster diameters. We also note that, in the case of l, while TEM measurements clearly distinguish a larger average dimension of the particles, XPS results are distinct from the analogous s and m, but they could be mainly related to the outer shell of the

[96] M. W. Heaven, A. Dass, P. S. White, K. M. Holt, R. W. Murray, J. Am. Chem. Soc. 2008, 130, 3754.

[97] a) R. Jin, Nanoscale 2010, 2, 343. b) R. L. Whetten, R. C. Price, Science 2007, 318, 407 and references therein.

[98] H. Tsunoyama, N. Ichikuni, H. Sakurai, T. Tsukuda, J. Am. Chem. Soc. 2009, 131, 7086.

particle, since its experimental diameter range becomes comparable to the inelastic mean free path for Au 4f photoelectrons, at the photon energy applied.

The MPC synthesis reaction described by Murray considers the reduction of aurate to Au(I) by the thiols and the formation of a polymer where the Au(I) species are coordinated by two sulphur groups.[64] The reduction of this polymeric structure gives the nanocluster (see Paragraph 2.4). We analyzed the product of the synthesis before the addition of the $NaBH_4$ reducer. The Au 4f spectrum revealed the presence of a single Au species assigned to Au(I), confirming the hypothesis of the formation of the polymer (Figure 6.2.7).

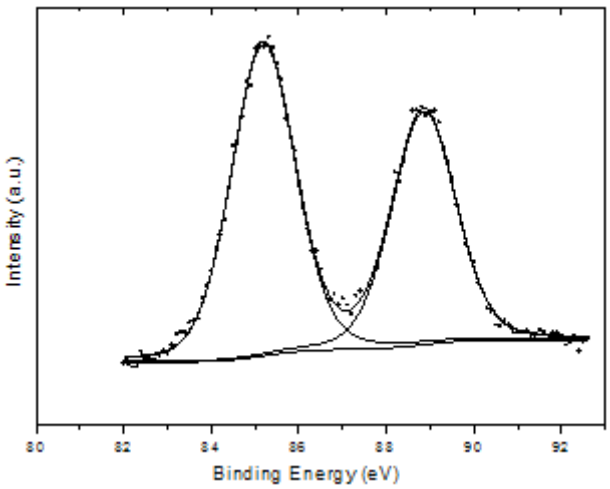

Figure 6.2.7: Au 4f XPS spectral regions of non reduced product of synthesis.

6.3 – Conclusions

A series of differently sized AuNPs stabilized by monodentate, bidentate, tridentate and tetradentate thiolate calix[n]arene ligands prepared by the Brust-Schiffrin two-phase synthesis were characterized by TEM and XPS. The experimental data showed that the multidentate structure of calix[n]arene derivatives introduced a control element in the preparation that allows to obtain very small (< 1 nm) AuNPs.

XPS measurements have shown that gold is present in the core in different chemical states assigned on the basis of their energy separation: Au (Au-Au, central and surface atoms), Au(I) (Au-S) and Au(III) (due to residual $AuCl_4^-$). The S 2p spectra presented a major component due to thiolate-Au bond compatible with the staple motif evidenced by the X-ray

structure of the Au_{25} nanoclusters reported in the literature, and accompanied in some cases by a small contribution of disulphide bridges.

Since smaller NPs have a larger percentage of surface Au atoms, we can take the experimental S:Au and Au(b):Au(a) ratios as an indirect measure of the cluster nuclearity: they were found inversely proportional to the size of the nanoclusters.

We also characterized NPs obtained from Au_{11} clusters exchanged with bidentate calix[4]arene. The Au 4f and S 2p spectra and the quantitative ratios of this sample are closely comparable to that of 2s, 3s and 4s, supporting the assignment to Au_{11} or Au_{13} subnanometric clusters.

The analysis of Au 4f of the product of the synthesis before the addition of $NaBH_4$ revealed the presence of a Au(I) species, compatible with the polymeric -AuSR- structure, hypothesized by Murray.

Acknowledgments

Ringrazio tutte le persone che mi hanno sempre consigliato e appoggiato.
Il Prof. Robertino Zanoni, che mi ha seguito negli ultimi 4 anni, la Prof. Valeria Di Castro, i Prof. Franco Decker e Stefano Stranges e i Dott. Fabrizio Caprioli e Valeria Lanzilotto, qui all'Università La Sapienza.
Il gruppo del Prof. Pochini dell'Università di Parma, in particolare i Prof. Arturo Arduini e Andrea Secchi e il Dott. Luca Pescatori.
L'ultimo ringraziamento va alla mia famiglia e agli amici di sempre.